



INAOE

# **Elaborating a new technique for acousto-optical spectrum analysis of ultra-high-frequency radio-wave signals with an improved resolution, using collinear wave heterodyning**

Principal contributors:

**Alexandre S. Shcherbakov<sup>(1)</sup>, Alexej M. Bliznetsov<sup>(2)</sup>,  
Jewgenij Maximov<sup>(3)</sup>, Olga I. Belokurova<sup>(2)</sup>,  
Daniel Sanchez Lucero<sup>(1)</sup>, Abraham Luna Castellanos<sup>(1)</sup>,  
Sergey A. Nemov<sup>(2)</sup> & Karla J. Sanchez Perez<sup>(1)</sup>.**

- 1) National Institute for Astrophysics, Optics & Electronics (INAOE), Puebla, Mexico.
- 2) St.-Petersburg State Polytechnic University, Saint-Petersburg, Russian Federation.
- 3) Molecular Technology GmbH, Berlin, Germany.

**Technical report**

**Optics Department, INAOE.**

**©INAOE 2010**

The authors hereby grant to INAOE permission to reproduce and distribute copies of this technical report.



## INDEX

<b>Introduction</b>	2
<b>1. Formulating the problem. Frequency performances and resolution of the Bragg acousto-optical deflector operating in a one-phonon Bragg normal light scattering regime</b>	3
1.1. References	5
<b>2. Collinear acoustic wave heterodyning: theoretical consideration and experimental investigation using acousto-optical technique</b>	6
2.1. Introductory remarks	6
2.2. Co-directional collinear propagation and interaction of the longitudinal acoustic waves of finite amplitudes	6
2.3. Experimental verifications and modeling using acousto-optical technique	10
2.4. Potential acousto-optical efficiency	11
2.5. Conclusion	13
2.6. References	13
<b>3. Practical estimations and proof-of-principle experimental studies of the potentials peculiar to optical spectrum analysis with a novel lead molybdate crystalline acousto-optical cell</b>	14
3.1. General remarks	14
3.2. Potential performances of a novel lead molybdate crystalline acousto-optical cell with $\gamma < 1$	15
3.3. Potential performances of a novel lead molybdate crystalline acousto-optical cell with $\gamma > 1$	19
3.4. Brief comparative discussion	23
3.5. Characterizing the optical part of experimental set-up and various practical estimations	24
3.6. Conclusion	28
3.7. References	28
<b>4. Potentials of the acousto-optical spectrum analysis on a basis of a novel algorithm of the collinear wave heterodyning in a large-aperture KRS-5 crystalline cell</b>	29
4.1. Preliminary remarks	29
4.2. Efficiency of acousto-optical interaction in a KRS-5 cubic crystal	30
4.3. Efficiency of the co-directional collinear acoustic wave heterodyning	33
4.4. Estimating the frequency potentials peculiar to a multi-channel direct optical spectrum analysis with a KRS-5 cell	37
4.5. Estimating the efficiency of collinear wave heterodyning	42
4.6. Proof-of-principal experimental modeling	44
4.7. Brief comparative discussion	47
4.8. Conclusion	48
4.9. References	48
<b>5. Acknowledgment</b>	49

## INTRODUCTION

This technical report is devoted to the problem of improving the frequency resolution inherent in a parallel acousto-optical spectrum analysis via involving an additional nonlinear phenomenon into the data processing. In so doing, we examine possible application of the wave heterodyning to the real-time scale acousto-optical analysis of the frequency spectrum belonging to ultra-high-frequency radio-wave signals peculiar, for example, for radio-astronomy. The nonlinear process of wave heterodyning is realized through providing a co-directional collinear interaction of the longitudinal acoustic waves of finite amplitudes. This process, which is beforehand studied theoretically and investigated experimentally via the acousto-optical technique as well, allows us either to improve the frequency resolution of spectrum analysis at a given frequency range or to increase by a few times the current frequencies of radio-wave signals under processing. The first step along this way is connected with experimental modeling of the acoustic wave heterodyning in solids via exploitation of specific acousto-optical cell based on a liquid, which allows the simplest realization of a cell with the needed properties. Then, these theoretical and practical findings are used in our experimental studies aimed at creating a new type of acousto-optical cells, which are able to improve the resolution inherent in acousto-optical spectrum analyzer operating over ultra-high-frequency radio-wave signals. In particular, the possibility of upgrading the frequency resolution through the acoustic wave heterodyning is experimentally demonstrated using the cell made of lead molybdate crystal. The obtained results demonstrate practical efficiency of the novel approach presented. Thereafter, potentials peculiar to the acousto-optical spectrum analysis of a gigahertz-frequency range radio-wave signals with essentially improved relative value of the frequency resolution, which can be in the order of  $10^{-5}$  in our case, is considered with exploiting a new type of the acousto-optical cell made of really effective **KRS-5** cubic single crystal. The obtained estimations show that the elaborated approach, based algorithmically on a two-cascade processing, allows the direct **5000**-channel parallel optical analysis of spectra inherent in ultra-high-frequency radio-wave signals. In frames of the performed investigations, the efficiencies of both non-collinear acousto-optical and collinear acoustic interactions are analytically estimated. Moreover, analytic expression for the corresponding effective acoustic modulus of the third order in **KRS-5** has been found for the first time in our knowledge. In so doing, contrary to our previously developed theoretical approach based on the technique of substantial approximations, a regime of the coupled acoustic modes is considered, which provides more accurate analysis. These findings make it possible first to estimate the technical requirements to performance data of the acousto-optical cell as well as to acceptable values of the operating frequencies. At the end, above-proposed methodology for the experimental simulation is practically applied and exploited within a specific example of the liquid-made cell to estimate performances of the parallel spectrum analysis with the new **KRS-5**-crystal based acousto-optical cell.

# 1. FORMULATING THE PROBLEM. FREQUENCY PERFORMANCES AND RESOLUTION OF THE BRAGG ACOUSTO-OPTICAL DEFLECTOR OPERATING IN A ONE-PHONON BRAGG NORMAL LIGHT SCATTERING REGIME

Let us start from preliminary estimations of the frequency bandwidth  $\Delta f$ , the frequency resolution  $\delta f$ , and the number  $N$  of resolvable spots inherent in the Bragg acousto-optical deflector operating in a one-phonon normal light scattering regime. A one-phonon non-collinear light scattering in isotropic medium, see Fig.1.1a, is associated with the Bragg condition [1.1, 1.2]

$$\sin \theta = -\mathbf{K}/(2\mathbf{k}_0) = -\lambda f/(2nV) \quad (1.1)$$

for normal process without changing the state of light polarization. Here,  $\theta$  is the Bragg angle of light scattering,  $\mathbf{k}_0$  and  $\lambda$  are the wave number and the wavelength of light,  $n$  is the corresponding refractive index,  $\mathbf{K}$ ,  $f$ , and  $V$  are the wave number, carrier frequency, and phase velocity of the acoustic wave. The corresponding wave vector diagram is depicted in Fig.1.1b. The frequency bandwidth of acousto-optical interaction  $\Delta f$  can be estimated through differentiating this Bragg condition in Eq.(1.1) as  $\Delta f = \Delta \theta (2nV/\lambda) \cos \theta$ , where  $\Delta \theta$  is the variation of the angle of light incidence associated with the variation of the acoustic frequency  $\Delta f$  needed to provide the Bragg condition. In the case of light modulation, we have usually the geometry of interaction with rather wide optical beam, whose angle of spreading  $\delta \theta$  is small, and rather narrow aperture of the acoustic beam, whose angle of spreading is  $\delta \phi \approx (V/fL) \gg \delta \theta$ , where  $L$  is the length of acousto-optical interaction, see Fig.1.1a. Assuming that  $\delta \phi \approx \Delta \theta$  and  $\cos \theta \approx 1$ , we yield the following approximation

$$\Delta f \approx \frac{2nV^2}{\lambda Lf} \quad (1.2)$$

for the bandwidth of a normal Bragg acousto-optical interaction in isotropic medium. This approximate equality follows geometrically from the plot in Fig.1.1b, because  $\Delta K = 2\pi(\Delta f)/V$  and  $2\mathbf{k}_0 \delta \phi \cos \theta \approx 4\pi nV/(\lambda Lf)$ .

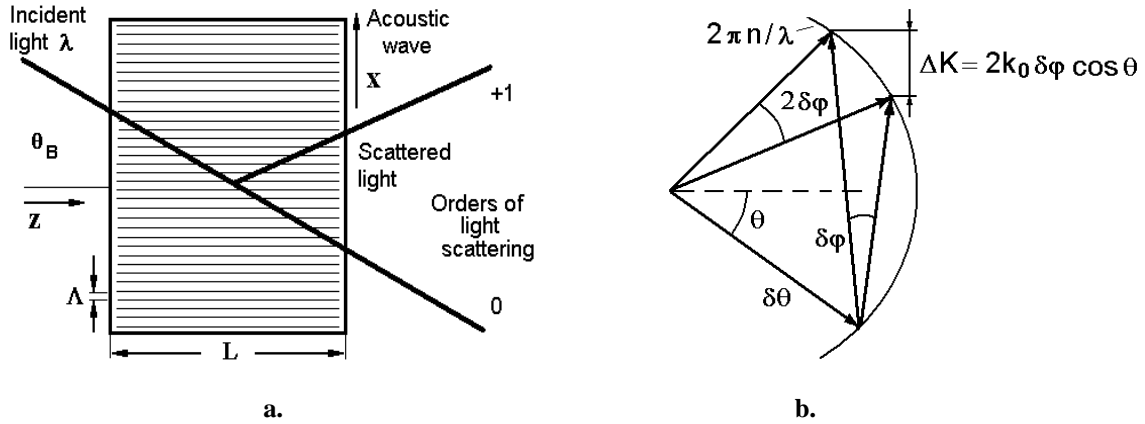


Figure 1.1. A one-phonon normal light scattering regime: principal schematic arrangement for the Bragg light scattering (a) and vector diagram determining the frequency bandwidth (b).

Generally, the momentum  $\mathbf{p}$  of a photon is connected with the wave number  $\mathbf{k}$  as  $\mathbf{p} = \hbar\mathbf{k}/(2\pi)$ , where  $\hbar$  is the Planck constant, so an uncertainty  $\delta \mathbf{p} = \hbar(\delta \mathbf{k})/(2\pi)$  in the momentum related to the uncertainty in the wave number  $\delta \mathbf{k}$  of a photon. The same view is true, if one will consider the phonons. Namely, the momentum  $\mathbf{P}$  of a phonon is

connected with the wave number  $\mathbf{K}$  as  $\mathbf{P} = \mathbf{h}\mathbf{K}/(2\pi)$ , and an uncertainty  $\delta\mathbf{P} = \mathbf{h}(\delta\mathbf{K})/(2\pi)$  in the momentum related to the uncertainty in the wave number  $\delta\mathbf{K}$  of a phonon. Then, because the phonon wave number is  $\mathbf{K} = 2\pi\mathbf{f}/\mathbf{V}$ , one can note that an uncertainty of the phonon wave number, in its turn, can be explained in terms of an uncertainty in the phonon frequency  $\delta\mathbf{f}$  as  $\delta\mathbf{K} = 2\pi(\delta\mathbf{f})/\mathbf{V}$ . The limiting case of just Bragg light scattering in acousto-optics is determined by the well-known [1.1 – 1.3] dimensionless inequality for the Klein-Cook parameter

$$Q = \lambda f^2 L / V^2 \gg 1 . \quad (1.3)$$

In this limit an uncertainty in the momentum of the issuing photon is characterized by the relation  $\delta\mathbf{p} \approx \delta\mathbf{P}$ , and, consequently,  $\delta\mathbf{k} \approx \delta\mathbf{K}$ , because they both are localized inside the same spatial area determined by the aperture  $\mathbf{D}$ . Together with this, the value of  $\delta\mathbf{k}$  is significantly smaller than the photon wave number variation connected with scattering from the order  $\mathbf{j}$  to the order  $\mathbf{j}+1$ , i.e.  $|\bar{\mathbf{k}}_{\mathbf{j}+1} - \bar{\mathbf{k}}_{\mathbf{j}}| \approx \mathbf{K} \gg \delta\mathbf{K} \approx \delta\mathbf{k}$ . By this is meant that the wave numbers of both the photons and the phonons are well determined in the Bragg limit of acousto-optical interaction. Due to the Heisenberg uncertainty principle [1.4] proclaims that  $\delta\mathbf{p} \delta\mathbf{x} \sim \mathbf{h}$  with  $\delta\mathbf{x} \approx \mathbf{D}$ , one can found that

$$\delta\mathbf{f} \approx \mathbf{V}/\mathbf{D} = \mathbf{T}^{-1}, \quad (1.4)$$

where  $\mathbf{T}$  is the time of passing the acoustic wave through the aperture  $\mathbf{D}$ . Just this value determines the frequency resolution of acousto-optical modulator operating in a one-phonon Bragg normal light scattering regime. The number  $\mathbf{N}$  of resolvable spots in the regime under consideration is given by the ratio

$$\mathbf{N} = \Delta\mathbf{f} / \delta\mathbf{f} = \mathbf{T} \Delta\mathbf{f} . \quad (1.5)$$

In high-frequency devices, the value of  $\mathbf{N}$  is restricted by both the geometrical factors and the acoustic attenuation in a medium. The first geometrical factor is the maximal aperture  $\mathbf{D}$  of a deflector. In connection with this, one can estimate the maximal bandwidth as  $\Delta\mathbf{f} \approx \mathbf{f}_0/2$ , where  $\mathbf{f}_0$  is the central carrier frequency of the acoustic wave, and obtain the first limitation

$$\mathbf{N}_1 \leq \frac{\mathbf{D}\mathbf{f}_0}{2\mathbf{V}} . \quad (1.6)$$

The second factor is determined by the acoustic beam spreading. One can assume that the aperture  $\mathbf{D}$  of that deflector belongs to the near zone of radiation from the piezo-electric transducer, whose size can be taken to be equal to  $\mathbf{L}$ , so that  $\mathbf{D} \approx \mathbf{L}^2 \mathbf{f}_0 / (2\mathbf{V})$ . This relation leads to  $\mathbf{L} = \mathbf{n} \mathbf{V}^2 \mathbf{Q} / (2\pi\lambda \mathbf{f}_0^2)$  and to the second limitation

$$\mathbf{N}_2 \leq \left( \frac{\mathbf{n} \mathbf{V} \mathbf{Q}}{4\pi\lambda \mathbf{f}_0} \right)^2 . \quad (1.7)$$

The third principal limitation is conditioned by acoustic attenuation. It can be also represented as a function of  $\mathbf{f}_0$ . Let us use the factor  $\Gamma_0$  of acoustic attenuation expressed in [dB/(cm GHz<sup>2</sup>)], so that  $\chi$ -dB level of attenuation will require the aperture  $\mathbf{D} \leq \chi \Gamma_0^{-1} \mathbf{f}_0^{-2}$ . Substituting this formula into Eq.(1.6), one can find

$$\mathbf{N}_3 \leq \frac{\chi}{2\Gamma_0 \mathbf{V} \mathbf{f}_0} . \quad (1.8)$$

Thus, the number of resolvable spots is restricted by a triplet of the above-mentioned independent limitations. To make illustrating numerical estimations one can take, for example, an acousto-optical deflector made of such widely

exploited crystalline material as a lead molybdate ( $\text{PbMoO}_4$ ). In this particular case of a one-phonon Bragg normal light scattering, one can take the following values inherent in this crystal:  $V = 3.63 \cdot 10^5$  cm/s,  $\lambda = 633$  nm,  $n = 2.26$ , and  $\Gamma_0 = 15$  dB/(cm GHz<sup>2</sup>) [1.1, 1.5]. The numerical estimations have been realized for the apertures  $D = 1-4$  cm; the attenuation factors along the total aperture  $\chi = 4$  and  $6$  (dB/aperture), and the Klein-Cook parameter  $Q = 2\pi, 3\pi, 4\pi$  providing just the Bragg regime of light scattering, see Fig.1.2. It is seen that a lead molybdate deflector with  $D \approx 2$  cm,  $Q = 2\pi$ , and  $\chi < 4$  (dB/aperture) is capable to provide  $N \approx 700$  resolvable spots with potential frequency resolution  $\delta f$  of approximately 180 KHz in the frequency bandwidth close to 120 MHz at a central frequency  $f_0$  of about 250 MHz. Together with this, using Fig.1.2 one can conclude that conventional lead molybdate deflector even with an aperture of 1 cm is not operable at the carrier frequencies exceeding 600 MHz. Thus, now one can formulate the problem facing this technical report. Taking alone a given lead molybdate optical deflector with the given aperture  $D = 2$  cm, is it possible to keep the same number of resolvable spots with the same potential frequency resolution in the same frequency bandwidth at significantly increased central carrier frequency  $f_0$  exceeding the above-mentioned 600 MHz? The main goal of our considerations is to give definitely positive answer to this question under condition of exploiting the collinear acoustic wave heterodyning in the taken optical deflector.

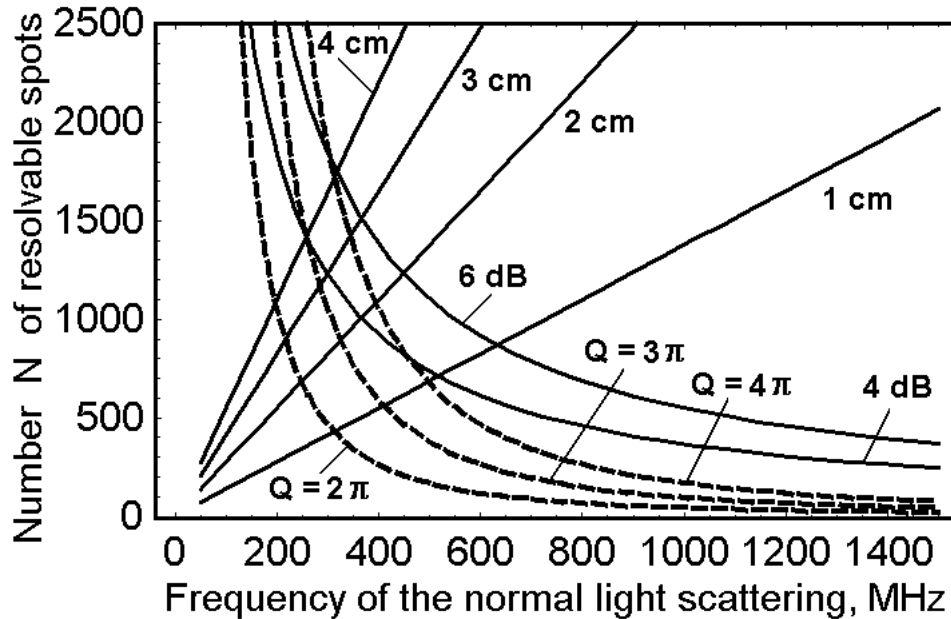


Figure 1.2. The combined diagram illustrating effect of a triplet of the restricting factors. The solid straight lines are related to  $N_1$ , the chosen apertures  $D$  are equal to 1, 2, 3, and 4 cm. The dashed lines regards to  $N_2$  in the particular cases of  $Q = 2\pi, 3\pi,$  and  $4\pi$ . The solid hyperbolic-like falling curves illustrate  $N_3$  and reflect contributions of the acoustic attenuation with total losses of 4 and 6 dB along the optical aperture.

### 1.1. REFERENCES

- 1.1. V.I.Balakshy, V.N.Parygin, L.E.Chirkov. *Physical Principles of Acousto-Optics*. (Radio i Szyaz, Moscow, 1985).
- 1.2. P.D.Das and C.M.DeCusatis. *Acousto-Optic Signal Processing: Fundamentals & Applications*. (Artech House, Boston, 1991).
- 1.3. R.W.Klein and B.D.Cook. A unified approach to ultrasonic light diffraction. *IEEE Transactions*, v. **SU-14**, no. 3, 123-134 (1967).
- 1.4. P.A.M.Dirac. *The Principles of Quantum Mechanics*. 4-th Ed. (Oxford University Press, Oxford, 1999).
- 1.5. V.G.Dmitriev, G. G. Gurzadyan and D. N. Nikogosyan, *Handbook of Nonlinear Optical Crystals* 3rd Ed. (Springer, Berlin, 1999).

## 2. COLLINEAR ACOUSTIC WAVE HETERODYNYING: THEORETICAL CONSIDERATION AND EXPERIMENTAL INVESTIGATION USING ACOUSTO-OPTICAL TECHNIQUE

### 2.1. INTRODUCTIVE REMARKS

A major portion of modern developments in a high-speed and extremely precise optical data processing is currently connected with applying various nonlinear effects, such as soliton phenomena and parametric processes, all-optical multi-stability, etc. [2.1, 2.2]. In this chapter, the practical potentials related to exploiting the nonlinear process of wave heterodyning in a medium with dispersive losses are considered. In the case of wave heterodyning, beneficial analogue information incorporated into the spectrum of a signal becomes to be converted from a high-frequency signal wave to a difference-frequency wave, so that just spectral components peculiar to the resulting difference-frequency wave are exploited during subsequent optical data processing. Usually, the precision of both spectral and frequency measurements for signals is determined by the uncertainty in the energy or momentum inherent in a photon localized in the interaction area [2.3]. Due to the dispersion of losses, heterodyning leads to increasing the characteristic length and/or time of propagation for the converted signal in that medium and to improving significantly the accuracy of optical data processing, because both spectral and frequency resolutions are in inverse proportion to the length or time of acousto-optical interaction. Here, we are reporting our investigations of the co-directional collinear longitudinal acoustic wave heterodyning through acousto-optic technique and its possible application to a real-time acousto-optical analysis of the frequency spectrum belonging to ultra-high-frequency (UHF) radio-wave analogue signals. The character of our studies is directly connected with actual absence of sufficiently effective acousto-optical materials suitable for processing ultra-high-frequency radio-wave analogue signals. Exploiting the introduced approximation, the theory of wave heterodyning in a medium with the dispersive losses has been progressed. Then, the developed theory was applied to our experiments directed to increasing the accuracy of acousto-optical spectrum analyzers working in the UHF-range. The obtained results confirm principally the advantages of our approach.

### 2.2. CO-DIRECTIONAL COLLINEAR PROPAGATION AND INTERACTION OF THE LONGITUDINAL ACOUSTIC WAVES OF FINITE AMPLITUDES

It is well known that co-directional collinear propagation of longitudinal acoustic waves of finite amplitudes in isotropic media and along the acoustic axes in crystalline materials, which do not have the group-velocity dispersion, but have the dispersive losses, is governed by the Burgers equation for the normalized distortion  $\xi = \mathbf{D}/\mathbf{D}_0$  [2.4]

$$\frac{\partial \xi}{\partial y} = \mathbf{B} \xi \frac{\partial \xi}{\partial \theta} + \frac{\partial^2 \xi}{\partial \theta^2} . \quad (2.1)$$

Here,  $\mathbf{D}$  is the amplitude of distortion,  $\mathbf{D}_0$  is the amplitude of acoustic pump distortion,  $\theta = \omega_{\mathbf{p}} (\mathbf{t} - \mathbf{x}/\mathbf{V})$ ,  $\mathbf{y} = \alpha_{\mathbf{p}} \mathbf{x}$ ,  $\omega_{\mathbf{p}} = 2\pi f_{\mathbf{p}}$ ,  $\mathbf{V}$ , and  $\alpha_{\mathbf{p}}$  are the cyclic frequency, velocity, and logarithmic attenuation of the pump acoustic wave. Then, the parameter  $\mathbf{B} = -\omega_{\mathbf{p}} \Gamma \mathbf{D}_0 / (2\alpha_{\mathbf{p}} \mathbf{V})$  describes a ratio of the acoustic nonlinearity to the acoustic dissipation;  $\Gamma$  is the constant of acoustic nonlinearity. Figure 2.1 illustrates arranging the interacting beams of the acoustic waves in a cell.

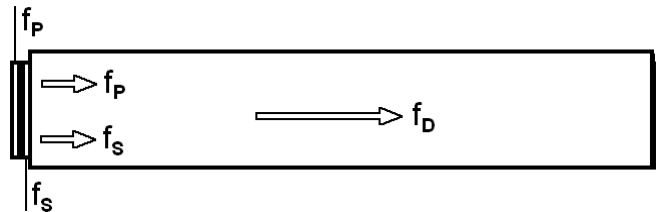


Figure 2.1. Arranging the interacting acoustic beams consisting of the longitudinal acoustic waves of finite amplitudes in a cell.

Broadly speaking, Eq.(2.1) can be analytically solved in its general form with arbitrary boundary conditions due to well-known Hopf-Cole substitution converting the nonlinear Burgers equation into linear heat conduction equation [2.4]. However, very cumbersome form of such a solution does not give a chance to perform the subsequent harmonic analysis. The spectral approach, when the project of solution has a given form, does not lead to a success as well, because in this case one has to solve an infinite set of the combined nonlinear equations. That is why the most worthwhile way is connected with finding an approximate solution by the method of successive approximations. The needed approximate solutions can be obtain rather fast when the parameter  $\mathbf{B}$  is not too large. In so doing, let us take the boundary condition to Eq.(2.1) in the form of a superposition of two longitudinal waves. One of them with unit amplitude and the above-noted cyclic frequency  $\omega_P = 2\pi f_P$  can be considered as a pump, while the other wave represents a signal with an amplitude of  $\delta$  and a cyclic frequency of  $\omega_S = 2\pi f_S$ , so that

$$\xi(y=0, \theta) = \sin(\theta + \psi) + \delta \sin(\gamma \theta), \quad (2.2)$$

where  $\gamma = \omega_S / \omega_P$ ,  $\psi$  is the phase shift between the signal and pump,  $\delta = \sqrt{P_S / P_P}$ ,  $P_P, S$  are the acoustic power densities for the pump and signal, respectively. Here, we restrict ourselves by the regime of non-degenerate acoustic interaction. Substituting Eq.(2.2) into Eq.(2.1), one can find the zero approximation solution describing the propagation of two attenuating non-interacting waves as

$$\xi^{(0)} = \exp(-y) \sin(\theta + \psi) + \delta \exp(-\gamma^2 y) \sin(\gamma \theta). \quad (2.3)$$

Now, using  $\xi^{(0)}$  in the nonlinear term of Eq.(2.1), one can estimate the first approximation solution as

$$\begin{aligned} \xi^{(1)} = & \xi^{(0)} + a_{P+P}^{(1)} \sin[2(\theta + \psi)] + a_{S+S}^{(1)} \sin(2\gamma\theta) + \\ & + a_{S+P}^{(1)} \sin[(\gamma+1)\theta + \psi] + a_{S-P}^{(1)} \sin[(\gamma-1)\theta + \psi]. \end{aligned} \quad (2.4)$$

Here,  $a_{P+P}^{(1)} = -\frac{\mathbf{B}}{4} [\exp(-2y) - \exp(-4y)]$  is the second harmonic amplitude of an acoustic pump wave, and

$a_{S+S}^{(1)} = -\frac{\mathbf{B} \delta^2}{4\gamma} [\exp(-2\gamma^2 y) - \exp(-4\gamma^2 y)]$  is the amplitude of the second harmonic of an acoustic signal wave.

Then, a pair of the following expressions:  $a_{S+P}^{(1)} = -\frac{\mathbf{B} \delta(\gamma+1)}{4\gamma} [\exp(2\gamma y) - 1] \exp[-y(1+\gamma)^2]$  and

$a_{S-P}^{(1)} = \frac{\mathbf{B} \delta(\gamma-1)}{4\gamma} [1 - \exp(-2\gamma y)] \exp[-y(1-\gamma)^2]$  gives the amplitudes of acoustic waves with the combined

and difference frequencies. Exploiting quite similar technique and neglecting the terms of the order of  $\delta^3$ , one can calculate approximate solutions of the second order. In the particular case of the second approximation for acoustic wave amplitude with the difference frequency, one can write

$$\begin{aligned} a_{S-P}^{(2)} = & \frac{\mathbf{B} \delta(\gamma-1)}{4\gamma} \exp[-y(\gamma-1)^2] \left\{ [1 - \exp(-2\gamma y)] + \frac{\mathbf{B}^2(\gamma+1)}{16} \left[ \frac{1 - \exp[-2y(\gamma+1)]}{\gamma+1} + \right. \right. \\ & \left. \left. + \frac{1 - \exp[-4y(\gamma+1)]}{2(\gamma+1)} - \frac{1 - \exp[-2y(\gamma+2)]}{\gamma+2} - \frac{1 - \exp[-2y(2\gamma+1)]}{2\gamma+1} \right] \right\}. \end{aligned} \quad (2.5)$$

In the case, when the nonlinearity does not exceed the dissipation, i.e. if  $\mathbf{B}^2 \leq 1$  and  $\delta^3 \ll 1$ , an additional acoustic wave with the difference frequency can be characterized by the first order solution as well. After squaring and normalizing, one obtains

$$\left( \mathbf{a}_{\mathbf{S}-\mathbf{P}}^{(1)} \right)^2 \mathbf{B}^{-2} \delta^{-2} = \left[ \frac{1}{4\gamma} (\gamma-1) \right]^2 E_i^2 \left( \gamma, \alpha_{\mathbf{S}} x \right), \quad (2.6)$$

$$E_i \left( \gamma, \alpha_{\mathbf{S}} x \right) = \left[ 1 - \exp \left( -\frac{2\alpha_{\mathbf{S}} x}{\gamma} \right) \right] \exp \left[ -\alpha_{\mathbf{S}} x \left( \frac{\gamma-1}{\gamma} \right)^2 \right]. \quad (2.7)$$

Here, the relations  $\mathbf{y} = \alpha_{\mathbf{P}} \mathbf{x} = \alpha_{\mathbf{S}} \gamma^{-2} \mathbf{x}$  were used;  $\alpha_{\mathbf{S}}$  is logarithmic decrement characterizing amplitude acoustic attenuation of the signal acoustic wave. The spatial dependences reflecting Eqs.(2.7) are presented in Fig.2.2. For the comparison, these plots include the exponential dependence  $\exp(-2\alpha_{\mathbf{S}} x)$ , which describes decreasing the acoustic signal power in zero approximation with  $\mathbf{B} = 1$ . One can see that the distributions of acoustic power on these plots are as more uniform as values of the parameter  $\gamma$  are closer to unity. However, therewith the intensity of an additional acoustic wave is decreasing directly proportional to  $(\gamma - 1)^2$ .

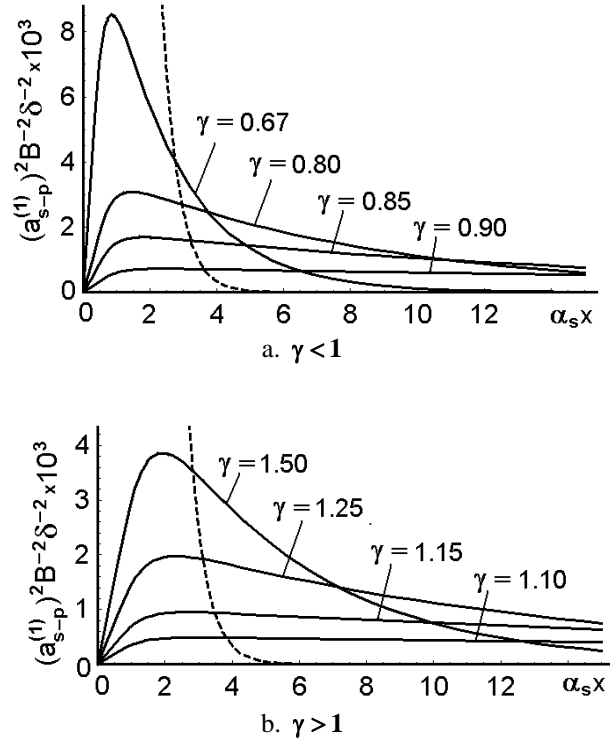


Figure 2.2. The spatial normalized plots of an additional acoustic wave power with the different frequency in the case of  $\mathbf{B} \leq 1$  and  $\delta^3 \ll 1$  for various values of the parameter  $\gamma$ .

It follows from Eq.(2.5) that the correction to the first order solution  $\mathbf{a}_{\mathbf{S}-\mathbf{P}}^{(1)}$  increases the amplitude of additional acoustic wave. By this it mean that when  $\mathbf{B}^2$ , which is directly proportional to the inputting power of acoustic pump, grows by ten times, the acoustic power of an additional wave becomes to be increased by more then ten times, see

Fig.2.3. Including the obtained corrections of the second order in the solution of the first order changes nothing in the character of these dependences and leads to only slight numerical additions in comparison with the first approximation.

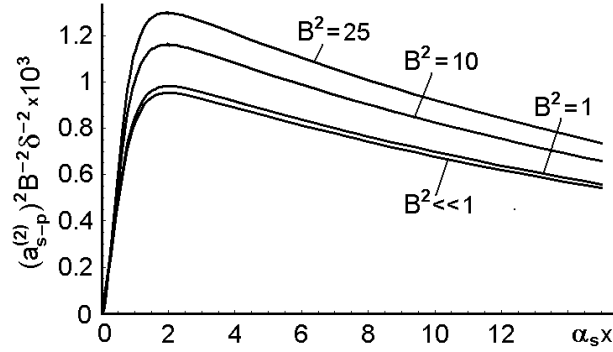


Figure 2.3. The spatial normalized plots of an additional acoustic wave power with the different frequency in the case of  $\gamma = 1.15$  and  $\delta^3 \ll 1$  for various values of the parameter  $B$

The power density  $P_D$  inherent in an additional acoustic wave of the difference frequency in the first approximation can be explained in dimensional values as

$$P_D(\gamma, \alpha_s x) = P_P P_S \left( \frac{f_D}{f_P f_S} \right)^2 m E_D^2(\gamma, \alpha_s x), \quad (2.8)$$

where  $f_D = |f_P - f_S|$ . Then, the value  $m = \frac{\pi^2 \Gamma^2}{8\rho V^5 \Gamma_0^2}$  determines the efficiency of generating an additional difference-frequency acoustic wave in a medium and takes into account the factor  $\Gamma_0$  characterizing the attenuation of acoustic waves. Usually, the acoustic attenuation is mentioned in bibliography in units of [ dB/(cm GHz<sup>2</sup>) ], but Eq.(2.8) needs it in the form recalculated for an acoustic power

$$\Gamma_0 \text{ (s}^2/\text{cm)} = 0.23 \Gamma_0 \text{ [ dB/(cm GHz}^2\text{)] } 10^{-18}. \quad (2.9)$$

Physical parameters for a few materials available for acoustic wave heterodyning are presented in Table 2.1.

Material	H <sub>2</sub> O	C <sub>2</sub> H <sub>5</sub> OH	PbMoO <sub>4</sub>	As <sub>2</sub> S <sub>3</sub>
Material density $\rho$ [g/cm <sup>3</sup> ]	1.00	0.787	6.95	3.20
Direction of propagation for the longitudinal acoustic waves	arbitrary	arbitrary	[001]	arbitrary
Velocity of propagation $V \cdot 10^{-5}$ [cm/s]	1.49	1.15	3.62	2.60
Modulus of the nonlinear parameter $ \Gamma $	8.0	12.3	17.5	21.5
Factor of the acoustic attenuation $\Gamma_0 \cdot 10^{18}$ [s <sup>2</sup> /cm]	552	1247	3.45	39.1
Acoustic quality factor $m \cdot 10^{-6}$ [s/g]	3.53	7.545	725	98.1
Acousto-optic figure of merit $M_2 \cdot 10^{18}$ [s <sup>3</sup> /g]	126	543	36.3	429

Table 2.1. Physical properties of some materials appropriate for the acousto-optic cell, see [2.5, 2.6].

Acousto-optical technique is one of the most sensitive methods to detect various acoustic signals. In connection with this, it would be worthwhile to discuss the efficiency  $I$  of light scattering by an additional acoustic wave in the linear regime of rather weak acoustic signals. In this particular case [2.5, 2.7],

$$I = \frac{\pi^2 M_2 P_D L^2}{2\lambda^2} . \quad (2.10)$$

where  $\lambda$  is the optical wavelength. Now, we can exploit Eq.(2.7) and (2.8) to rewrite Eq.(2.9) as

$$I = \frac{\pi^2 M_2 L^2}{2\lambda^2} P_P P_S \left( \frac{f_D}{f_P f_S} \right)^2 m E_D^2 (\gamma, \alpha_S x) , \quad (2.11)$$

which determines the combined efficiency of the acousto-optical cell in terms of light scattering.

### 2.3. EXPERIMENTAL VERIFICATIONS AND MODELLING USING ACOUSTO-OPTICAL TECHNIQUE

The obtained theoretical results related to collinear interaction of longitudinal acoustic waves were examined experimentally via exploitation of the acousto-optical technique. The main attention was paid to the process of generating an additional acoustic wave with the difference frequency. In so doing the experimental set-up, whose optical part is presented in Fig.2.4, were used. The collimated laser light beam with a wavelength of **633** nm was directed at the rotating mirror placed at the focus of the cylindrical lens 2. Rotation of this mirror provided the incidence of light beam at an arbitrary point of the acoustic duct. Light, scattered by an additional acoustic wave, was redirected to photo-detector placed at the focal plane of the cylindrical lens 1. At this step, one has to say that the analytical calculations allow the principal opportunity for experimental simulation of the desirable collinear interaction between high-frequency acoustic waves passing along the wave axes in anisotropic solid states through studying similar processes at low frequencies in isotropic media with acceptable characteristics, namely, parameters of acoustic nonlinearity, acoustic attenuation, acoustic and acousto-optical figures of merit. In particular, the performed investigations were oriented on experimental simulation of co-directional collinear interaction for acoustic waves of about 1 GHz, for example, in lead molybdate crystal (**PbMoO<sub>4</sub>**) through studying similar process in the acousto-optical cell exploiting ethanol (**C<sub>2</sub>H<sub>5</sub>OH**) at the frequencies of about **30 – 80** MHz, see Fig.2.5.

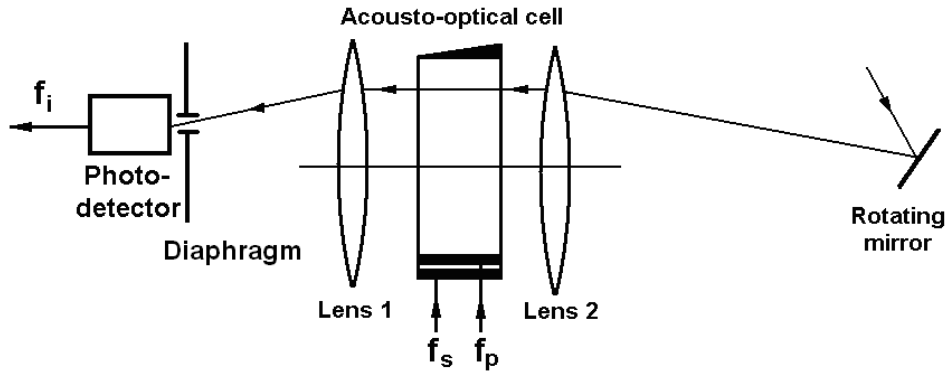


Figure 2.4. Optical scheme of the experimental set-up.

In fact, the experiments were carried out at the following pairs of the modeling frequencies in ethanol:

$f_S = 30$ MHz,	$f_P = 47.2$ MHz,	$f_D = 17.2$ MHz,	$\gamma = 0.64$ ;
$f_S = 57.3$ MHz,	$f_P = 82$ MHz,	$f_D = 24.7$ MHz,	$\gamma = 0.70$ ;
$f_S = 47$ MHz,	$f_P = 57$ MHz,	$f_D = 10$ MHz,	$\gamma = 0.82$ ;
$f_S = 28$ MHz,	$f_P = 31$ MHz,	$f_D = 3$ MHz,	$\gamma = 0.91$ .

(2.12)

Using Eq.(2.9), one can find that the experimental parameters of the modeling and real media are connected with each other as

$$\text{a) } f_S^2 = \frac{\Gamma_{0,M}}{\Gamma_0} f_{S,M}^2, \quad \text{b) } \gamma = \gamma_M, \quad \text{c) } \frac{P_P P_S}{\lambda^2 H^2} = \frac{\mu_M \Gamma_{0,M}}{\mu \Gamma_0} \left( \frac{P_P P_S}{\lambda^2 H^2} \right)_M, \quad (2.13)$$

where the index “M” is related to parameters of the modeling process. In the case of, for example, a lead molybdate crystal, these data are represented by:

$$\begin{aligned} f_S &= 0.53 \text{ GHz}, & f_P &= 0.84 \text{ GHz}, & f_D &= 0.31 \text{ GHz}, & \gamma &= 0.64; \\ f_S &= 1.02 \text{ GHz}, & f_P &= 1.46 \text{ GHz}, & f_D &= 0.44 \text{ GHz}, & \gamma &= 0.70; \\ f_S &= 0.83 \text{ GHz}, & f_P &= 1.01 \text{ GHz}, & f_D &= 0.18 \text{ GHz}, & \gamma &= 0.82; \\ f_S &= 0.49 \text{ GHz}, & f_P &= 0.54 \text{ GHz}, & f_D &= 0.05 \text{ GHz}, & \gamma &= 0.91. \end{aligned} \quad (2.14)$$

The normalized data reflecting the coordinate dependences of light scattering efficiency by an additional acoustic wave are presented in Fig.2.6. The points are experimental data, while the solid lines explain the corresponding calculations. The comparison of these data illustrates the possibility of applying the elaborated analytical method to describing co-directional collinear interaction of the longitudinal high-frequency acoustic waves, in particular, to the process of exiting an additional acoustic wave with the difference frequency and its visualizing via acousto-optic technique.

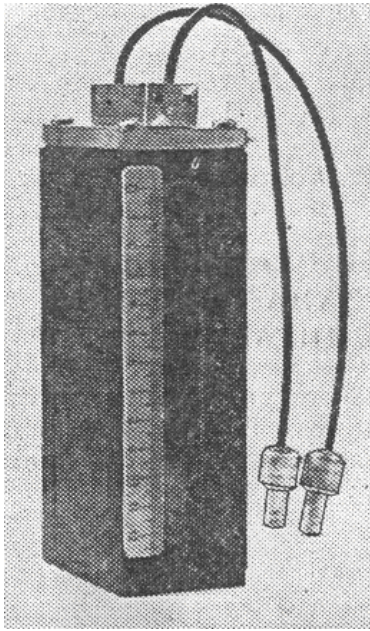


Figure 2.5. Acousto-optical cell with two piezo-electric transducers and with liquid medium represented by ethanol.

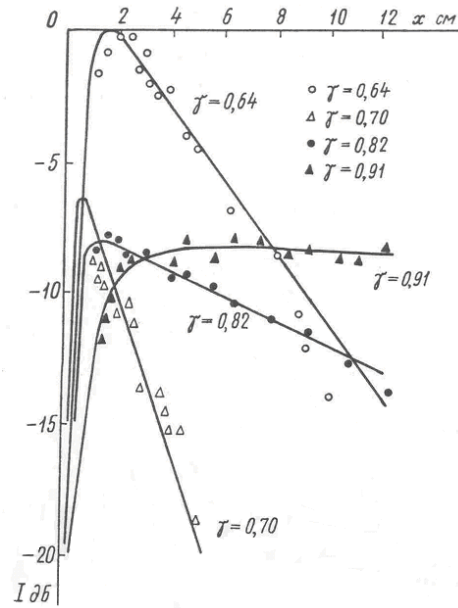


Figure 2.6. Normalized spatial dependences for the efficiency **I** of light scattering by the difference-frequency acoustic wave.

#### 2.4. POTENTIAL ACOUSTO-OPTICAL EFFICIENCY

Now, let us discuss the efficiency **I** of Bragg light scattering by the difference-frequency acoustic wave. In the case of weak acoustic signals, when nonlinearity inherent in acousto-optical interaction can be omitted [2.5], one can use the following expansion

$$\text{a) } \mathbf{I} = \sin^2(\mathbf{qL}) \approx \mathbf{q}^2 \mathbf{L}^2 - \frac{1}{3} \mathbf{q}^4 \mathbf{L}^4 + \dots, \quad \text{b) } \mathbf{q} \approx \pi \lambda^{-1} \sqrt{\mathbf{M}_2 \mathbf{P}_D / 2}. \quad (2.15)$$

Here,  $\lambda$  is the light wavelength in the air. The figure  $\mathbf{M}_2 = \mathbf{n}^6 \mathbf{p}_{\text{eff}}^2 / (\rho \mathbf{V}^3)$  of acousto-optical merit for the chosen crystal includes the refractive index  $\mathbf{n}$  and the effective photo-elastic constant  $\mathbf{p}_{\text{eff}}$ , which both depend on the crystal cut. Under condition  $\mathbf{q}^2 \mathbf{L}^2 \ll 3$ , i.e. within

$$\mathbf{P}_D \ll 6\lambda^2 / (\pi^2 \mathbf{M}_2 \mathbf{L}^2), \quad (2.16)$$

one may take only the first term in Eq.(2.15a). Exploiting Eqs.(2.8), one can rewrite Eq.(2.15a) as

$$\mathbf{I} = \frac{\pi^2 \mathbf{M}_2 \mathbf{L}^2}{2\lambda^2} \mathbf{P}_P \mathbf{P}_S \left( \frac{\mathbf{f}_D}{\mathbf{f}_P \mathbf{f}_S} \right)^2 \mathbf{m} \left[ 1 - \exp(-2\gamma \alpha_P \mathbf{x}) \right]^2 \exp \left[ -2\alpha_P \mathbf{x} (1 - \gamma)^2 \right], \quad (2.17)$$

which determines the combined efficiency of the acousto-optical cell under consideration in terms of light scattering. Now, the potential efficiency  $\mathbf{I}$  of Bragg light scattering by the difference-frequency acoustic wave has to be estimated in a lead molybdate ( $\text{PbMoO}_4$ ) single crystal; symmetry ( $4/m$ ). The crystal allows existing pure longitudinal elastic mode with velocity  $\mathbf{V} = 3.62 \cdot 10^5$  cm/s when this elastic wave is passing along the  $[001]$ -axis. Such an orientation has its original motivation in preliminary data related to linear and nonlinear manifestations of optical and acoustical properties inherent in this crystal. In particular, it exhibits rather high efficiency of collinear interaction for the longitudinal acoustic waves in the  $[001]$ -direction described by  $|\Gamma| = 17.5$  [2.6, 2.8]. Then, a maximal figure of acousto-optical merit  $\mathbf{M}_2 = 40.4 \cdot 10^{-18}$  s<sup>3</sup>/g is inherent in just normal light diffraction in the  $(110)$ -plane.

Now, the contribution of acousto-optical interaction should be estimated. The Bragg regime of light diffraction occurs when the angle of light incidence on the acoustic grating meets the corresponding Bragg condition and the inequality  $\mathbf{Q} = 2\pi\lambda \mathbf{L} \mathbf{f}_D^2 / (\mathbf{n} \mathbf{V}^2) \gg 1$  for the Klein-Cook parameter  $\mathbf{Q}$  [2.9] is satisfied. Taking  $\lambda = 532$  nm,  $\mathbf{n} \approx 2.26$  (in  $\text{PbMoO}_4$ ),  $\mathbf{L} = 1.0$  cm, and  $\mathbf{f}_D = 60$  MHz, one can estimate  $\mathbf{Q} \approx 4.04$ . Hence, the regime of light scattering, which is rather close to the Bragg regime at least in a small-signal linear region, could be expected for the acoustic different-frequencies of about 60 MHz. Using Eq.(2.16), the contribution of acousto-optical interaction can be sufficiently accurate estimated from the first term of Eq.(2.15a)

$$\mathbf{I}_{\text{max}} = \pi^2 \mathbf{M}_2 \mathbf{L}^2 \mathbf{P}_{D\text{max}} / (2\lambda^2). \quad (2.18)$$

With the maximally allowed level  $\mathbf{P}_{D\text{max}} \approx 4.5 \cdot 10^6$  g/s<sup>3</sup> = 0.45 W/cm<sup>2</sup> obtained from Eq.(2.16), one can find  $\mathbf{I}_{\text{max}} \approx 0.3$ . This estimation makes it possible to consider the above-chosen level of  $\mathbf{P}_D$  as more or less tolerable for an upper limit in lead molybdate under aforementioned condition given by Eq.(2.16). An undoubted merit of this characterization consists in practically convenient direct proportionality between the efficiency  $\mathbf{I}$  and the power density  $\mathbf{P}_D$ . At the second step, the contribution of acoustic wave mixing should be briefly analyzed. With this object in view, one can use Eq.(2.8) for estimating the acoustic pump power density  $\mathbf{P}_{P0}$  needed to reaching a pre-assigned peak level of the difference-frequency power density  $\mathbf{P}_{D\text{max}}$  within  $\delta^3 \ll 1$  at a given ratio  $\alpha = \mathbf{P}_S / \mathbf{P}_{P0}$ . From the start, it can be easily shown that a peak magnitude peculiar to the coordinate dependence in Eq.(2.8) is close to unity, i.e.  $\text{Max} \left\{ \left[ 1 - \exp(-2\gamma \alpha_P \mathbf{x}) \right]^2 \exp \left[ -2\alpha_P \mathbf{x} (1 - \gamma)^2 \right] \right\} \cong 1$ . Consequently, one can find

$$P_{P0} = \frac{f_S}{|1-\gamma|} \sqrt{\frac{P_{Dmax}}{\alpha m}}. \quad (2.19)$$

Let us consider an illustrative example for  $PbMoO_4$  when  $I_{max} = 3\%$  (which is quite natural for the spectrum analysis in a small-signal regime), so that Eq.(2.16) gives  $P_{Dmax} \approx 4 \cdot 10^5 \text{ g/s}^3 = 40 \text{ mW/cm}^2$ . Taking  $m = 7.25 \cdot 10^8 \text{ s/g}$ ,  $\alpha = 0.1$ ,  $\gamma = 1.15$ , and  $f_S = 1.0 \text{ GHz}$ , one can find  $P_{P0} \approx 50 \cdot 10^7 \text{ g/s}^3 = 50 \text{ W/cm}^2$  and  $P_S \approx 5.0 \text{ W/cm}^2$ . These data do not look unacceptable practically and can be improved with using more effective materials.

## 2.5. CONCLUSION

We have investigated both theoretically and experimentally the phenomenon of a co-directional collinear wave heterodyning, taken in the particular case of interaction the longitudinal acoustic waves of finite amplitudes. In so doing, the acousto-optical technique has been exploited. Possible applications of this phenomenon to the acousto-optical spectrum analysis of the UHF radio-wave signals have been tested as well. At the beginning, the experimental modeling of the acoustics wave mixing process in solids via application of acousto-optical cell based on liquid material, namely, liquid ethanol, which makes possible the simplest option for realizing the corresponding cells with the needed parameters, has been examined. The presented results demonstrate the possibility of applying co-directional collinear interaction of the longitudinal acoustic waves to resolving one of the problems related to acousto-optical spectrum analysis of just the UHF radio-wave signals. Devices of this sort provide an improved frequency resolution in that bandwidth of the working frequencies, where conventional acousto-optical cells made of given materials cannot operate. The functional scheme of the devices under proposal differs from the scheme for spectrum analysis with the electrical heterodyning that it does not require a mixer for microwave signals or a powerful intermediate-frequency amplifier. Both the acoustic wave heterodyning and the amplification of signal waves at the difference frequencies occur in a single solid-state circuit using the energy from the acoustic pump. Furthermore, the required relative frequency bandwidths of both the piezoelectric transducers on a facet of a cell are considerably small, so that the fabrication of these transducers could be simplified. The proposed scheme of acousto-optic spectrum analyzer may prove to be the most effective at frequencies above 1 GHz or more. Consequently, the results of these studies should also be thought of as an experimental modelling for gigahertz-range devices, where the choice of materials for effective acousto-optic cells is rather limited because of the increased (in fact, directly proportional to the carrier acoustic frequency squared) attenuation for acoustic waves.

## 2.6. REFERENCES

- 2.1. Yu.S.Kivshar and G.P.Agrawal. *Optical Solitons: from Fibers to Photonic Crystals*. (Academic Press, N.Y, 2003).
- 2.2. N.N.Akhmediev and A.Ankiewich. *Solitons: Nonlinear Pulses and Beams*. (Chapman & Hall, London, 1997).
- 2.3. P.A.M.Dirac. *The Principles of Quantum Mechanics*. 4-th Ed. (Oxford University Press, Oxford, 1999).
- 2.4. K.Dodd, J.C.Eilbeck, J.D.Gibbon, and H.Morris. *Solitons and Nonlinear Wave Equations*. (Academic Press, Orlando, 1984).
- 2.5. V.I.Balakshy, V.N.Parygin, L.E.Chirkov. *Physical Principles of Acousto-Optics*. (Radio i Szyaz, Moscow, 1985).
- 2.6. V.G.Dmitriev, G. G. Gurzadyan, D. N. Nikogosyan, *Handbook of Nonlinear Optical Crystals* 3rd Ed. (Springer, Berlin, 1999).
- 2.7. P.D.Das and C.M.DeCusatis. *Acousto-Optic Signal Processing: Fundamentals & Applications*. (Artech House, Boston, 1991).
- 2.8. A.A.Blistanov. *Crystals for Quantum and Nonlinear Optics*. (Moscow, MISIS, 2007).
- 2.9. R.W.Klein and B.D.Cook. A unified approach to ultrasonic light diffraction. *IEEE Transactions*, v. **SU-14**, no. 3, 123-134 (1967).

### 3. PRACTICAL ESTIMATIONS AND PROOF-OF-PRINCIPLE EXPERIMENTAL STUDIES OF THE POTENTIALS PECULIAR TO OPTICAL SPECTRUM ANALYSIS WITH A NOVEL LEAD MOLYBDATE CRYSTALLINE ACOUSTO-OPTICAL CELL

#### 3.1. GENERAL REMARKS

In a line with this, now we study potential possibilities related to using a collinear wave mixing in the specific case of a medium without any group-velocity dispersion while with strongly dispersive losses. Our approach allows realizing effective wave heterodyning, when the beneficial data in signal become to be converted from a relatively high-frequency carrier wave to a difference-frequency wave. The accuracy of spectral as well as frequency measurements is physically determined by the uncertainty in the energy or momentum inherent in a photon localized in the interaction area [3.1]. Due to a rather strong dispersion of losses, the heterodyning leads to increasing the characteristic length and time of propagation (they both are associated with a clear optical aperture) for the converted signal in that medium and to improving significantly the accuracy of signal processing. In this context, we present our results in the real-time optical analysis of frequency spectra, belonging to analogue ultra-high frequency radio-wave signals, with considerably improved frequency resolution. These results are based on a two-cascade processing, i.e. on exploiting a pair of different wave processes one after the other sequentially in the single crystalline cell. This cell includes two resonant piezoelectric transducers, converting the input electronic signals into gigahertz-frequency elastic waves, with the corresponding electronic ports on its upper facet, clear optical aperture  $D$ , and an effective acoustic absorber on its bottom facet, see Fig. 3.1.

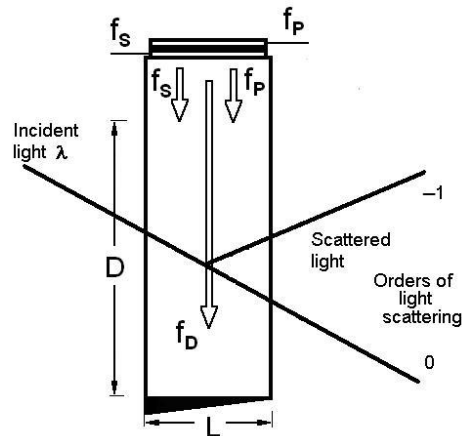


Figure 3.1. Schematic arrangement of the interacting beams in a two-cascade cell.

The first wave process represents mixing the longitudinal elastic waves of finite amplitudes in a compactly localized upper domain of a cell where relatively powerful pump of the frequency  $f_p$  interacts with relatively weaker signal elastic wave of the frequency  $f_s$ . During just this nonlinear process a collinear wave heterodyning takes place providing the appearance of an elastic wave of the difference-frequency  $f_D$ , which is able to propagate along a large-aperture cell due to weaker manifestation of strongly dispersive losses at lower frequencies. The second wave process is the subsequent Bragg light scattering by the difference-frequency elastic wave in as possible linear regime, i.e. in the regime of a given acoustic field for the incident light beam. This process occurs within a clear aperture  $D$  lighted by a wide incident optical beam of the wavelength  $\lambda$  and is able to realize optical spectrum analysis by itself. When, for example, the signal wave is rather intricate in behavior and consists of various frequencies, each individual spectral component from the difference-frequency elastic wave plays the role of a partial thick dynamic diffractive grating for the incident light beam. The length  $L$  of acousto-optical interaction has to provide performing the Bragg regime of light scattering.

In frames of the carried out studies, the technique of substantial approximations have been used to develop a theoretical description, which governs the difference-frequency elastic wave and adapts the corresponding expressions related to the light scattering. These findings make it possible first to estimate potential efficiencies for both the above-mentioned wave processes in optically transparent medium with square-law nonlinearity and dispersive acoustic losses. Then, analyzing the frequency properties and physical limitations gives us an opportunity to formulate requirements to performance data of the acousto-optical cell as well as to acceptable values of the operating frequencies. After that, the progressed theory is used in our experimental studies aimed at improving the accuracy of a multi-channel parallel optical data processing by an order of magnitude. In so doing, the acousto-optical spectrum analysis of a gigahertz-frequency range radio-wave signals with essentially improved frequency resolution is realized and investigated. During our proof-of-principle experiments a new type of the acousto-optical cell made of rather effective lead molybdate single crystal was exploited. These preliminary experimental data show that the elaborated approach, based algorithmically on a two-cascade processing, allows a direct multi-channel parallel optical analysis of spectra inherent in ultra-high-frequency radio-wave signals at relative accuracy of about  $10^{-4}$ .

### 3.2. POTENTIAL PERFORMANCES OF A NOVEL LEAD MOLYBDATE CRYSTALLINE ACOUSTO-OPTICAL CELL WITH $\gamma < 1$

In the first approximation, the normalized amplitude of the difference-frequency carrier acoustic wave passing along the optical aperture of a cell is given by Eq.(2.6), which can be rewritten as

$$a_{S-P}(x) = \left( \frac{\gamma-1}{4\gamma} \right) \left[ 1 - \exp(-2\gamma\alpha_P x) \right] \exp \left[ \alpha_P x (1-\gamma)^2 \right]. \quad (3.1)$$

Using Eq.(3.1), one can determine the point  $x_m$  associated with a maximum of the normalized amplitude distribution along the cell as

$$x_m = \left( \frac{-1}{2\alpha_P \gamma} \right) \ln \left[ \frac{(1-\gamma)^2}{1+\gamma^2} \right]. \quad (3.2)$$

The magnitude of this maximum can be estimated as

$$a_{S-P}(x=x_m) = \frac{\gamma-1}{2(1+\gamma^2)} \exp \left\{ \frac{(1-\gamma)^2}{2\gamma} \ln \left[ \frac{(1-\gamma)^2}{1+\gamma^2} \right] \right\}. \quad (3.3)$$

It is seen from Eq.(3.3) and Fig.2.2 that  $a_{S-P}^2(x=x_m)$  is the decreasing function of  $\gamma$ , see the solid line in Fig.3.2. However, such a dependence on  $\gamma$  leads to a non-uniformity of distributing signals associated with various difference-frequency components in a cell. To compensate this non-uniformity one can suggest to exploit the additionally needed pre-amplification  $G(\gamma)$ , which is shown by dashed line in Fig.3.2 and can be calculated as

$$G(\gamma) = \frac{a_{S-P}^2(x=x_m, \gamma = \gamma_0)}{a_{S-P}^2(x=x_m, \gamma)}, \quad (3.4)$$

where  $\gamma_0$  is an initially selected, minimal, and fixed value of the ratio  $\gamma$ .

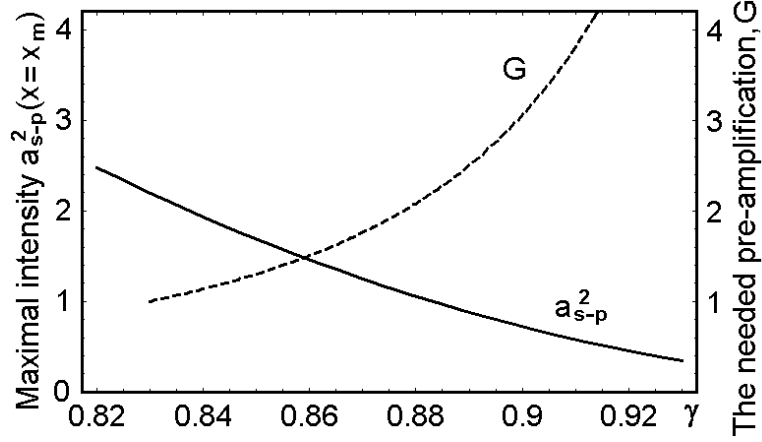


Figure 3.2. The plot of  $F(\gamma)$  for magnitudes of  $\gamma$  practically usable in the wave heterodyning.

Decreasing the normalized intensity  $a_{s-p}^2(\mathbf{x})$  of the difference-frequency acoustic wave down to a level of  $-3$  dB along the cell's optical aperture at a point  $\mathbf{x}_D$  gives the equality  $a_{s-p}(\mathbf{x} = \mathbf{x}_D) = (1/\sqrt{2}) a_{s-p}(\mathbf{x} = \mathbf{x}_m)$  in terms of the amplitudes, so that

$$\mathbf{x}_D = \frac{-1}{2\alpha_P(1-\gamma)^2} \left( \ln \left( \frac{\gamma\sqrt{2}}{1+\gamma^2} \right) + \left\{ \frac{(1-\gamma)^2}{2\gamma} \ln \left[ \frac{(1-\gamma)^2}{1+\gamma^2} \right] \right\} \right). \quad (3.5)$$

In fact, the value of  $\mathbf{x}_D$  determines the total length of acousto-optical cell with the collinear wave heterodyning. Now, an active part  $\mathbf{D}$  of the cell's optical aperture available for optical processing can be found as

$$\text{a) } \mathbf{D} = \mathbf{x}_D - \mathbf{x}_m = \frac{F(\gamma)}{\alpha_P}, \quad \text{b) } F(\gamma) = \frac{1}{(1-\gamma)^2} \ln \left( \frac{1+\gamma^2}{\gamma\sqrt{2}} \right). \quad (3.6)$$

The plot of  $F(\gamma)$  for values of  $\gamma$  neighboring unity and capable to be practically usable in the wave heterodyning is presented in Fig.3.3.

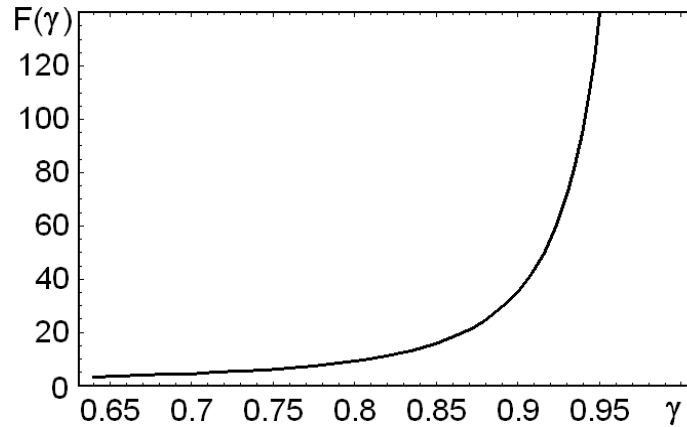


Figure 3.3. The plot of  $F(\gamma)$  for magnitudes of  $\gamma$  practically usable in the wave heterodyning.

Due to  $\alpha_P = 0.115 \Gamma_0 f_P^2$  ( $\text{cm}^{-1}$ ), the following expression for the pump frequency  $f_P$  and for the difference frequency  $f_D = f_P - f_S = f_P (1 - \gamma)$  appear

$$\text{a) } f_P = \sqrt{\frac{F(\gamma)}{0.115 \Gamma_0 D}} \quad \text{b) } f_D = (1 - \gamma) \sqrt{\frac{F(\gamma)}{0.115 \Gamma_0 D}} \quad (3.7)$$

In the particular case of a lead molybdate ( $\text{PbMoO}_4$ ) crystal ( $\Gamma_0 = 15 \text{ dB/cm GHz}^2$ ) with the active optical aperture  $D = 2 \text{ cm}$ , one can obtain from Eqs.(3.7) the following diagrams, see Fig.3.4.

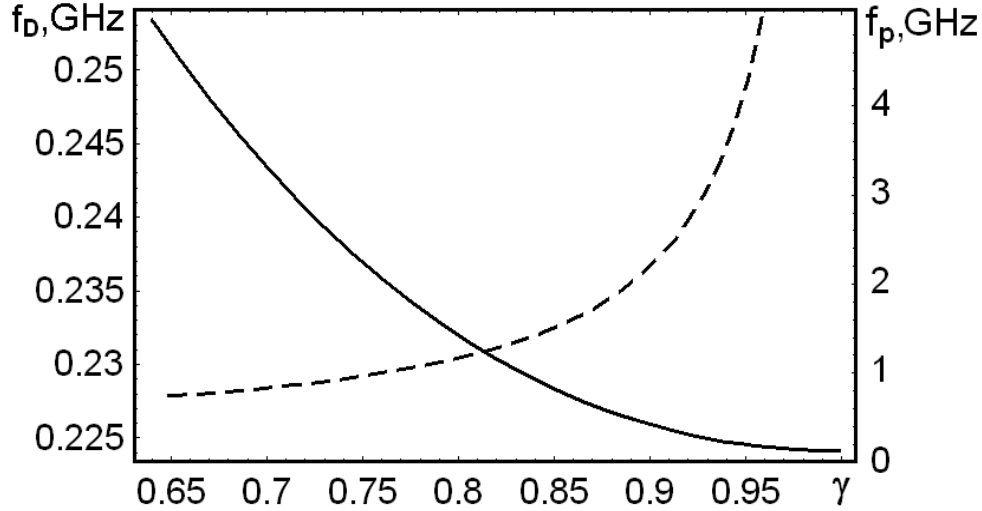


Figure 3.4. Plots for the pump frequency  $f_P$  (dashed line) and the difference frequency  $f_D$  (solid line) related to Eqs.(3.7) versus  $\gamma$  for magnitudes of  $\gamma$  practically usable in the wave heterodyning.

These dependencies allow the following estimation for practical realization. Let us take the upper difference-frequency as  $f_{UD} = 230 \text{ MHz}$  and the lower magnitude of  $\gamma$  as  $\gamma_L = 0.83$ , so that the pump frequency will be  $f_P = 1350 \text{ MHz}$  and the lower signal frequency will be  $f_{LS} = 1120 \text{ MHz}$ . Then, one can choose the bandwidth  $\Delta f$  of analysis, for example, in the range of  $110 \text{ MHz}$ , which leads to the lower difference-frequency  $f_{LD} = 120 \text{ MHz}$ , the upper signal frequency  $f_{US} = 1230 \text{ MHz}$ , and the upper magnitude  $\gamma_U = 0.91$ . These estimations are conditioned by the relations

$$\text{a) } f_{UD} = f_P - f_{LS} = f_P (1 - \gamma_L), \quad \text{b) } f_{LD} = f_P - f_{US} = f_P (1 - \gamma_U), \quad (3.8)$$

It is seen from Fig.1.2 that direct exploitation of similar lead molybdate cell with the active optical aperture  $D = 2 \text{ cm}$  at the signal frequencies of about  $1100 - 1200 \text{ MHz}$  is definitely impossible. Nevertheless, applying the collinear acoustic wave heterodyning allows to operate on these ultra-high carrier frequencies and to obtain the number of resolvable spots of about  $N = \Delta f / \delta f \approx 610$ . The above-mentioned non-uniformity in the distributions of signals, associated with various difference-frequency components in the lead molybdate cell, are illustrated in Fig.3.5.

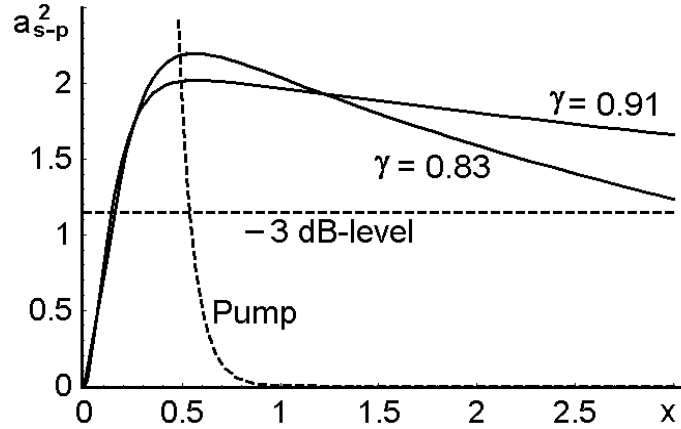


Figure 3.5. A non-uniformity in the distributions of various difference-frequency components in a  $\text{PbMoO}_4$ -cell.

Exploiting the modeling procedure discussed in sub-section 2.3 and the above-listed estimations, a novel solid-state acousto-optical cell had been designed and used in the standard scheme of a prototype for the acousto-optical spectrum analyzer of ultra-high-frequency radio-signals, see Fig.3.6. This scheme includes rather powerful laser ( $\lambda = 440$  nm, the issuing optical power exceeds 100 mW), a two-prism beam shaper, large-aperture achromatic doublet lens, and a 3000-pixel CCD linear array photo-camera. A lead molybdate ( $\text{PbMoO}_4$ ) single crystal of 25 mm in length, oriented along the [001]-axis for an acoustic beam along [100]-axis for an optical beam [2.5 – 2.7], was used in that cell. The cell completed with a pair of electronic input ports for the pump and signal on one of its facets as well as with acoustic absorber on the opposite facet.

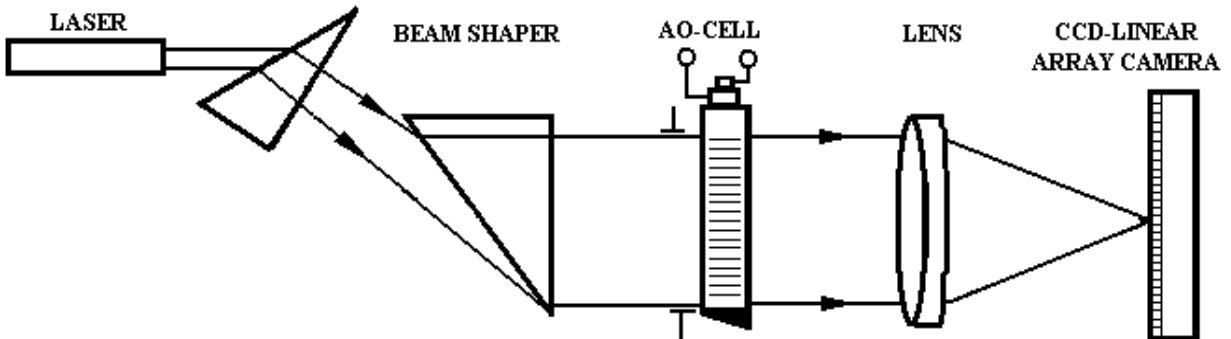


Figure 3.6. Schematic arrangement of a prototype for the acousto-optical spectrum analyzer.

This crystalline material was chosen because of its high value of the relative acousto-optic figure of merit that can be characterized by a value of  $M_2 \approx 36.3 \cdot 10^{-18} \text{ s}^3/\text{g}$  for both possible eigen-states of light polarization in this tetragonal crystal and its rather high acoustic interaction efficiency for collinear longitudinal waves in the [001]-direction described by  $|\Gamma| = 17.5$  [2.6]. As it was noted in section 1, the range of applicability for similar lead molybdate cell in conventional design is practically limited by frequencies of the order of 300–400 MHz. The piezo-electric transducer with an interaction length of 10 mm, generating the signal wave with power density of about 100 mW/mm<sup>2</sup>, was made of a thin ( $Y + 36^\circ$ )-cut lithium niobate, so that it excited purely longitudinal acoustic wave, with conversion losses of about 2 dB at its resonant frequency close to 1160 MHz. The single-frequency pumping longitudinal acoustic wave with the power density of up to 600 mW/mm<sup>2</sup> was generated at a carrier frequency of approximately 1350 MHz, so that the case of  $\gamma \in [0.80, 0.93]$  had been experimentally realized. During the experiments, we have placed a diaphragm in a few-millimeter vicinity of the piezo-electric transducers area (about 15% of the total aperture) to

minimize the effect of this area, where an increase in the power of difference frequency waves takes place. Consequently, the working optical aperture of a cell was slightly exceeding **2 cm**. The bandwidth of that prototype was about **120 MHz**. The efficiency of light scattering by an additional acoustic wave at the difference-frequency was slightly exceeding **1%**. Figure 3.7 shows the digitized oscilloscope traces of amplitude-frequency distribution peculiar to that prototype with the acousto-optical cell based on the collinear wave heterodyning. The digitized trace of this distribution had been recorded by a multi-pixel CCD linear array photo-camera through connecting the input signal port of a cell at an ultra-high-frequency radio-wave sweep-generator and fulfilling the acoustic wave heterodyning in a lead molybdate crystal. For a signal at the resulting carrier difference-frequency of about **230 MHz**, the attenuation is close to **3 dB** over the total cell aperture, while for a signal acoustic wave at the original frequency **1120 MHz** the attenuation exceeds **36 dB** along that aperture, which is perfectly unacceptable in practice. Within the second set of experimental tests, we examined the resolution of spectrum analyzer with the cell exploiting the acoustic wave heterodyning. The obtained data corresponds to a frequency resolution of about  $\delta f \approx 200$  KHz and  $N \approx 600$ , see Fig.3.8. This digitised trace had been recorded in the focal plane of lens, see Fig.3.6, via applying just a single-frequency excitation at the input signal port of a novel cell under consideration.

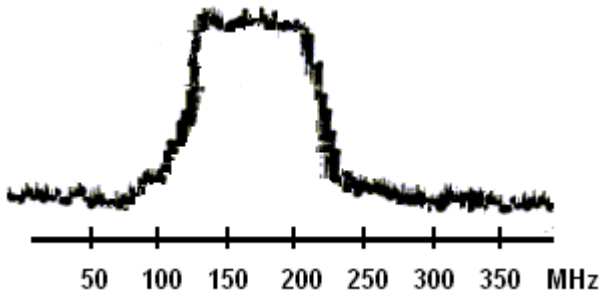


Figure 3.7. The digitized oscilloscope trace of the amplitude-frequency distribution inherent in the acousto-optical cell with collinear heterodyning exploiting the longitudinal elastic waves of a finite amplitude in **PbMoO<sub>4</sub>**-crystal.

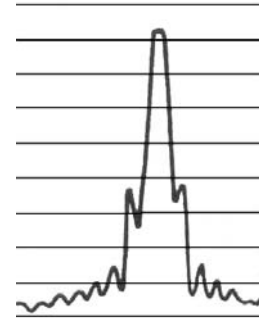


Figure 3.8. The digitized profile of an individual resolvable spot peculiar to a **PbMoO<sub>4</sub>**-cell with the most uniform ( $\gamma_L = 0.83$ ) distribution of the difference-frequency wave along **3.7 cm** aperture; horizontal lines are spaced by **2.5 dB**.

### 3.3. POTENTIAL PERFORMANCES OF A NOVEL LEAD MOLYBDATE CRYSTALLINE ACOUSTO-OPTICAL CELL WITH $\gamma > 1$

The normalized intensity  $J_{S-P}(x) = \left[ a_{S-P}^{(1)}(x) \right]^2 B^{-2} \delta^{-2}$  of the difference-frequency acoustic wave passing along the cell's optical aperture can be found from Eq.(2.6) in the following form [see an analogy in Eqs.(3.1) – (3.3) ]

$$J_{S-P}(x) = \left( \frac{\gamma-1}{4\gamma} \right)^2 \left[ 1 - \exp(-2\gamma\alpha_P x) \right]^2 \exp \left[ -2\alpha_P x (1-\gamma)^2 \right]. \quad (3.9)$$

From Eq.(3.9), as well as from the above-noted Eq.(3.1), one can find the point  $x_m$  associated with absolute maximum of the normalized intensity distribution inherent in the acoustic wave along the total cell's optical aperture as

$$x_m = \left( \frac{-1}{2\alpha_P \gamma} \right) \ln \left[ \frac{(1-\gamma)^2}{1+\gamma^2} \right], \quad (3.10)$$

which coincides with Eq.(3.2). The magnitude of this maximum can be estimated at the point  $x_m$  as

$$\mathbf{J}_{S-P}(\mathbf{x}=\mathbf{x}_m) = \frac{(\gamma-1)^2}{4(1+\gamma^2)^2} \exp \left\{ \frac{(1-\gamma)^2}{\gamma} \ln \left[ \frac{(1-\gamma)^2}{1+\gamma^2} \right] \right\}. \quad (3.11)$$

It is seen from Eq.(3.11) that the normalized intensity  $\mathbf{J}_{S-P}(\mathbf{x}=\mathbf{x}_m)$  is the decreasing function of  $\gamma$ , see the solid line in Fig.3.9. However, such a dependence on  $\gamma$  leads to a non-uniformity of distributing signals associated with various difference-frequency components inside the cell. To compensate this non-uniformity one can suggest exploiting the additionally needed preamplification  $\mathbf{G}(\gamma; \gamma_0)$ , which can be calculated as

$$\mathbf{G}(\gamma; \gamma_0) = \frac{3 \mathbf{J}_{S-P}(\mathbf{x}=\mathbf{x}_m, \gamma = \gamma_0)}{4 \mathbf{J}_{S-P}(\mathbf{x}=\mathbf{x}_m, \gamma)}, \quad (3.12)$$

where  $\gamma_0$  is initially selected and fixed value of the ratio  $\gamma$ . This fixed  $\gamma_0$  can be minimal or maximal, depending on the case  $\gamma < 1$  or  $\gamma > 1$  is chosen. An example of the needed preamplification  $\mathbf{G}(\gamma; \gamma_0)$  with  $\gamma_0 = 1.17$  is shown by the dashed line in Fig.3.9. Decreasing the normalized intensity  $\mathbf{J}_{S-P}(\mathbf{x}=\mathbf{x}_m)$  down to a level of  $-3$  dB along the optical aperture at a point  $\mathbf{x}_D$  gives the equality  $\mathbf{J}_{S-P}(\mathbf{x}=\mathbf{x}_D) = (1/2) \mathbf{J}_{S-P}(\mathbf{x}=\mathbf{x}_m)$ , so that one can find

$$\mathbf{x}_D = \frac{-1}{2\alpha_P(1-\gamma)^2} \left( \ln \left( \frac{\gamma\sqrt{2}}{1+\gamma^2} \right) + \left\{ \frac{(1-\gamma)^2}{2\gamma} \ln \left[ \frac{(1-\gamma)^2}{1+\gamma^2} \right] \right\} \right). \quad (3.13)$$

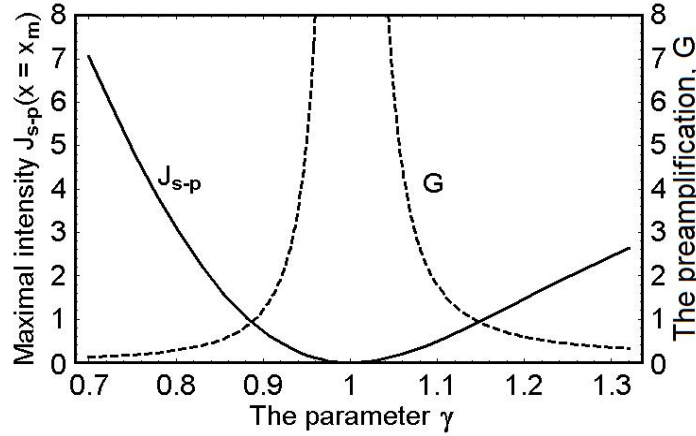


Figure 3.9. Plots of the maximal intensity  $\mathbf{J}_{S-P}(\mathbf{x}=\mathbf{x}_m)$  and the preamplification  $\mathbf{G}(\gamma; \gamma_0 = 1.17)$  versus the parameter  $\gamma$  for the magnitudes of  $\gamma$  practically usable within the wave heterodyning.

In fact, the magnitude of  $\mathbf{x}_D$  determines the total length of acousto-optical cell with the collinear wave heterodyning. Now, the really operating part  $\mathbf{D}$  of the cell's optical aperture available for optical processing can be found as

$$\text{a) } \mathbf{D} = \mathbf{x}_D - \mathbf{x}_m = \frac{\mathbf{F}(\gamma)}{\alpha_P}, \quad \text{b) } \mathbf{F}(\gamma) = \frac{1}{(1-\gamma)^2} \ln \left( \frac{1+\gamma^2}{\gamma\sqrt{2}} \right), \quad (3.14)$$

where the amplitude decrement is given by  $\alpha_P(\text{cm}^{-1}) = 0.115 \cdot \Gamma_0 \cdot [f_P(\text{GHz})]^2$ . Consequently, the following expressions for the pump frequency  $f_P$  and for the difference frequency  $f_D$  (where  $f_D = f_P - f_S = f_P(1-\gamma)$  if  $\gamma < 1$  or  $f_D = f_S - f_P = f_P(\gamma-1)$  if  $\gamma > 1$ ), appear

$$\text{a) } f_{\mathbf{P}} = \sqrt{\frac{\mathbf{F}(\gamma)}{0.115 \Gamma_0 \mathbf{D}}} \quad \text{b) } f_{\mathbf{D}} = |1-\gamma| \sqrt{\frac{\mathbf{F}(\gamma)}{0.115 \Gamma_0 \mathbf{D}}} \quad (3.15)$$

Now, let us direct our attention to the particular case of a lead molybdate crystalline cell ( $\Gamma_0 = 15 \text{ dB/cm GHz}^2$ ) with practically available optical aperture  $\mathbf{D} = 3.7 \text{ cm}$  and make a few estimations. At first, to provide higher operating frequencies together with the simplicity of realizing a low-frequency pump one can take an area of  $\gamma > 1$  with  $f_{\mathbf{D}} = f_{\mathbf{S}} - f_{\mathbf{P}} = f_{\mathbf{P}} (\gamma - 1)$ . It could be chosen in spite of the facts that the efficiency of frequency conversion in an area of  $\gamma \in [0.70, 0.95]$  exceeds a little bit the efficiency for  $\gamma \in [1.05, 1.30]$  and one will be in need of slightly higher preamplification with  $\gamma > 1$ . Applying Eqs.(3.15) to a lead molybdate cell with  $\mathbf{D} = 3.7 \text{ cm}$  and  $\gamma > 1$ , one can obtain the diagram shown in Fig.3.10.

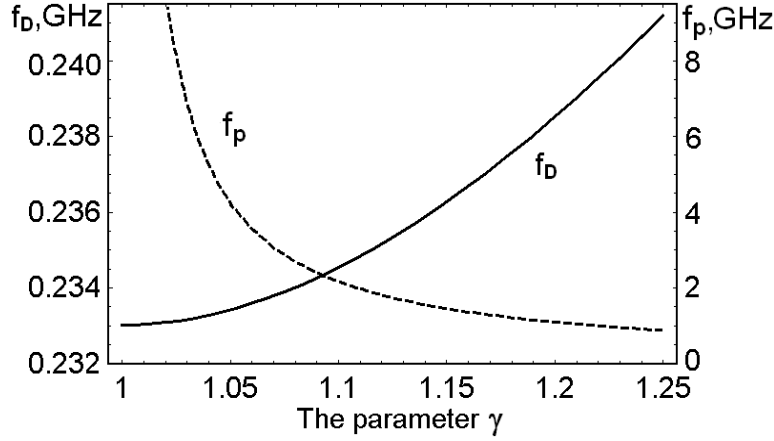


Figure 3.10. Plots for the pump frequency  $f_{\mathbf{P}}$  (dashed line) and the difference frequency  $f_{\mathbf{D}}$  (solid line) related to Eqs.(3.15) versus  $\gamma$  for magnitudes of  $\gamma$  practically usable in the wave heterodyning.

These dependencies allow the following estimations for practical realization. Let us take the upper difference-frequency as  $f_{\mathbf{UD}} = 236 \text{ MHz}$  and the upper magnitude of  $\gamma$  as  $\gamma_{\mathbf{U}} = 1.17$ , so that from Eq.(3.15a) the pump frequency will be  $f_{\mathbf{P}} = 1388 \text{ MHz}$  and the upper signal frequency will be  $f_{\mathbf{US}} = 1624 \text{ MHz}$ . Then, one can choose the bandwidth  $\Delta f$  of analysis, for example, in the range of  $180 \text{ MHz}$ , which leads to the lower difference-frequency  $f_{\mathbf{LD}} = 56 \text{ MHz}$  restricted by the Bragg regime condition. Consequently, the lower signal frequency is  $f_{\mathbf{LS}} = 1444 \text{ MHz}$ , and the lower magnitude of  $\gamma$  is  $\gamma_{\mathbf{L}} = 1.04$ . These estimations are conditioned by the following relations

$$\text{a) } f_{\mathbf{UD}} = f_{\mathbf{US}} - f_{\mathbf{P}} = f_{\mathbf{P}} (\gamma_{\mathbf{U}} - 1), \quad \text{b) } f_{\mathbf{LD}} = f_{\mathbf{LS}} - f_{\mathbf{P}} = f_{\mathbf{P}} (\gamma_{\mathbf{L}} - 1). \quad (3.16)$$

It should be noted that direct exploitation of similar lead molybdate cell with the active optical aperture  $\mathbf{D} = 3.7 \text{ cm}$  at the signal frequencies of about  $1000 \text{ MHz}$  is definitely impossible, because the acoustic attenuation exceeds  $55 \text{ dB}$  along this aperture. Nevertheless, applying the collinear acoustic wave heterodyning allows us to operate on these gigahertz-range carrier frequencies. Non-uniformities in the distributions of signals are illustrated in figure 5, where  $\mathbf{G} = 1$  for  $\gamma_{\mathbf{U}} = 1.17$  and  $\mathbf{G} = 6$ , as it follows from Eq.(3.15) and Fig.3.11 for  $\gamma_{\mathbf{L}} = 1.04$ . Using Eq.(3.10), one can estimate that  $x_{\mathbf{m}} = 0.58 \text{ cm}$  for  $\gamma_{\mathbf{U}} = 1.17$  and  $x_{\mathbf{m}} = 0.94 \text{ cm}$  for  $\gamma_{\mathbf{U}} = 1.04$  with  $\alpha_{\mathbf{P}} = 3.32 \text{ cm}^{-1}$ . Figure 6 shows that the really operating optical aperture  $\mathbf{D}$  lies between  $x = 0.4 \text{ cm}$  and  $x = 4.2 \text{ cm}$  for  $\gamma_{\mathbf{U}} = 1.17$ , resulting in at least  $\mathbf{D} \approx 3.8 \text{ cm}$ . Physical limit for potential frequency resolution of a cell is given by the value  $\delta f \approx \mathbf{V}/\mathbf{D}$ .

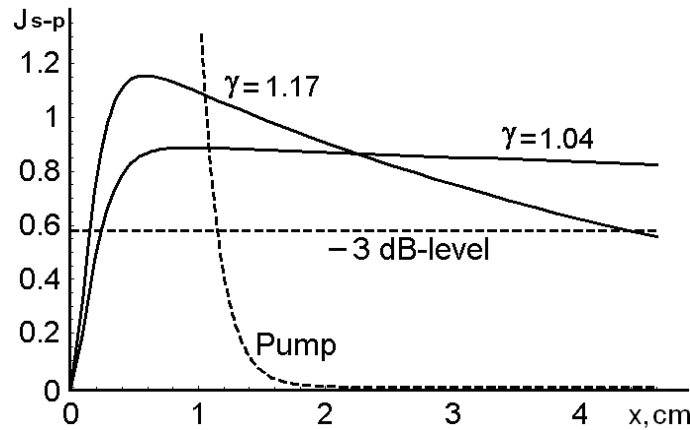


Figure 3.11. Non-uniformities in the distributions of signals associated with various difference-frequency acoustic wave components in the lead molybdate cell.

As it has been mentioned above, a novel acousto-optic cell was made of a lead molybdate single crystal and completed with a pair of electronic input ports for the pump and signal on one of its facets as well as with acoustic absorber on the opposite facet. The piezoelectric transducer with an interaction length of **1.0** cm, generating the signal wave with power density of about **100** mW/mm<sup>2</sup>, was made of a thin ( $\mathbf{Y} + 36^\circ$ ) -cut lithium niobate crystal, so that it excited purely longitudinal acoustic wave, with conversion losses of about **2** dB at its resonant frequency close to **1530** MHz. The single-frequency pumping longitudinal acoustic wave with the power density of up to **600** mW/mm<sup>2</sup> was generated at a carrier frequency of approximately **1390** MHz, so that the case of  $\gamma \in [1.04, 1.20]$  had been experimentally realized. During the experiments, we have placed a diaphragm in about **5**-millimeter vicinity of the piezoelectric transducers area (about **13.5** % of the total aperture) to minimize the effect of this area, where an increase in the power of difference frequency waves takes place. Consequently, the working optical aperture of a cell was a little bit longer than **37** mm. The bandwidth of that prototype was about **180** MHz. The efficiency of light scattering by an additional acoustic wave at the difference-frequency was slightly exceeding **1%**. Fig.3.12 shows the digitized oscilloscope traces of amplitude-frequency distribution peculiar to that prototype with the acousto-optical cell based on the collinear wave heterodyning. The digitized trace of this distribution had been recorded by a multi-pixel CCD linear array photo-camera through connecting the input signal port of a cell at an ultra-high-frequency radio-wave sweep-generator and fulfilling the acoustic wave heterodyning in a lead molybdate crystal. For a radio-wave signal, producing the dynamic acoustic grating on the resulting carrier difference-frequency of about **235** MHz, the attenuation is close to **3** dB over the total cell aperture. At the same time, for the signal acoustic waves at even the lower original frequency **1440** MHz the attenuation exceeds **100** dB along a **37** mm aperture, which is perfectly unacceptable in practice. Within the second set of our experimental tests, we examined the resolution of spectrum analyzer with the cell exploiting the collinear acoustic-wave heterodyning. In fact, the intensity distribution of an individual resolvable spot in the focal plane of the integrating lens had been considered. In so doing, the technique, which had long been in use, with very narrow slit diaphragm scanning over sufficiently sensitive photodetector and subsequent logarithmic amplifier was applied to our needs. Practically, this technique gives an opportunity to fix the continuous distribution of light intensity in the lobes of an individual spot really carefully in a rather wide dynamic range of about **25** dB [3.2]. One can see that the measured level of the first lobes lies at a level of about **-13** dB with initially homogeneous lighting of the operating cell's aperture, which is in good coincidence with the well-known theoretical prediction [3.3]. Figure 3.13 presents the digitized trace, which had been recorded in the focal plane of the integrating lens, see Fig.3.6, via applying just a single-frequency excitation at the input signal port of the proposed cell. In the case under consideration, physical limit of the frequency resolution is  $\mathbf{V/D} \approx 98$  KHz, while experimentally obtained value, affected by acoustic losses as well as by technical imperfectness of the integrating lens, corresponds to a frequency resolution of about  $\delta f \approx 120$  KHz at a level of **-10** dB and gives the number of resolvable spots or, what is the same, the number of parallel frequency channels  $\mathbf{N} \approx 1500$ . By this is meant that the proposed technique for direct parallel optical spectrum analysis of

gigahertz-frequency range radio-wave signals provides at least **1500**-channel processing even within our proof-of-principle experiment. As this takes place, the accuracy or the relative frequency resolution  $\delta f/f_{LS}$  (where  $f_{LS} = 1444$  MHz) is less than  $10^{-4}$ , which is practically unattainable for conventional direct acousto-optical methods of spectrum analysis.

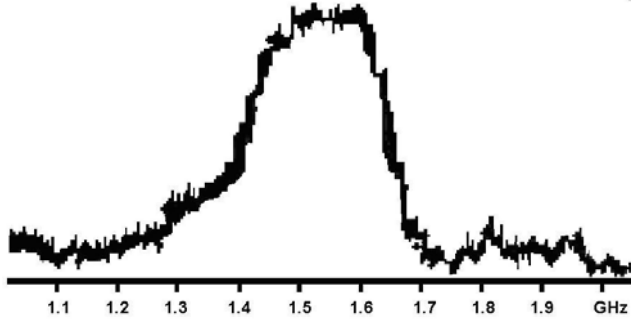


Figure 3.12. The digitized oscilloscope trace of the amplitude-frequency distribution inherent in the acousto-optical cell with collinear heterodyning exploiting the longitudinal elastic waves of a finite amplitude in **PbMoO<sub>4</sub>**-crystal.

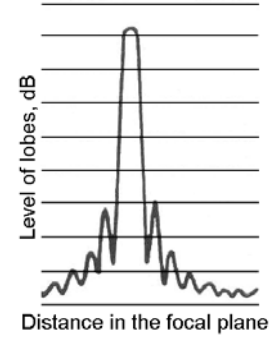


Figure 3.13. The digitized profile of an individual resolvable spot peculiar to a **PbMoO<sub>4</sub>**-cell with the most uniform ( $\gamma_U = 1.17$ ) distribution of the difference-frequency wave along 3.7 cm aperture; horizontal lines are spaced by **2.5** dB.

### 3.4. BRIEF COMPARATIVE DISCUSSION

At this step, it seems quite reasonable to compare operation characteristic of the proposed acousto-optical cell with the corresponding characteristics of an acceptable traditional high-frequency cell. Let us take a cell exploiting longitudinal acoustic wave along the **X**-axis of such a low-loss crystal as lithium niobate with  $M_2 = 7.0 \cdot 10^{-18} \text{ s}^3/\text{g}$ ,  $\Gamma = 0.15 \text{ dB}/(\text{cm GHz}^2)$ , and  $V_L = 6.57 \cdot 10^5 \text{ cm/s}$ . Each cell can be characterized in both frequency and amplitude domains. The best set of frequency characteristics for the chosen cell at the central frequency  $f_0 = 1.5 \text{ GHz}$  includes the frequency bandwidth  $\Delta f \approx f_0/2 = 750 \text{ MHz}$ , the upper signal frequency  $f_U = 1875 \text{ MHz}$ , the optical aperture  $D_0 = 3 [\text{dB}]/(\Gamma f_U^2) \approx 5.7 \text{ cm}$  associated with a 3-dB level of acoustic losses at the frequency  $f_U$ , the frequency resolution  $\delta f = V/D_0 = 115 \text{ KHz}$ , the number of resolvable spots  $N = \Delta f/\delta f \approx 6520$ , and the relative accuracy of analysis  $\delta f/f_0 \approx 0.77 \cdot 10^{-4}$ . The efficiency of this cell with  $L = 1.0 \text{ cm}$  and a given exciting acoustic wave power density  $P_0$  can be estimated by  $I_0 = \sin^2(q_0 L)$ , where  $q_0$  can be taken from Eq.(2.15b) at  $\lambda = 532 \text{ nm}$ . To make the comparison with the data in the end of section 2.4, let us take  $I_0 = 0.03$ , i.e. 3%. In this case, one can estimate  $q_0 = I_0^{1/2}/L \approx 0.173 \text{ cm}^{-1}$  and  $P_0 = (2I\lambda^2)/(\pi^2 L^2 M_2) \approx 0.25 \cdot 10^7 \text{ g/s}^3 = 0.25 \text{ W/cm}^2$ . Thus, the traditional **LiNbO<sub>3</sub>**-cell looks at the first glance slightly preferable than the above-proposed one. Nevertheless, to make the correct conclusion one has to take into account a few following circumstances. First, a large optical aperture requires growing large enough boule of lithium niobate. It should be the mono-domained sylvan-less single crystal exhibiting a high optical homogeneity and providing top-level conditions for propagation of both optical as well as UHF acoustic waves through a large-aperture cell. Practically, it is rather difficult to satisfy these requirements, but in the otherwise case, similar cell will have lost a significant part of its potential frequency resolution. Second, designing truly effective piezoelectric transducer with a 50% frequency bandwidth at a carrier frequency of about 1.5 GHz is not an ordinary task. The existing difficulties in technology of production as well as in subsequent acoustic and electronic matching of similar wide-band piezoelectric transducer can be resolved currently only within decreasing its efficiency or/and narrowing its bandwidth. This is why the above-noted potential frequency characteristics have to be considered as just

the limiting theoretical values. Third, the estimated efficiency for a lithium niobate cell cannot be applied directly to the comparison under consideration, because the proposed new cell involves two cascades of processing and provides an additional function, namely, the heterodyning, which needs naturally additional power consumption. Then, during this comparison one has to take into account that our experimentally tested lead-molybdate cell had not been really optimized, because the main purposes of this cell were to demonstrate a new principle of operation as well as to exhibit that it can be realized practically with more or less acceptable operation characteristics. Furthermore, in parallel with performing the cell's optimization more effective acoustically and acousto-optically materials, such as **KRS – 5** [3.4], can be examined within the proposed technique in expecting much better performance data. Together with this the proposed technique of spectral analysis, which includes the developed cell with two piezoelectric transducers and the frequency-dependent preamplification, should be in principle compared with the simplest technique based on preliminary electronic mixing of the high-frequency radio-wave signals with further launching of the resulting acoustic wave at the difference frequency. However, this kind of comparison exceeds evidently the limits of this article as far as, on the one hand side, it is mostly related to comparing electronic rather than acousto-optical components of the functional scheme under consideration and, on the other hand side, one needs more practical experience of exploiting the proposed technique than he has at the moment to make such a comparison really qualitatively.

### 3.5. CHARACTERIZING THE OPTICAL PART OF EXPERIMENTAL SET-UP AND SOME PRACTICAL ESTIMATIONS

Exploiting the above-listed estimations, a novel acousto-optical cell had been designed and used in almost standard optical scheme for acousto-optical spectrum analysis of a gigahertz-frequency range radio-signals, see Fig.3.6. This scheme includes green-light laser ( $\lambda = 532$  nm, the output optical power exceeds **100** mW), a four-prism beam expander (only two of them are shown), a rectangular selecting optical diaphragm, a single-crystal acousto-optical cell with acoustic absorber and two ultra-high-frequency electronic ports for the input signal and pump, a large-aperture achromatic doublet lens, and a **3000**-pixel CCD linear array photo-camera. A lead molybdate single crystal of **42** mm in total length, oriented as it had been described above, was used in that cell. The incident light was linearly polarized along the **[0,0,1]**-axis of the cell's crystal. It provided, on the one hand side, the maximal transmission of the prism beam expander due to coinciding the plane of expanding laser beam with the corresponding vector of light polarization and, on the other hand, the maximal efficiency of acousto-optical interaction in a lead molybdate single crystal (see sections **3.2** and **3.3**).

The size of an individual resolvable spot can be remarkably affected by a non-uniformity of light stream leaving the acousto-optical cell output facet. This non-uniformity governed by a combined distribution of the incident light field profile and the drooping distribution of the difference-frequency acoustic wave along cell's optical aperture. Usually, profile of the incident light field is close to a Gaussian shape, because it is conditioned, first of all, by the initial profile of laser beam. Together with this, just a Gaussian profile is commonly used within possible apodization of the incident beam profile. In addition, the apodization is originally directed to suppressing the side lobes, which are peculiar to light distribution of each individual resolvable spot in a Fourier transform plane of the integrating lens. In so doing, the apodization is capable to increase the potential dynamic range of spectrum analysis. Reasoning from the assumption that the electric field profile  $\mathbf{E}_{in}$  reaching the cell's optical aperture has a Gaussian shape, one can write (in both physical and dimensionless variables) that

$$\mathbf{E}_{in} = \mathbf{E}_0 \exp[-\sigma(\mathbf{x}_1 - \mathbf{x}_0)^2] = \mathbf{E}_0 \exp[-\beta(\mathbf{y} - \mathbf{y}_0)^2], \quad \mathbf{I}_{in} = \mathbf{E}_{in}^2. \quad (3.17)$$

where  $\mathbf{x}_1$  and  $\mathbf{D}$  are the physical coordinate across a beam and the physical cell's optical aperture measured in centimeters,  $\mathbf{y} = \mathbf{x}_1/\mathbf{D}$  is the normalized dimensionless coordinate, so that the coordinates  $\mathbf{x}_0$  and  $\mathbf{y}_0$  correspond to the center of distribution,  $\sigma$  and  $\beta = \sigma\mathbf{D}^2$  are physical and dimensionless parameters of the Gaussian-shape function.

Generally, the drooping intensity distribution of the difference-frequency acoustic wave along cell's optical aperture is characterized by Eq.(2.8) and it has to be taken into account in frames of our analysis. However in an area of the clear optical aperture  $\mathbf{D} = \mathbf{x}_D - \mathbf{x}_m$ , one can take only the reduced expression

$\mathbf{a}_{S-P}^{(1)}(\mathbf{x}) \propto \exp[-\alpha_P \mathbf{x}(1-\gamma)^2]$  with  $\mathbf{x} \in [\mathbf{x}_m, \mathbf{x}_D]$ . To have a chance of joining this formula with Eq.(3.17) one has to determine  $\mathbf{x}_1 = \mathbf{x} - \mathbf{x}_m$  and to normalize  $\mathbf{a}_{S-P}^{(1)}(\mathbf{x})$  by its magnitude just at the point  $\mathbf{x}_m$ . As a result, one can write

$$\mathbf{a}_{S-P}^{(N)} = \exp[-\alpha_P \mathbf{x}_1(1-\gamma)^2] = \exp[-\alpha_D y], \quad \mathbf{J}_{S-P}^{(N)} = [\mathbf{a}_{S-P}^{(N)}]^2, \quad (3.18)$$

where the amplitude decrement  $\alpha_D = \alpha_P D(1-\gamma)^2$  describes a total value of losses all over the cell's optical aperture  $D$  for the difference-frequency acoustic wave; it can be expressed in decibels or in a dimensionless form, because  $\alpha_P [\text{cm}^{-1}] = 0.115 \cdot \alpha_P [\text{dB/cm}]$ . To illustrate a sense of this reasoning let us consider the following example. Taking  $y_0 = 0.5$  and formulating the condition  $\mathbf{I}_{in}(y=0) = \mathbf{I}_{in}(y=1) = 0.5 \cdot \mathbf{I}_{in}(y=0.5)$ , one can find that the needed dimensionless parameter of the Gaussian-shape function is  $\beta = 1.382$ . Then, assuming that  $\mathbf{J}_{S-P}^{(N)}(y=1) = 0.5 \cdot \mathbf{J}_{S-P}^{(N)}(y=0)$ , one can estimate  $\alpha_D \approx 0.345$  in the worst case of  $\gamma_U = 1.17$ . The plots corresponding to this example are presented in Fig.3.14. The total intensity of light field passing through the cell's aperture can be estimated by the value

$$I_A = \left[ \int_0^1 \exp[-\beta(y-0.5)^2] \exp(-\alpha_D y) dy \right]^2 = \frac{\pi}{4\beta} \exp\left[\frac{\alpha_D}{2\beta}(\alpha_D - 2\beta)\right] \left[ \text{Erf}\left(\frac{\alpha_D + \beta}{2\sqrt{\beta}}\right) - \text{Erf}\left(\frac{\alpha_D - \beta}{2\sqrt{\beta}}\right) \right].$$

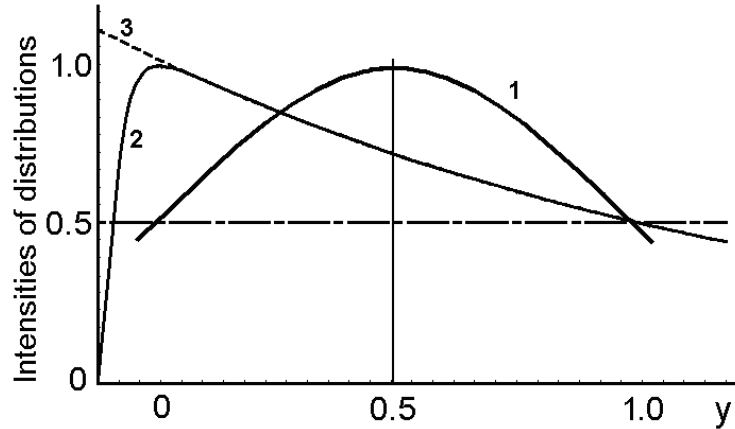


Figure 3.14. Intensity distributions for Gaussian profile of the incident light with  $\beta = 1.382$  (bold line 1) as well as for the difference-frequency acoustic wave with  $\alpha_D \approx 0.345$ ,  $\gamma_U = 1.17$  (solid line 2) along cell's aperture. For the comparison, the dependence reflecting Eq.(3.18) is shown (dashed line 3).

The shape of light field distribution  $\mathbf{E}(\mathbf{u})$  (the dimensionless coordinate  $\mathbf{u}$  is centered on a maximum of this distribution) peculiar to an individual resolvable spot in a Fourier-transform plane of the integrating lens can be estimated analytically as

$$\begin{aligned} \mathbf{E}(\mathbf{u}) &= \int_0^1 \exp[-\beta(y-0.5)^2] \exp(-\alpha_D y) \exp(-2i\pi u y) dy = \\ &= \frac{1}{2} \sqrt{\frac{\pi}{\beta}} \exp\left[-\beta\left(\frac{1}{4} - v^2\right)\right] \left\{ \text{Erf}\left[\sqrt{\beta}(1+v)\right] - \text{Erf}\left[\sqrt{\beta}v\right] \right\}, \end{aligned} \quad (3.19)$$

where the notation  $\mathbf{v} = \left( \frac{\alpha_D}{2\beta} - \frac{1}{2} \right) + i \frac{\pi \mathbf{u}}{\mathbf{b}}$  is used. Let us introduce  $\mathbf{v}(\mathbf{u} = \mathbf{0}) = \mathbf{v}_0 = \left( \frac{\alpha_D}{2\beta} - \frac{1}{2} \right)$  and obtain

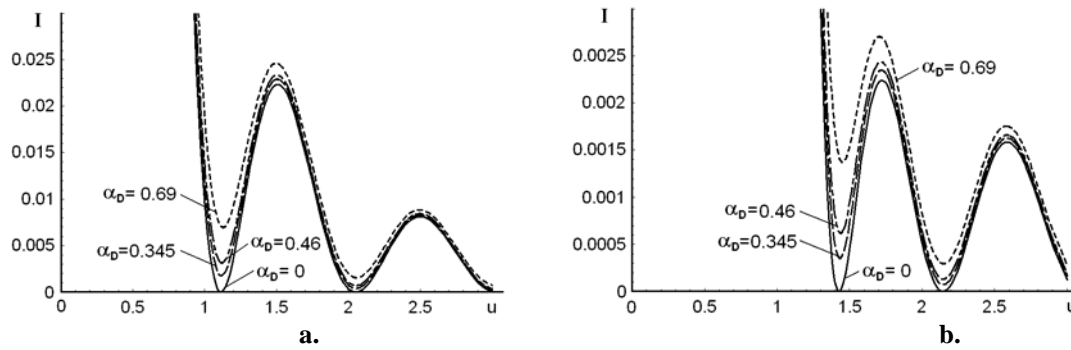
$$\mathbf{E}(\mathbf{u} = \mathbf{0}) = \frac{1}{2} \sqrt{\frac{\pi}{\beta}} \exp \left[ -\beta \left( \frac{1}{4} - \mathbf{v}_0^2 \right) \right] \left\{ \text{Erf} \left[ \sqrt{\beta} (1 + \mathbf{v}_0) \right] - \text{Erf} \left[ \sqrt{\beta} \mathbf{v}_0 \right] \right\}, \quad (3.20)$$

which is real-valued in behavior. Using Eqs.(3.19) and (3.20), the normalized distribution  $\mathbf{I}(\mathbf{u})$  of light intensity peculiar to an individual resolvable spot in a Fourier-transform plane of the integrating lens can be written as  $\mathbf{I}(\mathbf{u}, \beta, \alpha_D) = \mathbf{E}(\mathbf{u}) \mathbf{E}^*(\mathbf{u}) \mathbf{E}^{-2}(\mathbf{u} = \mathbf{0})$ . Generally,  $\mathbf{u} = \mathbf{w} \mathbf{D} / \lambda \mathbf{F}_L$ , where  $\mathbf{w}$  is the physical spatial coordinate in the focal plane and  $\mathbf{F}_L$  is the focal distance of the integrating lens. In the particular case of  $\beta \equiv 0$ , one can find

$$\mathbf{I}(\mathbf{u}, \beta = 0, \alpha_D) = \frac{\sin^2(\pi \mathbf{u}) + \sinh^2(\alpha_D/2)}{\left[ 1 + (2\pi \mathbf{u} / \alpha_D)^2 \right] \sinh^2(\alpha_D/2)}. \quad (3.21)$$

Results of numerical simulations for  $\mathbf{I}(\mathbf{u}, \beta, \alpha_D)$ , based on Eqs.(3.19) - (3.21), with practically useful values of  $\beta$  and  $\alpha_D$  are shown in Fig.3.15. It is seen from Fig.3.15 that increasing the amplitude decrement  $\alpha_D$  leads to growing of side lobes and minima of the normalized light intensity distribution inherent in each individual resolvable spot in the focal plane of the integrating lens. Moreover, the spatial width of the main lobe peculiar to each individual resolvable spot shows an increase due to the presence of losses, so that real magnitude of the frequency resolution  $\delta f$  is taking away from the limit  $\mathbf{V}/\mathbf{D}$ . Together with this, increasing the parameter  $\beta$  provides suppressing side lobes and minima of light distributions, so that as usually the dynamic range could be increased. Then, one can see from Figs.3.15b and 3.15c that for the magnitudes of  $\beta$  exceeding some value, which has been estimated by about 6.7, the second side lobe dominates over the first one. This fact and a tendency to broadening the main lobe due to losses are illustrated in Fig.3.16 in the particular case of  $\alpha_D = 0.345$ .

Now, let us estimate potential possibilities related to both the dynamic range and the width of an individual resolvable spot in a scheme of acousto-optical spectrometer with a co-directional collinear wave heterodyning. The most critical limitation for the dynamic range is related to the maximal level of side lobes. Figure 3.17 illustrates affecting the dynamic range by a maximal side lobe, so that one can clearly see that acoustic attenuation decreases the potential dynamic range, which grows by itself with escalating the parameter  $\beta$ .



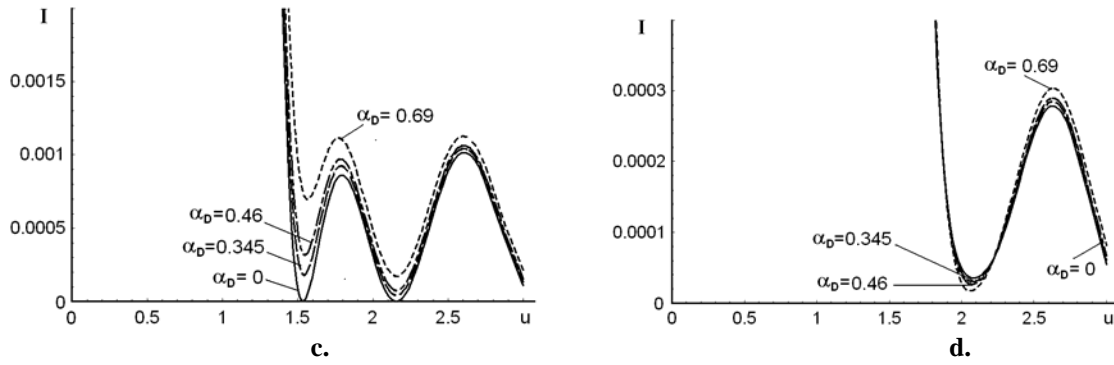


Figure 3.15. The combined effect of both the incident light apodization and the acoustic beam attenuation on the normalized light intensity in the focal plane of the integrating lens: (a) is for  $\beta = 2$ , (b) is  $\beta = 6$ , (c) is for  $\beta = 7$ , and (d) is for  $\beta = 10$ ; here, various vertical scales are taken for each magnitude of  $\beta$ .

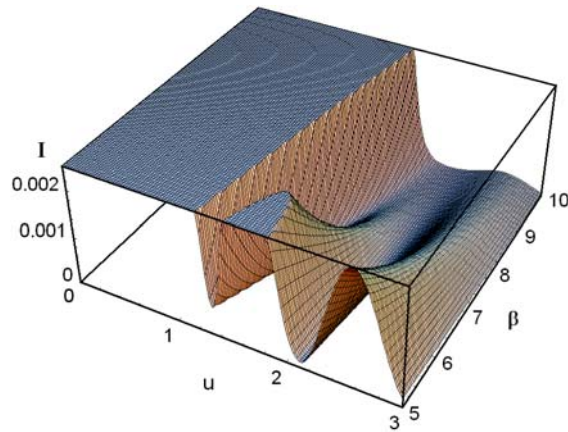


Figure 3.16. The general plot of the light intensity distribution peculiar to an individual resolvable spot in a Fourier plane with  $\alpha_D = 0.345$  and  $\beta \in [5, 10]$ .

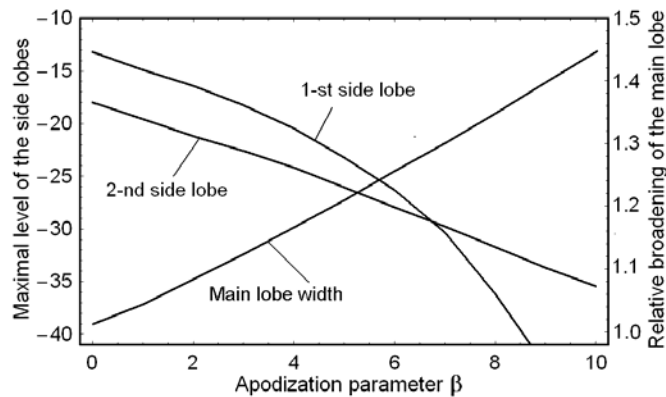


Figure 3.17. Width of the main lobe at a level of 0.405 and maximal levels of the side lobes, the first or second ones, versus the apodization parameter  $\beta$  with  $\alpha_D = 0.345$ .

Broadening the main lobe of an individual resolvable spot is characterized by the third curve in Fig.3.17, which reflects increasing its width at a level of 0.405 corresponding to the Rayleigh resolution criterion [3.5].

### 3.6. CONCLUSION

The presented data demonstrate both the possibility and the potential advantages of applying a co-directional collinear wave heterodyning to essential, about an order of magnitude, improvement of the frequency resolution within a multi-channel parallel acousto-optical spectrum analysis of gigahertz-frequency range analogue radio-wave signals. In so doing, we have theoretically investigated the phenomenon of a co-directional collinear wave heterodyning, taken in the particular case of mixing the longitudinal acoustic waves of finite amplitudes. Then, an opportunity of implementing acousto-optical data processing with the wave heterodyning has been experimentally performed utilizing the specially designed acousto-optical cell made of a lead molybdate single crystal. Together with this, the methods for estimating the total efficiency of operation and optimizing aperture parameters for the cell of a new type have been developed. Moreover, the phenomenon of affecting the light distribution inherent in an individual resolvable spot by joint action of the incident light beam non-uniformity and the natural presence of acoustical losses along cell's optical aperture has been estimated. The proposed technique exploits a two-cascade algorithm of processing and is intended for direct parallel and precise optical spectrum analysis and provides about **1500**-frequency-channels for processing analogue radio-wave signals in a gigahertz-frequency range with the accuracy or, what is the same, with the relative frequency resolution better than  $10^{-4}$ , which is usually unattainable for conventional direct acousto-optical methods. The obtained results reflect fruitful character of modern approaches based on applying various non-linear phenomena to improving the performance data of optical processing and give an appropriate example of this kind. At the moment, a few practical advantages of the presented approach can be noted. First, the proposed device need not additional electronic equipment for mixing the signals and selecting the resulting carrier frequency, because heterodyning can be performed directly in a cell and provides potentially the dynamic range of about **90** dB peculiar to wave processes in solids. Then, the approach under consideration decreases the required relative bandwidth of piezoelectric transducer from **50–100%** at the resulting frequency within a conventional cell to **10–15%** at the initial carrier frequency. Within our proof-of-principle experiment the acousto-optical cell with **2** piezoelectric transducers was used, but generally it is not necessary. Due to the relative bandwidth does not exceed **15%**, potentially it is quite reasonable to exploit just only one transducer. Third, in the case of a spatially multi-channel arrangement of the acousto-optical cell, the identity of neighboring spatial channels to each other can be provided by adjusting the corresponding heterodynes. Finally, one should note that the number of isotropic or crystalline materials, which are appropriate for acousto-optical cells processing signals in a gigahertz-frequency range, is definitely restricted due to fast-growing influence of a square-law frequency dependence for the acoustic attenuation in solids. For instance, one can easily show [3.6, 3.7] that the above-discussed lead molybdate crystal cannot be used for creating a conventional acousto-optical cell operating with signals whose carrier frequency exceeds about **300–400** MHz. Nevertheless, just this crystalline material had been exploited for the control over **1.5** GHz signals within these studies. Consequently, one can conclude that a two-cascade arrangement of a cell presented here allows extending the spectrum of acousto-optical materials being appropriate for direct processing of ultra-high-frequency analogue radio-wave signals.

### 3.7. REFERENCES

- 3.1. P.A.M.Dirac. *The Principles of Quantum Mechanics*. 4-th Ed. (Oxford University Press, Oxford, 1999).
- 3.2. A.S.Shcherbakov, E.Tepichin Rodriguez, A.Aguirre Lopes, and Je.Maximov. Frequency bandwidth and potential resolution of optical modulators exploiting a multi-phonon light scattering in crystals. *Optik: Int. J. Light. Electron. Opt.*, v.**120**, issue 7, 301-312 (2009).
- 3.3. J.W.Goodman, *Introduction to Fourier Optics*, 2-nd Ed., (McGraw-Hill, N.Y., 1996).
- 3.4. A.S.Shcherbakov, Je.Maximov, and D.Sanchez Lucero. Potentials of the acousto-optical spectral data processing on the basis of a novel algorithm of the collinear wave heterodyning in a large-aperture KRS-5 crystalline cell. *Proc. of SPIE*, vol.7598, p. 75981J-1 – 75981J-11 (2010).
- 3.5. M.Born and E Wolf. *Principles of Optics*. 3-rd Ed. (Pergamon Press, Oxford, 1970).
- 3.6. V.G.Dmitriev, G. G. Gurzadyan, D. N. Nikogosyan, *Handbook of Nonlinear Optical Crystals* 3rd Ed. (Springer, Berlin, 1999).
- 3.7. A.A.Blistanov. *Crystals for Quantum and Nonlinear Optics*. (Moscow, MISIS, 2007).

#### 4. POTENTIALS OF THE ACOUSTO-OPTICAL SPECTRUM ANALYSIS ON THE BASIS OF COLLINEAR ACOUSTIC WAVE HETERODYNING IN A LARGE-APERTURE KRS-5 CRYSTALLINE CELL

The technique under consideration imposes specific requirements on the cell's material, namely, a high optical quality of large-size crystalline boules, high-efficient acousto-optical and acoustic interactions, and low group velocity of acoustic waves together with square-low dispersion for linear acoustic losses. With these requirements in mind, we focus our attention on the solid solutions of thallium chalcogenides and take the TlBr-TlI (thallium bromine – thallium iodine) solution, which forms **KRS – 5** cubic-symmetry crystals with the mass-ratio **58%** of TlBr to **42%** of TlI. Analysis shows that the acousto-optical cell made of a **KRS – 5** crystal oriented along the **[111]**-axis and the corresponding longitudinal elastic mode for producing the dynamic diffractive grating can be exploited. With the acoustic velocity of about **1.92 mm/μs** and attenuation of approximately **10 dB/(cm GHz<sup>2</sup>)**, similar cell is capable to provide an optical aperture of about **5.0 cm** and one of the highest figures of acousto-optical merit in solid states in the visible range. Such a cell is rather desirable for the application to direct 5000-channel parallel spectrum analysis with improved up to **10<sup>-5</sup>** relative frequency resolution.

##### 4.1. PRELIMINARY REMARKS

The proposed approach makes possible providing effective wave heterodyning, when the beneficial data in signal become to be converted from a relatively high-frequency carrier wave to a difference-frequency wave. Because of rather strong square-law dispersion of linear acoustic losses, the heterodyning leads to increasing the characteristic length and time of propagation (they both are associated with a clear optical aperture) for the converted signal in that medium and to improving significantly the accuracy of signal processing as it follows from the uncertainty principle in quantum mechanics [4-6]. In this context, we consider an opportunity for real-time scale optical analysis of frequency spectra, belonging to analogue ultra-high frequency radio-wave signals, with significantly improved frequency resolution. This consideration is based on a two-cascade processing, i.e. on exploiting a pair of different wave processes one after the other sequentially in the single crystalline cell, which includes the piezoelectric transducer, converting the inputting electronic signals into gigahertz-frequency elastic waves, with two electronic ports on its upper facet, clear optical aperture **D**, and an effective acoustic absorber on its bottom facet, see Fig.4.1a.

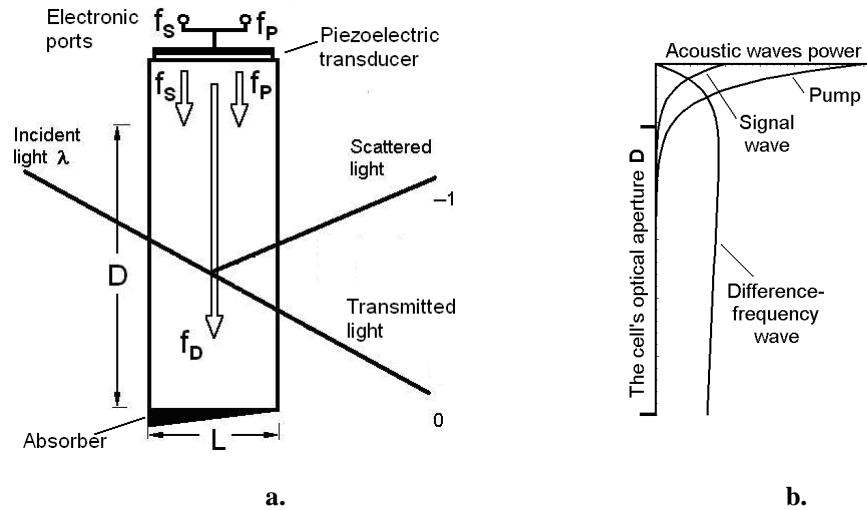


Figure 4.1. Schematic arrangement of the interacting beams in a two-cascade acousto-optical cell (a) and the illustrating spatial distributions for powers of the interacting acoustic waves (b).

The first wave process represents mixing the longitudinal elastic waves of finite amplitudes in a compactly localized upper domain of a cell where relatively powerful pump of the frequency  $f_P$  interacts with relatively weaker signal

elastic wave of the frequency  $\mathbf{f}_S$ . During just this nonlinear process a collinear wave heterodyning takes place providing the appearance of an elastic wave of the difference-frequency  $\mathbf{f}_D$ , which is able to propagate along a large-aperture cell due to weaker manifestation of strongly dispersive losses at lower frequencies, see Fig.4.1b. The second wave process is the subsequent Bragg light scattering by the difference-frequency elastic wave in as possible linear regime, i.e. in the regime of a given acoustic field for the incident light beam. This process occurs within a clear aperture  $\mathbf{D}$  lighted by a wide incident optical beam of the wavelength  $\lambda$  (in air) and is able to realize optical spectrum analysis by itself. When, for example, the signal wave is rather intricate in behavior and consists of various frequencies, each individual spectral component from the difference-frequency elastic wave plays the role of a partial thick dynamic diffractive grating for the incident light beam. The length  $\mathbf{L}$  of acousto-optical interaction has to provide performing the Bragg regime of light scattering.

Generally, the term “resolution” can be interpreted in slightly different from one another ways. One of these ways can be naturally related to the number  $\mathbf{N}$  of resolvable spots, because increasing the number  $\mathbf{N}$  undoubtedly means improving the resolution. Nevertheless, the resolution can be characterized from the other side as well if one will consider the absolute value of, for example, frequency resolution: as less is an individual resolvable frequency interval as more is the frequency resolution. Moreover, within designing a system (for instance, for the star radio-astronomy) one can meet a specific situation when it is so desirable to improve just an absolute value of the frequency resolution that the penalty for that even in the form of decreasing the number  $\mathbf{N}$ , when the bandwidth of processing is not fixed, becomes to be acceptable. In connection with this refining, we would like to say that just the last option is the case under our consideration. Namely, we aspire first of all to improving the frequency resolution, while reasonably large number  $\mathbf{N}$  serves us to be an illustration that it could be done algorithmically in a multi-channel parallel regime. Therefore, potentials peculiar to the acousto-optical spectrum analysis of a gigahertz-frequency range radio-wave signals with essentially improved relative value of the frequency resolution, which can be in the order of  $10^{-5}$  in our case, is considered with exploiting a new type of the acousto-optical cell made of really effective **KRS-5** cubic single crystal. The obtained estimations show that the elaborated approach, based algorithmically on a two-cascade processing, allows the direct **5000**-channel parallel optical analysis of spectra inherent in ultra-high-frequency radio-wave signals. In frames of the performed investigations, the efficiencies of both non-collinear acousto-optical and collinear acoustic interactions are analytically estimated. Moreover, analytic expression for the corresponding effective acoustic modulus of the third order in **KRS-5** has been found for the first time in our knowledge. In so doing, contrary to our recently developed theoretical approach based on the technique of substantial approximations [4.4, 4.5], a regime of the coupled acoustic modes is considered, which provides more accurate analysis. These findings make it possible first to estimate the technical requirements to performance data of the acousto-optical cell as well as to acceptable values of the operating frequencies. At the end, previously proposed methodology for the experimental simulation [4.4] is practically applied and exploited within a specific example of the liquid-made cell to estimate performances of the parallel spectrum analysis with the new **KRS-5**-crystal based acousto-optical cell.

## 4.2. EFFICIENCY OF ACOUSTO-OPTIC INTERACTION IN A KRS-5 CUBIC CRYSTAL

One can start from estimating the potential efficiency  $\mathbf{I}$  of Bragg light scattering by the longitudinal acoustic waves in a **KRS-5** single crystal. At first, let us take the cell’s orientation shown in Fig.4.2. Such a selection has its origins in preliminary known data related to linear and nonlinear manifestations of optical and acoustical properties inherent in this crystal. To obtain the figure of acousto-optical merit  $\mathbf{M}_2$  inherent in the selected cut of a **KRS-5** crystal first of all the effective photo-elastic constant  $\mathbf{p}_{\text{eff}}$  has to be found. For this purpose one has to take into account that a **KRS-5** single crystal belongs to the **m3m**-cubic symmetry group. This crystal allows existing pure longitudinal elastic waves with the wave vector  $\vec{\mathbf{K}}$  and the displacement vector  $\vec{\mathbf{u}} = \mathbf{u}\vec{\mathbf{m}}$ , when these waves are passing along the crystallographic axis **[111]**, so that  $\vec{\mathbf{K}} \parallel \vec{\mathbf{m}} \parallel \mathbf{[111]}$ . Each dynamic acoustic grating can be characterized by its deformation tensor of the second rank. Because of  $\vec{\mathbf{K}} \parallel \mathbf{[111]}$  and  $\vec{\mathbf{u}} \parallel \mathbf{[111]}$ , one can write  $\vec{\mathbf{q}} = \vec{\mathbf{K}} / |\vec{\mathbf{K}}| = (1/\sqrt{3})(1,1,1)$  and  $\vec{\mathbf{u}} = (1/\sqrt{3})(1,1,1)$ , so that the corresponding deformation tensor  $\gamma^{(\mathbf{L})}$  takes the form

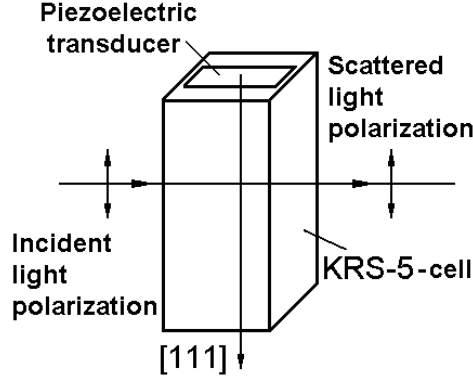


Figure 4.2. Crystallographic orientations for the piezoelectric transducer and the crystalline material in a **KRS-5**-cell.

$$\gamma^{(L)} = \frac{1}{2} (\bar{\mathbf{u}} \cdot \bar{\mathbf{q}} + \bar{\mathbf{q}} \cdot \bar{\mathbf{u}}) = \frac{1}{3} \begin{pmatrix} 1 & 1 & 1 \\ 1 & 1 & 1 \\ 1 & 1 & 1 \end{pmatrix}. \quad (4.1)$$

The tensor  $\gamma^{(L)}$  of the second rank with the components  $\gamma_{kl}^{(L)}$  ( $k, l=1, 2, 3$ ) can be converted into a 6-dimension vector  $\bar{\gamma}^{(L)} = (1/3) (1, 1, 1, 2, 2, 2)$  [4.7]. This expression for the deformation tensor makes it possible to estimate the velocity of the longitudinal wave. For this purpose one can use the tensor  $\mathbf{C}$  of elastic moduli of the second order. If now one will use the same procedure [4.7] and take the tensor  $\mathbf{C}$  of the fourth rank for the **KRS-5** crystal in the form of a 6 x 6 matrix, its components  $C_{\lambda\mu}$  will be non-zero only with  $C_{11} = C_{22} = C_{33}$ ,  $C_{44} = C_{55} = C_{66}$ , and  $C_{12} = C_{13} = C_{21} = C_{23} = C_{31} = C_{32}$ . Utilizing similar representation, one can find the corresponding effective elastic modulus of the second order

$$\mathbf{C}_2 = \gamma^{(L)} \mathbf{C} \gamma^{(L)} = \bar{\gamma}_\lambda^{(L)} C_{\lambda\mu} \bar{\gamma}_\mu^{(L)} = (1/3) (C_{11} + 2C_{12} + 4C_{44}), \quad (4.2)$$

which describes the velocity  $\mathbf{V}_L$  inherent in the selected pure elastic longitudinal mode as  $\mathbf{V}_L = \sqrt{C_2/\rho}$ , where  $\rho$  is the material density. One can use  $C_{11} = 3.4 \cdot 10^{11}$  dyne/cm<sup>2</sup>,  $C_{12} = 1.3 \cdot 10^{11}$  dyne/cm<sup>2</sup>,  $C_{44} = 0.58 \cdot 10^{11}$  dyne/cm<sup>2</sup>, and  $\rho = 7.37$  g/cm<sup>3</sup> peculiar to a **KRS-5** crystal and estimate  $\mathbf{V}_L = 1.92 \cdot 10^5$  cm/s. Together with this, one has to note that acoustic attenuation peculiar to this acoustic mode is not too low and is characterized by the factor  $\Gamma = 10$  dB/(cm GHz<sup>2</sup>) [4.8, 4.9].

Now, one is ready to estimate the efficiency of acousto-optical interaction associated with the above selected longitudinal elastic wave. By this is meant that the photo-elastic tensor  $\mathbf{p}$  of the fourth rank should be taken and converted into the form of a 6 x 6 matrix with the components  $p_{\lambda\mu}$ . For the cubic **KRS-5** crystal (symmetry group **m3m**), matrix representation for the tensor  $\mathbf{p}$  gives the following non-zero components:  $p_{11} = p_{22} = p_{33}$ ,  $p_{44} = p_{55} = p_{66}$ , and  $p_{12} = p_{13} = p_{21} = p_{23} = p_{31} = p_{32}$ . Consequently, one can calculate the matrix product  $\mathbf{p} \bar{\gamma}^{(L)} = (1/3) (p_{11} + 2p_{12}, p_{11} + 2p_{12}, p_{11} + 2p_{12}, 2p_{44}, 2p_{44}, 2p_{44})$  and convert it back to the form of a standard tensor ( $\mathbf{p} \gamma^{(L)}$ ) of the second rank [4.7]. The effective photo-elastic constant can be written from the scalar form

$$\mathbf{p}_{\text{eff}} = \bar{\mathbf{e}}_1 (\mathbf{p} \gamma^{(L)}) \bar{\mathbf{e}}_0 = \frac{1}{3} \bar{\mathbf{e}}_1 \begin{pmatrix} p_{11} + 2p_{12} & 2p_{44} & 2p_{44} \\ 2p_{44} & p_{11} + 2p_{12} & 2p_{44} \\ 2p_{44} & 2p_{44} & p_{11} + 2p_{12} \end{pmatrix} \bar{\mathbf{e}}_0, \quad (4.3)$$

where as before the vectors  $\bar{\mathbf{e}}_0$  and  $\bar{\mathbf{e}}_1$  describe the polarization states of incident and scattered light beams, respectively. Due to  $\bar{\mathbf{K}} \parallel [\mathbf{111}]$ , it is obvious that if the Bragg angles are omitted as small values, the wave vectors  $\bar{\mathbf{k}}_0$  and  $\bar{\mathbf{k}}_1$  of the incident and scattered light beams, respectively, should lie in the  $(\mathbf{111})$ -plane to be orthogonal to  $\bar{\mathbf{K}}$ . Moreover, one can put  $\bar{\mathbf{k}}_0 = \bar{\mathbf{k}}_1 = \bar{\mathbf{k}}$  when the Bragg angles are neglected. Due to optical isotropy of cubic **KRS – 5** crystal, one can select, for example,  $\bar{\mathbf{k}} \parallel [\mathbf{1}\bar{\mathbf{1}}\mathbf{0}]$ . In this particular case, one has an opportunity to consider the vectors  $\bar{\mathbf{e}}_0$  and  $\bar{\mathbf{e}}_1$  belonging to  $(\mathbf{1}\bar{\mathbf{1}}\mathbf{0})$ -plane, which includes  $[\mathbf{110}]$ ,  $[\mathbf{111}]$ , and  $[\mathbf{001}]$  axes; therewith the axes  $[\mathbf{110}]$  and  $[\mathbf{001}]$  give us an orthogonal basis, because  $[\mathbf{110}] \perp [\mathbf{001}]$ . In so doing, let us take at first the angles  $\alpha_{0,1}$  as current angles between  $\bar{\mathbf{e}}_{0,1}$  and the  $[\mathbf{001}]$ -axis. Consequently, one can easily obtain that  $\bar{\mathbf{e}}_{0,1} = \left( \sin \alpha_{0,1} / \sqrt{2}, \sin \alpha_{0,1} / \sqrt{2}, \cos \alpha_{0,1} \right)$ , so that  $\bar{\mathbf{e}}_{0,1} \parallel [\mathbf{001}]$  when  $\alpha_{0,1} = 0$ . Now, one can change the initial position for the vectors  $\bar{\mathbf{e}}_{0,1}$  via the substitution the angles  $\alpha_{0,1}$  by the new angles  $\alpha_{0,1} + \beta_1$ , where  $\beta_1 = \arccos(1/\sqrt{3})$ ; i.e. one can write

$$\bar{\mathbf{e}}_{0,1} = \left( \frac{1}{\sqrt{2}} \sin(\alpha_{0,1} + \beta_1), \frac{1}{\sqrt{2}} \sin(\alpha_{0,1} + \beta_1), \cos(\alpha_{0,1} + \beta_1) \right). \quad (4.4)$$

After such a substitution, one will have finally obtained that  $\bar{\mathbf{e}}_{0,1} \parallel [\mathbf{111}]$  when  $\alpha_{0,1} = 0$ . As usually, two regimes of light scattering can be realized. At first, one can consider the normal regime of scattering when  $\alpha_1 = \alpha_0$ . In this regime,

$$\mathbf{p}_{\text{eff}}^{(n)} = \frac{1}{3} \left\{ (\mathbf{p}_{11} + 2\mathbf{p}_{12} + 2\mathbf{p}_{44}) \sin^2(\alpha_0 + \beta_1) + 2\sqrt{2} \mathbf{p}_{44} \sin[2(\alpha_0 + \beta_1)] + (\mathbf{p}_{11} + 2\mathbf{p}_{12}) \cos^2(\alpha_0 + \beta_1) \right\}. \quad (4.5)$$

This formula can be simulated numerically with  $\mathbf{p}_{11} = 0.21$ ,  $\mathbf{p}_{12} = 0.22$ , and  $\mathbf{p}_{44} = 0.15$ , see Fig.4.3a. The oscillating plot exhibits a maximum magnitude  $\mathbf{p}_{\text{eff max}}^{(n)} = 0.417$  at  $\alpha_0 = \pi \mathbf{k}$ ,  $\mathbf{k} = \{\dots, -2, -1, 0, 1, 2, \dots\}$  and a minimum magnitude  $\mathbf{p}_{\text{eff min}}^{(n)} = 0.117$  at  $\alpha_0 = (\pi/2) + \pi \mathbf{k}$ . The second regime is associated with the anomalous light scattering when  $\alpha_1 = \alpha_0 + (\pi/2)$ . This regime is characterized by the formula

$$\mathbf{p}_{\text{eff}}^{(\text{an})} = \frac{\mathbf{p}_{44}}{3} \left\{ \sin[2(\alpha_0 + \beta_1)] + 2\sqrt{2} \cos[2(\alpha_0 + \beta_1)] \right\}. \quad (4.6)$$

This regime provides its maxima  $\mathbf{p}_{\text{eff max}}^{(\text{an})} = 0.15$  with  $\alpha_0 = (\pi/4) + (\pi \mathbf{k}/2)$ . The plots associated with these angular distributions for the effective photo-elastic constants in a **KRS – 5** single crystal are shown in Fig.4.3b. The maximal magnitude inherent in the corresponding figures of acousto-optical merit is related to the normal regime in a **KRS – 5** single crystal and equals to  $\mathbf{M}_2 = \mathbf{n}^6 (\mathbf{p}_{\text{eff max}}^{(n)})^2 / (\rho \mathbf{V}_L^3) \approx 930 \cdot 10^{-18} \text{ s}^3/\text{g}$  with  $\mathbf{n} = 2.57$  at the wavelength  $\lambda = 671 \text{ nm}$ . The performed calculations demonstrate that the normal regime of light scattering by the longitudinal elastic wave is a few times more efficient than the anomalous one.

The other side of estimating the efficiency of acousto-optic interaction is connected with choosing the regime of light scattering. The most efficient one is the Bragg regime, which is shown in fact in Fig.4.1a. It allows a 100% efficiency of light scattering and occurs with large enough length  $\mathbf{L}$  of interaction between light and acoustic waves when the dynamic acoustic diffractive grating is sufficiently thick. Such a regime can be realized only when the angle of light incidence on that acoustic grating meets the corresponding Bragg condition (which can be assumed to be

provided in advance) and the inequality  $Q = 2\pi\lambda L f_D^2 / (n V_L^2) \gg 1$  for the Klein-Cook factor  $Q$  [4.10] is satisfied. Taking, for example,  $\lambda = 671$  nm,  $L = 1.0$  cm, and  $V_L = 1.92 \cdot 10^5$  cm/s, one can estimate  $Q \geq 7$  for  $f_D > 40$  MHz. Thus, the Bragg regime of light scattering could be expected for the acoustic difference-frequencies at least exceeding **40** MHz in a **KRS – 5** single crystal, so that the acoustic frequency  $f_D = 40$  MHz can be considered as a lower limit for the Bragg regime of light scattering.

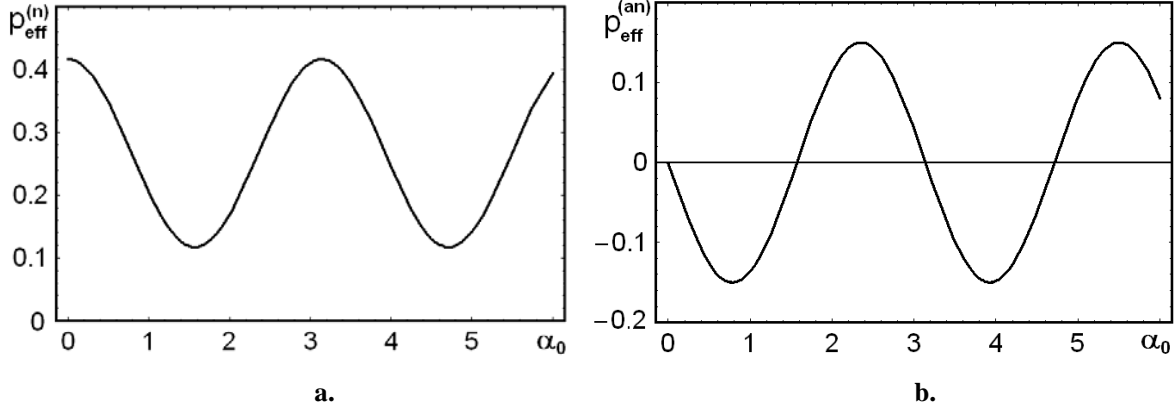


Figure 4.3. Absolute dependences for the effective photo-elastic constants in a **KRS – 5** single crystal versus the angle  $\alpha_0$  : normal light scattering (a) and anomalous light scattering (b).

### 4.3. EFFICIENCY OF THE CO-DIRECTIONAL COLLINEAR ACOUSTIC WAVE HETERODYNING

At this stage, effect of the second acoustic harmonic generation associated with the longitudinal elastic wave propagating along the **[111]**-axis in a **KRS – 5** single crystal is under consideration. It can be done using the Shapiro-Thurston equation [4.11] reduced down to terms of the third order in its general form

$$\rho \frac{\partial^2 \mathbf{u}_i}{\partial t^2} - C_{ijkl} \frac{\partial^2 \mathbf{u}_k}{\partial x_j \partial x_l} = \tilde{C}_{ijklqr} \frac{\partial \mathbf{u}_q}{\partial x_r} \frac{\partial^2 \mathbf{u}_k}{\partial x_j \partial x_l}, \quad (4.7)$$

$$\tilde{C}_{ijklqr} = C_{ijklqr} + C_{ijlq} \delta_{kr} + C_{ilrq} \delta_{jk} + C_{iklq} \delta_{jr}. \quad (4.8)$$

These equations include all the components. In the above-chosen case of propagating pure longitudinal elastic mode along the crystallographic axis **[111]** with  $\vec{\mathbf{K}} \parallel \vec{\mathbf{m}} \parallel [111]$ , see section 4.2, the directing cosines  $\mathbf{n}_i$  ( $i = 1, 2, 3$ ) should satisfy a pair of the following obvious conditions  $\mathbf{n}_1 = \mathbf{n}_2 = \mathbf{n}_3$  and  $\mathbf{n}_1^2 + \mathbf{n}_2^2 + \mathbf{n}_3^2 = 1$ , so that  $\mathbf{n}_i = 1/\sqrt{3}$ . Using Eqs.(4.7), (4.8), and after easy, but cumbersome algebraic calculations, one can obtain the following effective elastic modulus of the third order

$$C_3 = C_{111} + 2C_{123} + 6C_{112} + 12C_{144} + 16C_{456} + 24C_{155} + 9C_{11} + 18C_{12} + 36C_{44} \quad (4.9)$$

and (exploiting, for example, the data from Ref.[4.12]) conclude that the longitudinal elastic wave propagating along the **[111]**-axis is definitely capable of generating the second harmonic in a **KRS – 5** single crystal.

Now, one can introduce the new coordinate axis  $\mathbf{x}$  oriented along the **[111]** crystallographic axis of **KRS – 5**, so that  $\vec{\mathbf{x}} \parallel \vec{\mathbf{m}} \parallel [111]$  and Eq.(4.7) takes the form

$$\frac{\partial^2 \mathbf{u}}{\partial t^2} - \mathbf{V}_L^2 \frac{\partial^2 \mathbf{u}}{\partial \mathbf{x}^2} = \frac{C_3}{\rho} \frac{\partial \mathbf{u}}{\partial \mathbf{x}} \frac{\partial^2 \mathbf{u}}{\partial \mathbf{x}^2}. \quad (4.10)$$

The first term in Eq.(4.10) can be approximately converted within quasi-linear linear form of  $\partial \mathbf{u} / \partial t \approx -\mathbf{V}_L (\partial \mathbf{u} / \partial \mathbf{x})$  as  $\partial^2 \mathbf{u} / \partial t^2 \approx -\mathbf{V}_L (\partial^2 \mathbf{u} / \partial \mathbf{x} \partial t)$ . Then, using the obvious relation  $2(\partial \mathbf{u} / \partial \mathbf{x})(\partial^2 \mathbf{u} / \partial \mathbf{x}^2) = (\partial / \partial \mathbf{x})(\partial \mathbf{u} / \partial \mathbf{x})^2$ , one can integrate Eq.(4.10) with respect to  $\mathbf{x}$ . After that an additional phenomenological term  $\alpha \mathbf{V}_L \mathbf{u}$  can be included to take into account linear acoustic losses, which are physically characterized by the amplitude decrement  $\alpha [\mathbf{cm}^{-1}]$  reflecting usually just the square-law frequency dispersion of losses in solids. As a result, one can write

$$\frac{\partial \mathbf{u}}{\partial t} + \mathbf{V}_L \frac{\partial \mathbf{u}}{\partial \mathbf{x}} + \alpha \mathbf{V}_L \mathbf{u} = \frac{\Gamma}{2} \mathbf{V}_L \left( \frac{\partial \mathbf{u}}{\partial \mathbf{x}} \right)^2, \quad (4.11)$$

where  $\Gamma = -C_3 / C_2$ ,  $\mathbf{V}_L = \sqrt{C_2 / \rho}$ , and  $C_2 = (C_{11} + 2C_{12} + 4C_{44}) / 3$  is the elastic modulus of the second order for  $\bar{\mathbf{x}} \parallel \bar{\mathbf{m}} \parallel [111]$ . A one-dimensional wave equation (4.11) for the complex amplitude of elastic wave is peculiar for characterizing a three-wave mixing in a medium with linear dispersive losses and square-law nonlinearity. Because of a square-law dispersion of acoustic losses, the complex amplitude  $\mathbf{u}$  can be taken in the form of a superposition of only a triplet of waves including the pump, the signal wave, and the difference-frequency wave, namely,  $\mathbf{u} = \mathbf{u}_P + \mathbf{u}_S + \mathbf{u}_D$ , while the second harmonics of both the pump and the signal wave as well as their sum-frequency component can be omitted in this project of the chosen solution. Starting, for example, from the pump, one can write the corresponding complex amplitude as  $\mathbf{u}_P(\mathbf{x}, t) = \mathbf{A}_P(\mathbf{x}) \exp[i(\mathbf{k}_P \mathbf{x} - \omega_P t)] + \mathbf{A}_P^*(\mathbf{x}) \exp[-i(\mathbf{k}_P \mathbf{x} - \omega_P t)]$  and note its losses as  $\alpha_P$ . Substituting this formula into the left hand side of Eq.(4.11), one can calculate

$$\mathbf{V}_L^{-1} \frac{\partial \mathbf{u}_P}{\partial t} + \frac{\partial \mathbf{u}_P}{\partial \mathbf{x}} + \alpha_P \mathbf{u} = \left[ \alpha_P \mathbf{A}_P + \frac{d\mathbf{A}_P}{d\mathbf{x}} \right] \exp[i(\mathbf{k}_P \mathbf{x} - \omega_P t)] + \left[ \alpha_P \mathbf{A}_P^* + \frac{d\mathbf{A}_P^*}{d\mathbf{x}} \right] \exp[-i(\mathbf{k}_P \mathbf{x} - \omega_P t)]. \quad (4.12)$$

It is seen that the relations analogous to Eq.(4.12) can be obtained for the signal and difference-frequency waves. To construct the contribution  $(\partial \mathbf{u} / \partial \mathbf{x})^2$  in the right hand side of Eq.(4.11) one has to estimate the summands. Applying the slowly varying amplitudes technique, one has to take into account the inequalities  $|d\mathbf{A}_j(\mathbf{x}) / d\mathbf{x}| \ll \mathbf{k}_j |\mathbf{A}_j(\mathbf{x})|$ ,  $\mathbf{j} \in \{P, S, D\}$ . Consequently, the following approximation appears

$$\begin{aligned} \left( \frac{\partial \mathbf{u}}{\partial \mathbf{x}} \right)^2 \approx & \left( \mathbf{i} \mathbf{k}_P \left\{ \mathbf{A}_P(\mathbf{x}) \exp[i(\mathbf{k}_P \mathbf{x} - \omega_P t)] - \mathbf{A}_P^*(\mathbf{x}) \exp[-i(\mathbf{k}_P \mathbf{x} - \omega_P t)] \right\} + \right. \\ & + \mathbf{i} \mathbf{k}_S \left\{ \mathbf{A}_S(\mathbf{x}) \exp[i(\mathbf{k}_S \mathbf{x} - \omega_S t)] - \mathbf{A}_S^*(\mathbf{x}) \exp[-i(\mathbf{k}_S \mathbf{x} - \omega_S t)] \right\} + \\ & \left. + \mathbf{i} \mathbf{k}_D \left\{ \mathbf{A}_D(\mathbf{x}) \exp[i(\mathbf{k}_D \mathbf{x} - \omega_D t)] - \mathbf{A}_D^*(\mathbf{x}) \exp[-i(\mathbf{k}_D \mathbf{x} - \omega_D t)] \right\} \right)^2. \end{aligned} \quad (4.13)$$

Now, one has to consider two different regimes of a three-wave mixing. The right hand sides of Eqs.(4.12) and (4.13) give

1)  $\mathbf{f}_S = \mathbf{f}_P + \mathbf{f}_D$ :

$$\text{a) } \frac{d\mathbf{A}_S}{d\mathbf{x}} + \alpha_S \mathbf{A}_S = \beta_S \mathbf{A}_D \mathbf{A}_P, \quad \text{b) } \frac{d\mathbf{A}_P}{d\mathbf{x}} + \alpha_P \mathbf{A}_P = -\beta_P \mathbf{A}_D^* \mathbf{A}_S, \quad \text{c) } \frac{d\mathbf{A}_D}{d\mathbf{x}} + \alpha_D \mathbf{A}_D = -\beta_D \mathbf{A}_P^* \mathbf{A}_S; \quad (4.14)$$

2)  $\mathbf{f}_P = \mathbf{f}_S + \mathbf{f}_D$ :

$$\text{a) } \frac{d\mathbf{A}_P}{dx} + \alpha_P \mathbf{A}_P = \beta_P \mathbf{A}_D \mathbf{A}_S, \quad \text{b) } \frac{d\mathbf{A}_S}{dx} + \alpha_S \mathbf{A}_S = -\beta_S \mathbf{A}_D^* \mathbf{A}_P, \quad \text{c) } \frac{d\mathbf{A}_D}{dx} + \alpha_D \mathbf{A}_D = -\beta_D \mathbf{A}_S^* \mathbf{A}_P. \quad (4.15)$$

where  $\beta_S = 0.5 \Gamma \mathbf{k}_P \mathbf{k}_D$ ,  $\beta_P = 0.5 \Gamma \mathbf{k}_S \mathbf{k}_D$ , and  $\beta_D = 0.5 \Gamma \mathbf{k}_P \mathbf{k}_S$  are the coupling factors. At this step, one can take  $\mathbf{A}_{D,S,P} = \mathbf{a}_{D,S,P} \exp[i(\varphi_{D,S,P})]$ , where  $\mathbf{a}_{D,S,P}$  and  $\varphi_{D,S,P}$  are the real-valued amplitudes and phases of non-optical waves. Let us consider, for example, Eqs.(4.14) governing the system in a regime of  $\mathbf{f}_S = \mathbf{f}_P + \mathbf{f}_D$  with  $\text{sign}(\mathbf{f}_P - \mathbf{f}_S) = -1$ . Dividing real and imaginary parts in Eqs.(4.14), one can find two groups of the real-valued equations

$$\begin{aligned} \text{a) } \frac{d\mathbf{a}_S}{dx} + \alpha_S \mathbf{a}_S &= \beta_S \mathbf{a}_D \mathbf{a}_P \cos(\varphi_S - \varphi_D - \varphi_P), & \text{b) } \frac{d\mathbf{a}_D}{dx} + \alpha_D \mathbf{a}_D &= -\beta_D \mathbf{a}_S \mathbf{a}_P \cos(\varphi_S - \varphi_D - \varphi_P), \\ \text{c) } \frac{d\mathbf{a}_P}{dx} + \alpha_P \mathbf{a}_P &= -\beta_P \mathbf{a}_D \mathbf{a}_S \cos(\varphi_S - \varphi_D - \varphi_P); \end{aligned} \quad (4.16)$$

$$\begin{aligned} \text{a) } \frac{d\varphi_S}{dx} \mathbf{a}_S &= \beta_S \mathbf{a}_D \mathbf{a}_P \sin(\varphi_S - \varphi_D - \varphi_P), & \text{b) } \frac{d\varphi_D}{dx} \mathbf{a}_D &= -\beta_D \mathbf{a}_S \mathbf{a}_P \sin(\varphi_S - \varphi_D - \varphi_P), \\ \text{c) } \frac{d\varphi_P}{dx} \mathbf{a}_P &= -\beta_P \mathbf{a}_D \mathbf{a}_S \sin(\varphi_S - \varphi_D - \varphi_P). \end{aligned} \quad (4.17)$$

Equations (4.16) and (4.17) can be analyzed with the natural for similar problems boundary conditions  $\mathbf{U}_P \neq \mathbf{0}$ ,  $\mathbf{U}_S \neq \mathbf{0}$ , and  $\mathbf{U}_D = \mathbf{0}$ , where  $\mathbf{U}_{P,S,D} = \mathbf{A}_{P,S,D}(\mathbf{x} = \mathbf{0})$ . With these conditions, one can find from Eq.(4.16b) that  $\frac{d\mathbf{a}_D}{dx}(\mathbf{x} = \mathbf{0}) = -\beta_D \mathbf{U}_P \mathbf{U}_S$ . Here, the following quite natural approximation can be done; namely, let us put  $\mathbf{a}_P \gg \mathbf{a}_S, \mathbf{a}_D$  almost everywhere in an area of interaction. In this particular case, Eq.(4.16c) can be solved in a given field approximation as  $\mathbf{a}_P = \mathbf{U}_P \exp(-\alpha_P \mathbf{x})$ , while Eq.(4.17c) gives  $\frac{d\varphi_P}{dx} = \mathbf{0}$ . Substituting these solutions into Eqs.(4.16) and (4.17) and dividing real and imaginary parts, one can obtain

$$\begin{aligned} \text{a) } \frac{d\mathbf{a}_S}{dx} + \alpha_S \mathbf{a}_S &= \beta_S \mathbf{a}_D \mathbf{U}_P \exp(-\alpha_P \mathbf{x}) \cos \varphi, & \text{b) } \frac{d\mathbf{a}_D}{dx} + \alpha_D \mathbf{a}_D &= -\beta_D \mathbf{a}_S \mathbf{U}_P \exp(-\alpha_P \mathbf{x}) \cos \varphi; \\ \text{c) } \frac{d\varphi}{dx} &= \mathbf{U}_P \exp(-\alpha_P \mathbf{x}) \sin \varphi \left( \beta_D \frac{\mathbf{a}_S}{\mathbf{a}_D} - \beta_S \frac{\mathbf{a}_D}{\mathbf{a}_S} \right), & \text{d) } \varphi &= \varphi_S - \varphi_P - \varphi_D. \end{aligned} \quad (4.18)$$

From the first integral of Eqs.(4.18), with allowance for the boundary condition  $\mathbf{a}_D(\mathbf{x} = \mathbf{0}) = \mathbf{0}$ , which is characteristic of wave heterodyning, one can find that  $d\varphi/dx \equiv \mathbf{0}$  and  $\sin \varphi \equiv \mathbf{0}$ , so that one can take, for example,  $\cos \varphi = \mathbf{1}$ . Equations (4.15), associated with the regime  $\mathbf{f}_P = \mathbf{f}_S + \mathbf{f}_D$  with  $\text{sign}(\mathbf{f}_P - \mathbf{f}_S) = +1$ , can be analyzed by similar way via substituting  $\beta_S \rightarrow -\beta_S$ . Consequently, Eqs.(4.18a) and (4.18b) give two following pairs of the combined ordinary differential equations of the first order

$$\text{a) } \frac{d\mathbf{a}_S}{dx} + \alpha_S \mathbf{a}_S = -\text{sign}(\mathbf{f}_P - \mathbf{f}_S) \beta_S \mathbf{a}_D \mathbf{U}_P \exp(-\alpha_P \mathbf{x}), \quad \text{b) } \frac{d\mathbf{a}_D}{dx} + \alpha_D \mathbf{a}_D = -\beta_D \mathbf{a}_S \mathbf{U}_P \exp(-\alpha_P \mathbf{x}). \quad (4.19)$$

Excluding  $\mathbf{a}_S$  from Eqs.(4.19), one can write a linearized version for the needed second order ordinary differential equation

$$\frac{d^2 \mathbf{a}_D}{dx^2} + (\alpha_P + \alpha_S + \alpha_D) \frac{d\mathbf{a}_D}{dx} + \left[ \alpha_D (\alpha_P + \alpha_S) - \text{sign}(f_P - f_S) \beta_S \beta_D U_P^2 \exp(-2\alpha_P x) \right] \mathbf{a}_D = 0. \quad (4.20)$$

Due to the above-mentioned dispersion of losses included in the factors  $\alpha_P$ ,  $\alpha_S$ , and  $\alpha_D$ , one can extract their square-law proportionalities to the corresponding carrier frequencies of acoustic waves  $\alpha_{P,S,D} \sim f_{P,S,D}^2$  and write

$$\text{a) } \alpha_P + \alpha_S + \alpha_D = 2\alpha_P [1 + \delta \text{sign}(f_P - f_S) + \delta^2], \quad \text{b) } \alpha_P + \alpha_S - \alpha_D = 2\alpha_P [1 + \delta \text{sign}(f_P - f_S)], \quad (4.21)$$

with  $\delta = f_D/f_P \ll 1$ . Introducing the notations  $\mathbf{g} = -\delta \text{sign}(f_P - f_S) + \delta^2$ , and  $\mathbf{h} = \delta \text{sign}(f_P - f_S)$ , so that  $\mathbf{g} \approx -\mathbf{h}$  due to the smallness of  $\delta$ , one can express the exact solution to Eq.(4.20) in terms of the Bessel functions as

$$\mathbf{a}_D(x) = \exp[-\alpha_P x (1 + \mathbf{g})] \left\{ C_1 Z_{(\mathbf{h}-1)}[\xi \exp(-\alpha_P x)] + C_2 Z_{(1-\mathbf{h})}[\xi \exp(-\alpha_P x)] \right\}, \quad (4.22)$$

where  $\xi = \alpha_P^{-1} U_P \sqrt{\beta_S \beta_D}$  is the normalized acoustic wave amplitude. Then,  $Z_{\mathbf{v}} = J_{\mathbf{v}}$  when  $f_P < f_S$  and  $\text{sign}(f_P - f_S) = -1$ , while  $Z_{\mathbf{v}} = I_{\mathbf{v}}$  with  $f_P > f_S$  and  $\text{sign}(f_P - f_S) = +1$ ; for example, see [4.13]. Exploiting the above-mentioned boundary conditions for  $\mathbf{a}_D$  and its spatial derivative, one can determine the constants  $C_{1,2}$  of integration in Eq.(4.22) as

$$\text{a) } C_1 = \left( \frac{-2 \beta_D U_P U_S}{\alpha_P \xi} \right) \frac{Z_{(1-\mathbf{h})}(\xi)}{W(\xi, \mathbf{h})}, \quad \text{b) } C_2 = \left( \frac{2 \beta_D U_P U_S}{\alpha_P \xi} \right) \frac{Z_{(\mathbf{h}-1)}(\xi)}{W(\xi, \mathbf{h})}, \quad (4.23)$$

$$W(\xi, \mathbf{h}) = Z_{(1-\mathbf{h})}(\xi) [Z_{(\mathbf{h}-2)}(\xi) + \text{sign}(f_P - f_S) Z_{(\mathbf{h})}(\xi)] - Z_{(\mathbf{h}-1)}(\xi) [Z_{(-\mathbf{h})}(\xi) + \text{sign}(f_P - f_S) Z_{(2-\mathbf{h})}(\xi)] \quad (4.24)$$

Thus, Eqs.(4.22) – (4.24) represent the solution describing the spatial distribution for the difference-frequency acoustic wave along the acousto-optical cell exploiting collinear acoustic wave heterodyning. In the noted above particular cases, Eq.(4.24) can be simplified as  $W(\xi, \mathbf{h}) = -4(\pi \xi)^{-1} \sin(\pi \delta) \text{sign}(f_P - f_S)$ , so that one can write

1)  $f_S = f_P + f_D$ ,  $\text{sign}(f_P - f_S) = -1$ :

$$\mathbf{a}_D(\alpha_P x) = \frac{\pi \beta_D U_P U_S \left\{ J_{(-\delta-1)}(\xi) J_{(1+\delta)}[\xi \exp(-\alpha_P x)] - J_{(1+\delta)}(\xi) J_{(-\delta-1)}[\xi \exp(-\alpha_P x)] \right\}}{2\alpha_P \sin(\pi \delta) \exp[\alpha_P x (1 + \delta + \delta^2)]}; \quad (4.25)$$

2)  $f_P = f_S + f_D$ ,  $\text{sign}(f_P - f_S) = +1$ :

$$\mathbf{a}_D(\alpha_P x) = \frac{\pi \beta_D U_P U_S \left\{ I_{(1-\delta)}(\xi) I_{(\delta-1)}[\xi \exp(-\alpha_P x)] - I_{(\delta-1)}(\xi) I_{(1-\delta)}[\xi \exp(-\alpha_P x)] \right\}}{2\alpha_P \sin(\pi \delta) \exp[\alpha_P x (1 - \delta + \delta^2)]}; \quad (4.26)$$

The amplitude distributions, which are inherent in the difference-frequency acoustic wave components and normalized by the factor  $\pi \beta_D U_P U_S / (2\alpha_P)$ , for the same pairs of the normalized acoustic wave amplitudes  $\xi$  are presented in Figs.4.4 and 4.5.

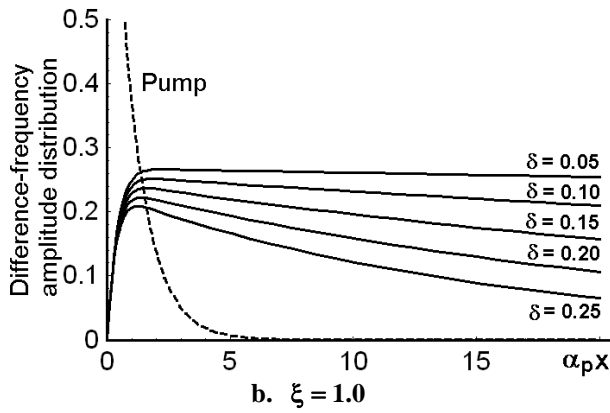
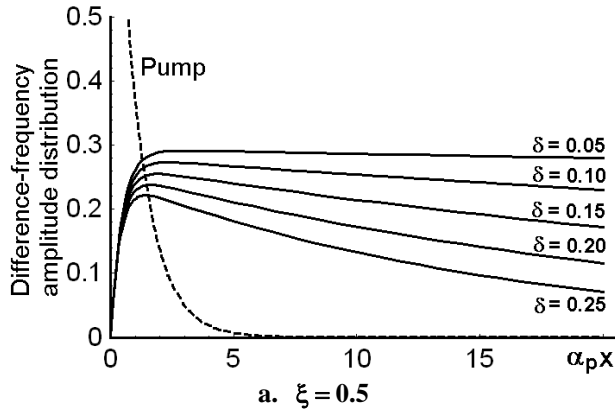


Figure 4.4. The normalized amplitudes for the difference-frequency acoustic waves versus the product  $\alpha_p x$  when  $f_S = f_P + f_D$ .

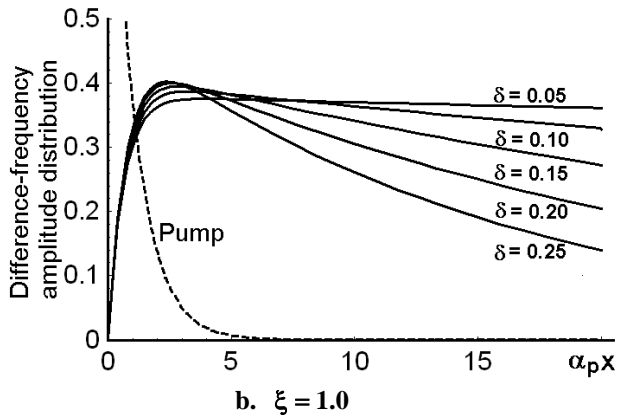
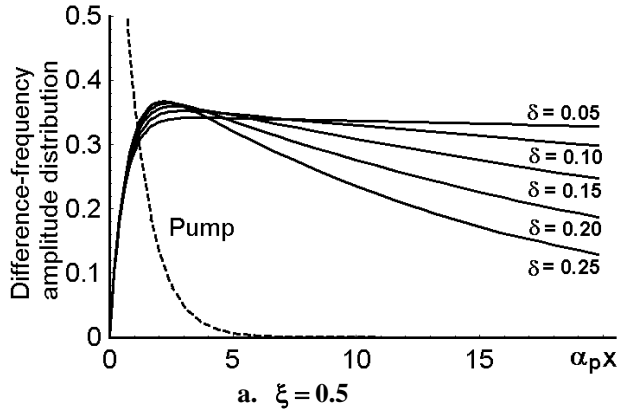


Figure 4.5. The normalized amplitudes for the difference-frequency acoustic waves versus the product  $\alpha_p x$  when  $f_P = f_S + f_D$ .

#### 4.4. ESTIMATING THE FREQUENCY POTENTIALS PECULIAR TO A MULTI-CHANNEL DIRECT OPTICAL SPECTRUM ANALYSIS WITH A KRS-5 CELL

Potential frequency limitations can be analyzed within nonlinear acoustic mechanisms of collinear heterodyning. Without the loss of generality, let us take Eq.(4.25) for further analysis at length. This equation, related as before to the case of  $f_S = f_P + f_D$ , can be rewritten with  $z = \alpha_p x$  as

$$a) a_D(z) = F_D \Phi(z, \delta, \xi), \quad b) F_D = \frac{\pi \beta_D U_P U_S}{2\alpha_P}, \quad (4.27)$$

$$c) \Phi(z, \delta, \xi) = \frac{J_{(-\delta-1)}(\xi) J_{(1+\delta)}[\xi \exp(-z)] - J_{(1+\delta)}(\xi) J_{(-\delta-1)}[\xi \exp(-z)]}{\sin(\pi\delta) \exp[z(1+\delta+\delta^2)]}.$$

At this stage, the coordinate  $z_m$  of a maximum of the amplitude function  $\Phi(z, \delta, \xi)$  has to be found. For this purpose, one has to analyze the condition  $[d\Phi(z_m, \delta, \xi)/dz] = 0$ . The condition of existing a maximum for  $\Phi(z, \delta, \xi)$  takes the form

$$\begin{aligned} & \mathbf{J}_{(-1-\delta)}(\xi) \left\{ \delta^2 \mathbf{J}_{(1+\delta)}[\xi \exp(\mathbf{z}_m)] + \xi \exp(\mathbf{z}_m) \mathbf{J}(\delta)[\xi \exp(\mathbf{z}_m)] \right\} - \\ & - \mathbf{J}_{(1+\delta)}(\xi) \left\{ \delta^2 \mathbf{J}_{(-1-\delta)}[\xi \exp(\mathbf{z}_m)] - \xi \exp(\mathbf{z}_m) \mathbf{J}(-\delta)[\xi \exp(\mathbf{z}_m)] \right\} = 0 . \end{aligned} \quad (4.28)$$

This condition can be easily analyzed numerically within considering  $\delta$  and  $\mathbf{z}_m$  as the independent and dependent variables, while  $\xi$  plays the role a discrete independent parameter. One can find from Eq.(4.28) that:

$$\begin{aligned} \text{a) } & \mathbf{z}_m(\delta, \xi = 0.5) \approx 2.66 - 2.1 \cdot 10^{-4} \delta^{-2} + 0.0405 \delta^{-1} - 8.17 \delta + 10.3 \delta^2 , \\ \text{b) } & \mathbf{z}_m(\delta, \xi = 1.0) \approx 2.587 - 6.0 \cdot 10^{-6} \delta^{-2} + 0.0016 \delta^{-1} - 8.26 \delta + 11.4 \delta^2 , \end{aligned} \quad (4.29)$$

see Fig.4.6a. These formulas are rather important practically because they make it possible to estimate potential frequency limitations for optical spectrum analysis.

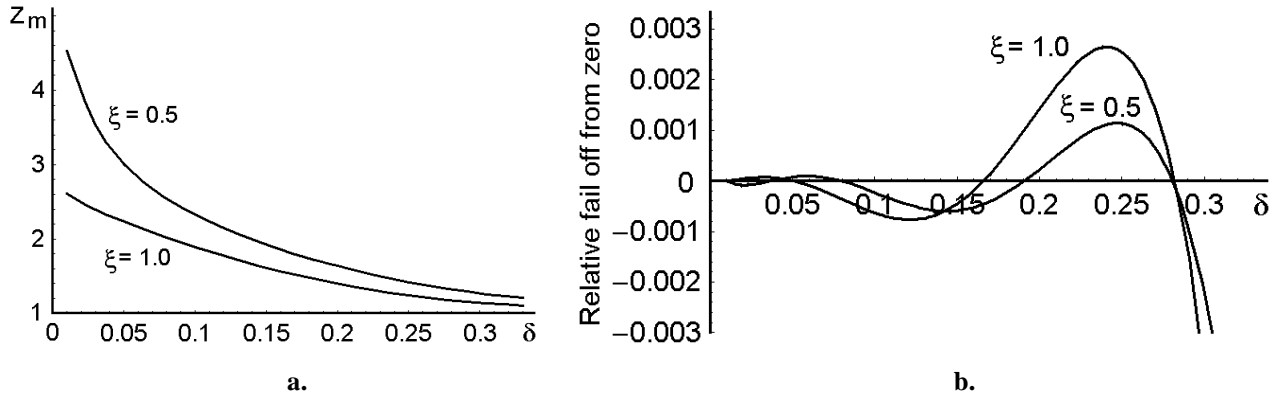


Figure 4.6. The plots (a) determine the coordinate  $\mathbf{z}_m$  as an approximate function of the frequency ratio  $\delta$  from numerical solution to Eq.(4.28), while curves (b) characterize the relative accuracy of approximate plots in Fig.4.6a.

On the one hand side, substituting the obtained  $\mathbf{z}_m(\delta, \xi)$  into Eq.(4.28) allows us, first, to estimate the accuracy of the performed approximations. Figure 4.6b illustrates the closeness of the derivative  $\mathbf{d}\Phi[\mathbf{z}_m(\delta, \xi), \delta, \xi]/\mathbf{d}\mathbf{z}$  to zero in terms of its relative fail off from zero for two particular cases of  $\xi = 0.5$  and  $\xi = 1.0$ . One can see from Fig.4.6b that maximal value of an error does not exceed **0.3%** within  $\delta \in [0.01; 0.30]$ . Then, Figs.4.4 and 4.5 exhibit a non-uniformity of distributing signals associated with various difference-frequency acoustic components inside the cell, so that a larger non-uniformity is associated with the component of a higher value of  $\delta$ . Thus, one can take the upper-difference frequency component and restrict itself by an upper value  $\delta_U$  of the parameter  $\delta$ . Then, substituting the obtained  $\mathbf{z}_m(\delta_U, \xi)$  into  $\Phi(\mathbf{z}, \delta, \xi)$  makes it possible to formulate the requirement to the cell's optical aperture. One can take it as follows: decreasing the normalized acoustic field distribution down to a level of  $-3$  dB along the cell's optical aperture at a point  $\mathbf{z}_D(\delta_U, \xi)$  gives the equality

$$\Phi^2[\mathbf{z}_D(\delta_U, \xi), \delta_U, \xi] = 0.5 \Phi^2[\mathbf{z}_m(\delta_U, \xi), \delta_U, \xi] \quad (4.30)$$

in terms of the intensities. In fact, the value of  $\mathbf{z}_D(\delta_U, \xi)$  determines the total geometric length  $\mathbf{x}_D(\delta_U, \xi)$  of acousto-optical cell with the collinear wave heterodyning. Then, one can explain  $\mathbf{x}_{m,D} = \alpha_P^{-1} \mathbf{z}_{m,D}$  and obtain

$$\mathbf{D} = \mathbf{x}_D(\delta_U, \xi) - \mathbf{x}_m(\delta_U, \xi), \quad (4.31)$$

where  $\mathbf{D}$  is the really operating part of the cell's optical aperture available for parallel optical processing at given  $\xi$  and some range of the parameter  $\delta$ . Nevertheless, it is seen from Figs.4.4 and 4.5 that the normalized intensity distributions  $\Phi^2(z, \delta, \xi)$  are the obviously decreasing functions of the parameter  $\delta$ . As a result, similar dependences on  $\delta$  lead to a non-uniformity of distributing signals associated with various difference-frequency components inside the cell. Moreover, this non-uniformity is as larger as higher is the corresponding parameter  $\delta$ , so that the lowest magnitude  $\delta_L$  of the parameter  $\delta$  leads to almost uniform acoustic signal distribution along the cell's optical aperture. Together with this, Figs.4.4 and 4.5 show that as higher is the parameter  $\delta$ , as lower is the absolute maximum of the corresponding dependence, and, consequently, the corresponding frequency components have to be adequately preamplified. Under these circumstances, one can suggest the following criterion for such a pre-amplification, namely, let us equalize various frequency components in a central vicinity of the above-noted operating part  $\mathbf{D}$  inherent in the cell's optical aperture. In so doing, one can suggest re-normalizing maximal intensity determined by the expression

$$\Phi_m^2[z_m(\delta, \xi), \delta, \xi, G] = \frac{G}{z_m(\delta, \xi)} \Phi^2[z_m(\delta, \xi), \delta, \xi] \quad (4.32)$$

with possible linear gain  $G$ , whose magnitude can be taken rather arbitrary. The corresponding distributions, both allowing  $\delta_U$  up to **0.35** and  $\delta_L$  down to **0.05**, are presented in Fig 4.7 in the particular case of, for instance,  $G = 4$ . This diagram illustrates the simplest (and definitely non-optimized) possibility of the above-noted equalizing the frequency components involved.

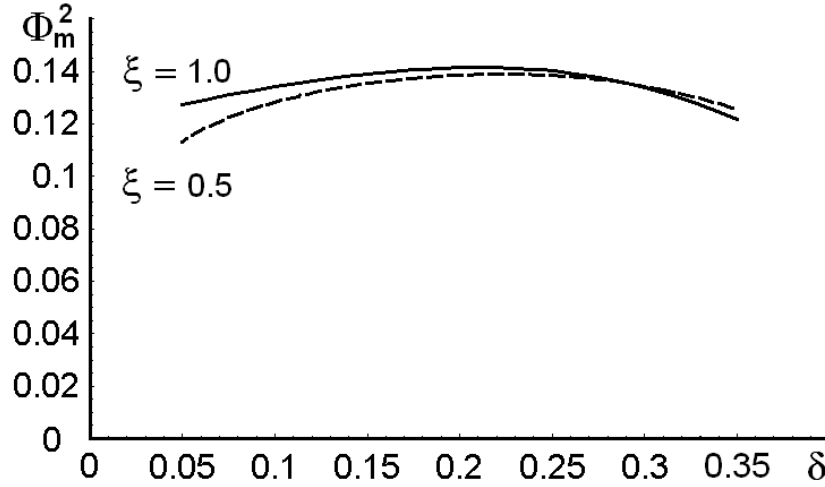


Figure 4.7. Re-normalized maximal intensities  $\Phi_m^2[z_m(\delta), \delta, \xi]$  versus the parameter  $\delta$  with  $G = 4$ : the dashed line is for  $\xi = 0.5$ , while the solid line is for  $\xi = 1.0$ .

Then, one can consider the re-normalized spatial intensity distributions

$$\Phi_0^2(z, \delta, \xi) = \frac{G}{z_m(\delta)} \Phi^2(z, \delta, \xi) \quad (4.33)$$

along the cell's aperture. These distributions are depicted in Fig.4.8 in the same particular case of  $G = 4$  together with the magnitudes  $\delta_U = 0.17$  and  $\delta_L = 0.034$ , taken for example as well as in a view of the further consideration.

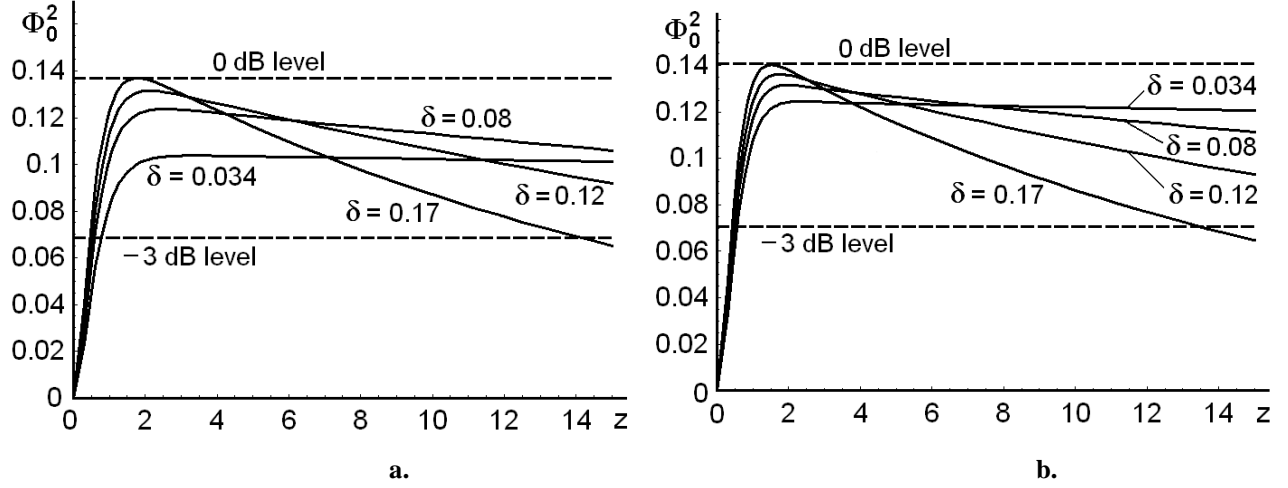


Figure 4.8. Re-normalized spatial intensity distributions  $\Phi_0^2(z, \delta, \xi)$  along the cell's aperture with  $G = 4$  for various  $\delta$ : (a) is for  $\xi = 0.5$  and (b) is for  $\xi = 1.0$ .

Taking into account Eq.(4.30), one can find from Fig.4.8 that the really operating part  $\mathbf{D}$  of the cell's optical aperture available for parallel optical processing in Eq.(4.31) is practically independent on the magnitude of  $\xi$ . Very slight dependence on  $\xi$  manifests itself mainly in concrete localization of  $\mathbf{D}$  within total aperture of the cell. However, this dependence is rather weak as it follows from the data in Fig.4.8, so that potentially it could be neglected in practice.

At this point, an opportunity exists to simplify the process of determining the value of  $\mathbf{x}_D(\delta_U, \xi)$ . In so doing, let us rewrite Eq.(4.27b) as  $\Phi(z, \delta, \xi) = \Phi_1 + \Phi_2$ , where:

$$\begin{aligned} \text{a) } \Phi_1(z, \delta, \xi) &= \frac{J_{(-\delta-1)}(\xi) J_{(1+\delta)}[\xi \exp(-z)]}{\sin(\pi\delta) \exp[z(1+\delta+\delta^2)]}, \\ \text{b) } \Phi_2(z, \delta, \xi) &= \frac{-J_{(1+\delta)}(\xi) J_{(-\delta-1)}[\xi \exp(-z)]}{\sin(\pi\delta) \exp[z(1+\delta+\delta^2)]}. \end{aligned} \quad (4.34)$$

Comparisons of these contributions to the right from the planes  $\mathbf{z}_m(\delta)$  in two chosen above cases of  $\xi = 0.5$  and  $\xi = 1.0$  are presented in Fig.4.9. It is clearly seen from Fig.4.9 that  $\Phi_1 \rightarrow 0$  and  $\Phi_1 \ll \Phi_2$  in those areas, so that one can motivatively take the reduced form of  $\Phi(z, \delta, \xi)$  and put  $\Phi(z, \delta, \xi) \approx \Phi_2(z, \delta, \xi)$  within at least  $z \geq 2z_m(\delta, \xi)$  in Eq.(4.27b) and take the reduced, but well-approximated form of Eq.(4.27a)

$$\mathbf{a}_{DR}(z) = - \left( \frac{\pi \beta_D U_P U_S}{2\alpha_P} \right) \frac{J_{(1+\delta)}(\xi) J_{(-\delta-1)}[\xi \exp(-z)]}{\sin(\pi\delta) \exp[z(1+\delta+\delta^2)]}; \quad (4.35)$$

The corresponding contributions after substituting  $\Phi(z, \delta, \xi) \approx \Phi_2(z, \delta, \xi)$  in Eq.(4.33), i.e. after normalizing, are presented in Fig.4.10 with  $\delta = 0.17$  in the cases of  $\xi = 0.5$  and  $\xi = 1.0$  under discussion.

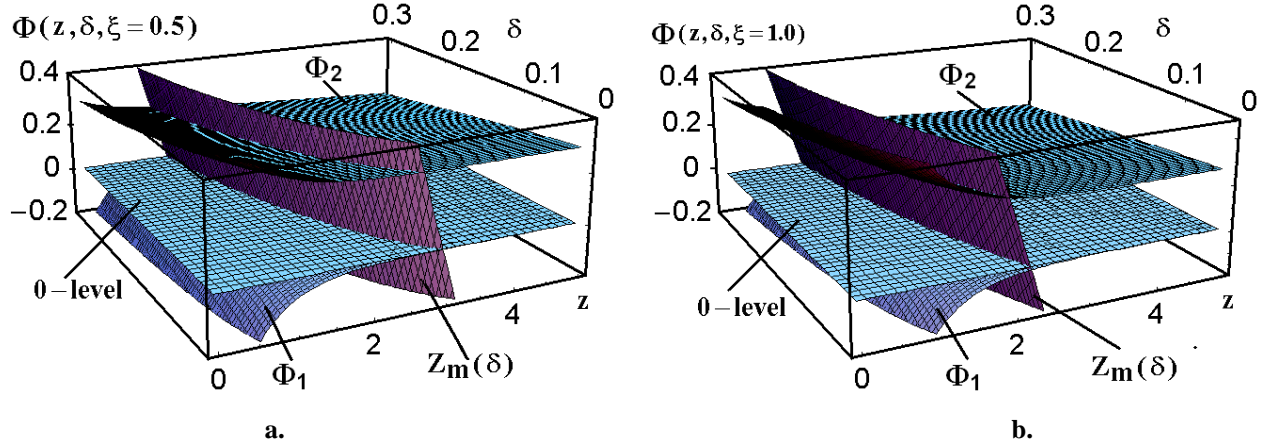


Figure 4.9. Comparing the contributions of the terms  $\Phi_1$  and  $\Phi_2$  from Eq.(4.34) to the right of the plane  $z_m(\delta, \xi)$  with: (a)  $\xi = 0.5$  and (b)  $\xi = 1.0$ ; the 0 dB-levels are shown as well for a convenience.

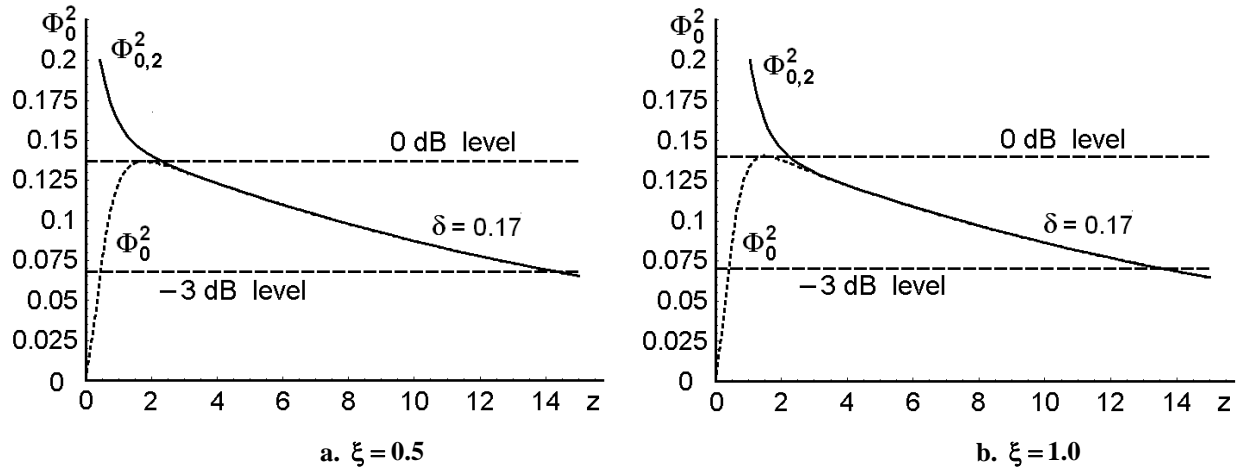


Figure 4.10. Coinciding the terms  $\Phi_0^2$  and  $\Phi_{0,2}^2$  obtained from Eqs.(4.33) and (4.34) to the right of the area  $2z_m(\delta, \xi)$  with  $G = 4$ ,  $\delta = 0.17$  and: (a)  $\xi = 0.5$  and (b)  $\xi = 1.0$ . The 0 dB and -3 dB levels are shown as well.

Now, let us direct our attention to the particular case of a **KRS-5** crystalline cell with  $\Gamma_0 = 10$  dB/(cm GHz<sup>2</sup>) and practically operating optical aperture  $D = 5.0$  cm and make a few practical estimations. At first, to provide higher operating frequencies inherent in the cell under consideration together with the simplicity of realizing a low-frequency pump, it looks preferable to choose an area of  $f_S = f_P + f_D$  and  $\text{sign}(f_P - f_S) = -1$  related to Eq.(4.25) in spite of the fact that this area is more sensitive to variations of the parameter  $\delta$ , see Fig.4.4. Applying Eq.(4.35) and Figs.(4.10), one can find that the upper difference-frequency about  $f_{UD} \approx 250$  MHz provides approximately a **3 dB**-level of acoustic losses along the taken optical aperture  $D \approx 5.0$  cm of the cell. It should be noted at this step that the numerical estimations adduced here should be considered as rather simplified illustrations, while practically notable technical calculations have to be performed much more precisely, of course. Nevertheless, one can say that these estimations reflect the proposed principle of operation in the full measure. Due to the upper magnitude of  $\delta$  in this case is  $\delta_U = 0.17$ , as it follows also from Figs.4.10, and initial determination of the parameter  $\delta$  gives  $f_{UD} / \delta_U = f_P$ , one can find that the pump frequency will be  $f_P = 1470$  MHz and the upper signal frequency will be

$f_{US} = 1720$  MHz. Then, one can choose the bandwidth  $\Delta f$  of spectrum analysis, for example, in the range of **200** MHz, which leads to the lower difference-frequency  $f_{LD} = 50$  MHz restricted by the Bragg regime condition, see the corresponding estimation at the end of section 4.2. Consequently, the lower signal frequency is  $f_{LS} = 1520$  MHz, and the lower magnitude of the parameter  $\delta$  is  $\delta_L = 0.034$ . These estimations are conditioned by the relations

$$\text{a) } f_{UD} = f_{US} - f_P = f_P \delta_U, \quad \text{b) } f_{LD} = f_{LS} - f_P = f_P \delta_L, \quad (4.36)$$

It should be noted that direct exploitation of similar **KRS-5** cell with the active optical aperture  $D = 5.0$  cm at the signal frequencies of already **1000** MHz is definitely impossible, because the acoustic attenuation is about **50** dB along this aperture. Nevertheless, applying the collinear acoustic wave heterodyning allows us to operate on these gigahertz-range carrier frequencies. The above-mentioned non-uniformities in the distributions of signals associated with various difference-frequency components in the **KRS-5** cell under consideration are illustrated in Fig.4.8. Using Eq.(4.29) at the pump frequency  $f_P = 1470$  MHz providing  $\alpha_P = 2.485 \text{ cm}^{-1}$ , one can estimate with  $\delta_U = 0.17$  that  $z_m = 1.80$  and  $x_m = 0.720$  cm for  $\xi = 0.5$  as well as  $z_m = 1.52$  and  $x_m = 0.608$  cm for  $\xi = 1.0$ . Then, estimating these non-uniformities in the distributions of acoustical signals along the cell's aperture at  $\delta_U = 0.17$  even graphically makes it possible to conclude from Figs.4.8 and 4.10 that one can obtain  $z_D = 14.2$  and  $x_D = 5.71$  cm for  $\xi = 0.5$  as well as  $z_D = 13.8$  and  $x_D = 5.55$  cm for  $\xi = 1.0$ . At this point, it is worthwhile to make two refining remarks. First, the analysis should, naturally, include considering the behavior of another frequency components inherent in the complete spectrum of the difference-frequency signal, in particular, the component with  $\delta_L = 0.034$ . Nevertheless, one can see from Fig.4.8 (as well as from Figs.4.4 and 4.5) that total irregularity inherent in this lowest-frequency component is practically insignificant even taking into account the appropriateness  $z_m(\delta_L) > z_m(\delta_U)$ . Second, some small part of the cell's aperture placed to the left of  $z_m(\delta_U)$ , which exhibit more or less "acceptable" level of signal irregularity can be also exploited practically. Thus, the really operating optical aperture  $D$ , lying between  $z_m(\delta_U)$  and  $z_D(\delta_U)$  for  $\delta_U = 0.17$  at a level of  $-3$  dB with the above-mentioned remarks, consists in approximately  $D = 5.0$  cm.

#### 4.5. ESTIMATING THE EFFICIENCY OF COLLINEAR WAVE HETERODYNING

Now, the efficiency of collinear wave heterodyning in the chosen regime of a given pump intensity and coupling between signal and difference-frequency acoustic modes has to be estimated. Again, without the loss of generality, let us take Eq.(4.25) in the form of Eq.(4.27), which describes the case of  $f_S = f_P + f_D$ , for further analysis. At this case, let us estimate the contributions involved in the term  $F_D$  from Eq.(4.27), which does not include any coordinate dependence contrary to the function  $\Phi(z, \delta, \xi)$ . One can start from the pump losses that are described by the factor  $\alpha_P = \tilde{\Gamma}_0 f_P^2$ . Usually, the acoustic attenuation factor  $\Gamma_0$  is used in bibliography (see for instance, Ref.[4.8, 4.9]) in the units of dB/(cm GHz<sup>2</sup>), but here one needs it in the form of  $\tilde{\Gamma}_0 \text{ (s}^2/\text{cm)} = [(\ln 10)/10] \cdot 10^{-18} \cdot \Gamma_0 \text{ [dB/(cm GHz}^2\text{)]}$  within estimating the efficiency of collinear wave heterodyning. Then, the factor  $\beta_D$ , introduced in Eqs.(4.14) and (4.15), takes the form  $\beta_D = 2\pi^2 V_L^{-2} \Gamma f_P f_S$ . Finally, the deformation tensor  $\gamma^{(L)}$ , described initially by Eq.(4.1) in the normalized form, can be converted to the axes chosen in connection with orienting the coordinate axis  $\mathbf{x}$  as  $\bar{\mathbf{x}} \parallel \bar{\mathbf{m}} \parallel [111]$  in Eq.(4.10). In so doing, one can write  $\gamma^{(L)} = \bar{\mathbf{u}} \cdot \bar{\mathbf{q}}$  for the longitudinal acoustic mode. After that, recovering the magnitudes of the vectors included into  $\gamma^{(L)}$ , one explain the unique non-zero component of this tensor in dimensional form as  $\gamma_j^{(11)} \equiv \gamma_j = U_j k_j$ , where  $\mathbf{j} \in [P, S, D]$  as before, see comments to Eq.(4.13). This dimensional form represents a scalar relation as well, so that it can be inverted as  $U_j = \gamma_j / k_j$ , where  $\mathbf{k}_j = 2\pi f_j / V_L$ .

In its turn, the chosen component of deformations can be explained in terms of the corresponding acoustic power density  $\mathbf{P}_j$  as  $\gamma_j^2 = 2\mathbf{P}_j / (\rho \mathbf{V}_L^3)$  [4.14]. Exploiting these relations, one can obtain from Eq.(4.27) that

$$\mathbf{F}_D^2 = \frac{\pi^2 \Gamma^2 \mathbf{P}_P \mathbf{P}_S}{4 \tilde{\Gamma}_0^2 \rho^2 \mathbf{V}_L^6 \mathbf{f}_P^4} . \quad (4.37)$$

Together with this, the left hand side of Eq.(4.27a) gives

$$\mathbf{a}_D^2(\mathbf{z}) \Phi^{-2}(\mathbf{z}, \delta, \xi) = \frac{\mathbf{P}_D}{2\pi^2 \rho \mathbf{V}_L \mathbf{f}_D^2} . \quad (4.38)$$

Combining Eqs.(4.37) and (4.38), one can find the power density of the difference-frequency acoustic wave

$$\text{a) } \mathbf{P}_D = 4\pi^2 \mathbf{P}_P \mathbf{P}_S \mathbf{m} \left( \frac{\mathbf{f}_D^2}{\mathbf{f}_P^4} \right) \Phi^2(\mathbf{z}, \delta, \xi) , \quad \text{b) } \mathbf{m} = \frac{\pi^2 \Gamma^2}{8 \rho \tilde{\Gamma}_0^2 \mathbf{V}_L^5} . \quad (4.39)$$

Now, one can estimate the total efficiency  $\mathbf{I}$  of Bragg light scattering by the difference-frequency acoustic wave. In the particular case of rather weak acoustic signals, when nonlinearity inherent in acousto-optical interaction can be omitted [4.14], one can use only a few terms from the corresponding expansion (see sub-section 2.4) and write

$$\text{a) } \mathbf{I} = \sin^2(\mathbf{qL}) \approx \mathbf{q}^2 \mathbf{L}^2 - \frac{1}{3} \mathbf{q}^4 \mathbf{L}^4 + \dots , \quad \text{b) } \mathbf{q} \approx \pi \lambda^{-1} \sqrt{\mathbf{M}_2 \mathbf{P}_D / 2} . \quad (4.40)$$

Under natural condition  $\mathbf{q}^2 \mathbf{L}^2 \ll 3$ , i.e. under inequality

$$\mathbf{P}_D \ll 6\lambda^2 / (\pi^2 \mathbf{M}_2 \mathbf{L}^2) , \quad (4.41)$$

one may restrict himself by the first term in the right side of Eq.(4.40a) and rewrite Eq.(4.40a) as  $\mathbf{I} = \pi^2 \mathbf{M}_2 \mathbf{L}^2 \mathbf{P}_D / (2\lambda^2)$ . Sometimes, see for instance below Eq.(4.4b), it is worthwhile to exploit the parameter  $\mu = (\pi^2/2) \mathbf{M}_2 \mathbf{m}$ , which combines characterization of both nonlinear acoustic and linear acousto-optic properties of material under consideration. The magnitude of  $\mathbf{I}$  determines the combined efficiency of the acousto-optical cell under consideration in terms of light scattering. This result makes it possible to characterize the contribution of acousto-optical interaction exploiting Eq.(4.40a) in the form of

$$\mathbf{I}_{\max} = \pi^2 \mathbf{M}_2 \mathbf{L}^2 \mathbf{P}_{D\max} / (2\lambda^2) . \quad (4.42)$$

With a maximally allowed level  $\mathbf{P}_{D\max} \approx 5 \cdot 10^5 \text{ g/s}^3 = 50 \text{ mW/cm}^2$ , obtained from Eq.(4.41), one can find  $\mathbf{I}_{\max} \approx 0.3$ . This estimation makes it possible to consider the above-chosen level of  $\mathbf{P}_D$  as more or less tolerable for an upper limit in a **KRS-5** single crystal under aforementioned condition given by Eq.(4.41). An undoubted merit of this characterization consists in practically convenient direct proportionality between the efficiency  $\mathbf{I}$  and the power density  $\mathbf{P}_D$ .

After that the contribution of acoustic wave mixing should be briefly analyzed. With this object in view, one can use Eqs.(4.25) and (4.26) for estimating the acoustic pump power density  $\mathbf{P}_{P0}$  needed to reaching a pre-assigned peak level of the difference-frequency power density  $\mathbf{P}_{D\max}$  at a given ratio  $\alpha = \mathbf{P}_S / \mathbf{P}_{P0}$ . From the start, it should be noted that a peak magnitude peculiar to the squared coordinate dependence

$\Phi_m^2 [z_m(\delta, \xi), \delta, \xi, G] = \frac{G}{z_m(\delta, \xi)} \Phi^2 [z_m(\delta, \xi), \delta, \xi]$  in, for example, Eq.(4.32) can be estimated as  $\Phi_m^2 [z_m(\delta, \xi), \delta, \xi, G] \approx 0.1$  with  $G = 4$ , see Fig.4.7. Consequently, one can find

$$P_{P0} = \frac{f_P}{2\pi\delta\Phi_m [z_m(\delta, \xi), \delta, \xi, G]} \sqrt{\frac{P_{Dmax}}{\alpha m}}. \quad (4.43)$$

Let us consider the particular example related to a **KRS – 5** single crystal. When the required magnitude of  $I_{max}$  is, for instance, equal to **3%** (which is quite reasonable for the spectrum analysis in a small-signal linear regime), Eq.(4.42) gives  $P_{Dmax} \approx 3.0 \cdot 10^4 \text{ g/s}^3 = 3 \text{ mW/cm}^2$ . Then, taking  $m \approx 1.1 \cdot 10^{11} \text{ s/g}$ ,  $\alpha = 0.1$ ,  $G = 4$ ,  $\delta = 0.15$ ,  $\xi = 1.0$ , and  $f_P = 1.5 \text{ GHz}$ , one can estimate from Eq.(4.43) the needed value of the acoustic pump power density by  $P_{P0} \leq 0.83 \cdot 10^7 \text{ g/s}^3 = 0.83 \text{ W/cm}^2$ , which looks quite acceptable practically.

#### 4.6. PROOF-OF-PRINCIPAL EXPERIMENTAL MODELING.

The obtained theoretical results related to the collinear acoustic wave heterodyning were examined experimentally via exploitation of the acousto-optic technique. The main attention was paid to the process of generating the difference-frequency acoustic wave and the effect of heterodyning by itself. At this step, one has to say that the above-presented analytical calculations allow mathematically scaling the parameters exploited within the problem. By this is meant that principal physical opportunity exists for experimental simulation of the desirable collinear interaction between high-frequency acoustic waves passing along the wave axes in anisotropic solid state through studying perfectly equivalent process at low frequencies in isotropic media with acceptable characteristics, namely, parameters of acoustic nonlinearity, acoustic attenuation, acoustic and acousto-optical figures of merit. In our particular case, one can perform experimental simulation of co-directional collinear acoustic wave heterodyning in a **1.5**-GHz frequency range in the **KRS – 5** crystal through studying the same process in the acousto-optical cell exploiting the distilled water ( $H_2O$ ) at frequencies of about **100** MHz. Analysis of Eq.(4.39) shows that, if the original parameter  $\gamma$  is saved during both the scaling and the experimental modeling, i.e.  $\gamma \equiv \gamma_M$  (where index “M” is related to the modeling process), one can write

$$\text{a) } f_j^2 = \frac{\tilde{\Gamma}_{0,M}}{\tilde{\Gamma}_0} f_{j,M}^2, \quad \text{b) } \frac{P_P P_S L^2}{\lambda^2} = \frac{\mu_M \tilde{\Gamma}_{0,M}}{\mu \tilde{\Gamma}_0} \left( \frac{P_{P,M} P_{S,M} L_M^2}{\lambda_M^2} \right). \quad (4.44)$$

The index “j” in Eq.(4.44a) represents a generalization for all the indices exploited above. Taking into account the properties of water:  $\rho_M = 1.0 \text{ g/cm}^3$ ,  $n_M = 1.33$ ,  $|\Gamma_M| = 8$ ,  $V_{L,M} = 1.49 \cdot 10^5 \text{ cm/s}$ ,  $\Gamma_{0,M} = 2400 \text{ dB/(cm GHz}^2)$ , and  $M_{2,M} = 126 \cdot 10^{-18} \text{ s}^3/\text{g}$ , one can find  $\tilde{\Gamma}_{0,M} \approx 5.52 \cdot 10^{-16} \text{ s}^2/\text{cm}$ ,  $m_M \approx 3.53 \cdot 10^6 \text{ s/g}$ , and  $\mu_M \approx 8.77 \cdot 10^{-9} \text{ s}^4/(\text{g cm})$ . Using Eq.(4.44a), which gives the frequency factor  $\sqrt{\tilde{\Gamma}_0 / \tilde{\Gamma}_{0,M}} \cong 0.0645$ , and utilizing the data from section 4.4, which are related to Eq.(4.36) and illustrated by Fig.4.8, one can calculate for the modeling medium, i.e. for the distilled water, that

$$\begin{aligned} \text{a) } f_{US,M} &= 110.940 \text{ MHz}, & \text{b) } f_{LS,M} &= 98.045 \text{ MHz}, & \text{c) } f_{P,M} &= 94.815 \text{ MHz}, \\ \text{d) } f_{DL,M} &= 3.225 \text{ MHz}, & \text{e) } f_{DU,M} &= 16.125 \text{ MHz}. \end{aligned} \quad (4.45)$$

General principle of the wave heterodyning and its experimental modeling are illustrated by Fig.4.11. The obtained magnitudes of the operating frequencies for liquid cell keep a pair of the previously chosen parameters  $\gamma_L \equiv \gamma_{L,M} = 1.034$  and  $\gamma_U \equiv \gamma_{U,M} = 1.17$ .

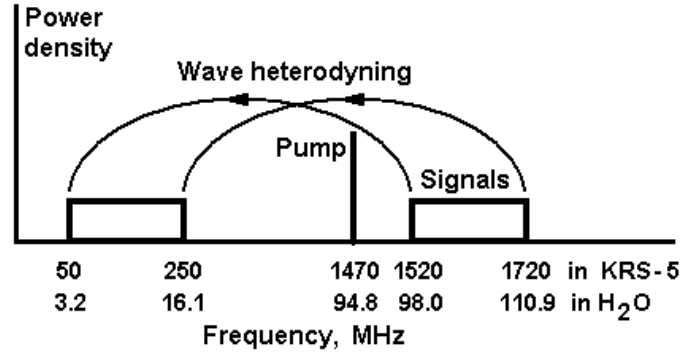


Figure 4.11. General principle of the wave heterodyning and its experimental modeling.

The frequency  $f_{DU,M}$  from Eq.(4.45e) makes it possible to exploit the results of section 4.4 for the modeling medium and to estimate potential clear aperture inherent in the water-based acousto-optical cell at a  $-3$  dB-level of acoustic losses along this aperture as  $D_M \approx 5.0$  cm. Together with this one has to estimate the Klein-Cook factor  $Q$  for the liquid cell. Taking, for example,  $\lambda_M = \lambda = 671$  nm and  $L_M = 2.5$  cm, one can estimate  $Q \approx 0.4$  for  $f_{DL,M} = 3.225$  MHz and  $Q \approx 9.1$  for  $f_{DU,M} = 16.125$  MHz. Thus, the Bragg region of light scattering could be expected for the acoustic difference-frequencies, which are close to  $f_{DU,M}$ , while for the acoustic difference-frequencies near  $f_{DL,M}$  the transition region [4.8] of light scattering could be expected in this water-based cell. Nevertheless, both these options are acceptable for our purposes. In fact, they both give almost the same linear approximation, and just this approximation is desirable within a small-signal linear regime of spectral data processing being under consideration here.

In so doing the experimental set-up, whose optical part had been presented in Fig.3.6, has been arranged. The goals of our experiment did not touch the principal possibility of modeling the power density relations, which are described by Eq.(4.44b). This fact is conditioned by really large technical difference in designing between a liquid-based acousto-optical cell and a solid-state one. In our opinion at the moment, similar modeling cannot give adequate data being practically useful to help in creating the ultra-high-frequency **KRS-5** based cell. This is why at this step of modeling our attention was mainly concentrated on the physical principles of collinear acoustic wave heterodyning and the corresponding frequency relations. Exploiting the above-listed estimations, the specific liquid-based acousto-optical cell of a new type had been designed and inserted in almost standard optical scheme for acousto-optical spectrum analysis. This scheme includes dark red-light laser ( $\lambda_M = 671$  nm, the output optical power about 40 mW), a four-prism beam expander (only two of them are shown), a rectangular selecting optical diaphragm, a liquid-based acousto-optical cell with acoustic absorber and two radio-wave frequency electronic ports for the input signal and pump (see Fig.4.12), a large-aperture achromatic doublet lens, and a 3000-pixel CCD linear array photo-camera. A water-based liquid cell of about 6.0 cm in total length was lighted by the expanded optical beam being linearly polarized along the acoustic beam inside the cell. It provided, on the one hand side, the maximal transmission of the prism beam expander due to coinciding the plane of expanding laser beam with the corresponding vector of light polarization and, on the other hand, the maximal efficiency of acousto-optical interaction in water, because the effective photo-elastic constant equals to the maximum value  $p_{11,M} = 0.274$ . The piezoelectric transducer with an interaction length of 2.5 cm was made of a thin ( $Y + 36^\circ$ )-cut lithium niobate crystal, so that it excited purely longitudinal acoustic wave at its resonant frequency close to  $f_{0,M} \approx 103$  MHz and within the total frequency bandwidth of  $\Delta f_M \geq 16$  MHz (i.e. 15.5%). The single-frequency pumping longitudinal acoustic wave with the power

density of up to  $0.6 \text{ mW/mm}^2$  was generated at the fixed carrier frequency of approximately  $95 \text{ MHz}$ , so that the case of  $\gamma \in [1.04, 1.18]$  had been experimentally realized in frames of modeling. During the experiments, we have placed a diaphragm in about  $8$ -millimeter vicinity of the piezoelectric transducers area (about  $13\%$  of the total  $6.0 \text{ cm}$  aperture) to minimize the effect of this area, where an increase in the power of difference frequency waves takes place. Consequently, the available optical aperture of a cell was exceeding  $5.0 \text{ cm}$ . The efficiency of light scattering by longitudinal acoustic wave at the difference-frequency was slightly exceeding  $2\%$ . Figure 4.13 shows the digitized oscilloscope trace of the light intensity distribution versus the difference-frequency inherent in the resulting acoustic wave, which was generated in water-based liquid cell realizing the algorithm of collinear wave heterodyning. This oscilloscope trace had been recorded by a multi-pixel CCD linear array photo-camera through connecting the input signal port of a cell at the radio-wave sweep-generator simulating the radio-wave signal. The scheme, connecting the sweep-generator with the cell's piezoelectric transducer, included a two-section wide-band matching circuit of the lumped components together with a two-cascade resistance step-down transformer assembled out of micro-coaxial cables. The signal-like frequency was sweeping in the range of about  $98 - 111 \text{ MHz}$ , so that the difference frequency was varied in the range of about  $3.0 - 16.5 \text{ MHz}$ . It should be noted that for radio-wave signals, producing the dynamic acoustic gratings on the resulting carrier difference-frequencies of about  $250 \text{ MHz}$  in the **KRS-5** crystal and about  $16.2 \text{ MHz}$  in the distilled water, the attenuation is close to a  $-3 \text{ dB}$  level over the corresponding total cell apertures. At the same time, for the signal acoustic waves at even the lower original frequencies of about  $1520 \text{ MHz}$  in **KRS-5** and about  $98 \text{ MHz}$  in water, the total attenuations exceed  $110 \text{ dB}$  along the corresponding apertures, which is perfectly unacceptable in practice.

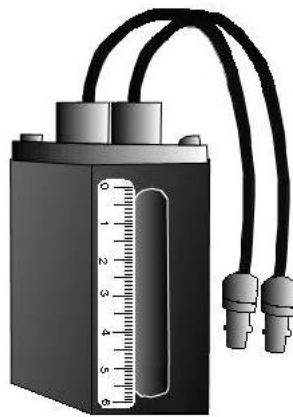


Figure 4.12. Water-based liquid acousto-optical cell with acoustic absorber and two radio-wave frequency electronic ports.

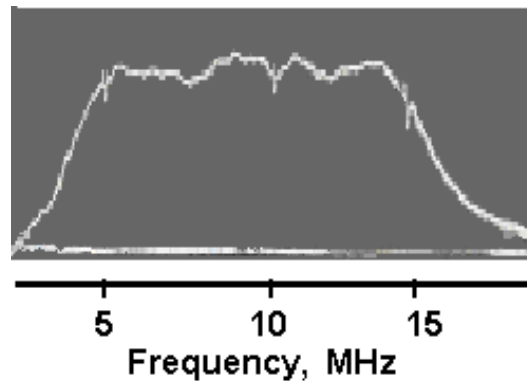


Figure 4.13. The digitized oscilloscope trace reflecting the frequency distribution of the light intensity scattered by the acoustic wave with the difference frequency within the modeling experiment.

#### 4.7. BRIEF COMPARATIVE DISCUSSION

The above-obtained results make it possible to perform theoretical estimations for potential number of parallel frequency channels and frequency resolution of spectrum analysis. Potential frequency resolution  $\delta f$  inherent in similar acousto-optical cell, operating in the regime of spectrum analysis, can be estimated from the following simple quantum mechanic consideration as  $\delta f \approx V/D$ . Just this value determines physical limit of the frequency resolution peculiar to an acousto-optical cell independently on the number of phonons taking part in a process of the Bragg light scattering. Taking into account the above listed values  $V_L = 1.92 \cdot 10^5$  cm/s and  $D = 5.0$  cm, one can find  $\delta f \approx 38.4$  KHz. The number of parallel frequency channels for spectrum analysis can be calculated as  $N = \Delta f / \delta f$ . In the case of  $\Delta f = 200$  MHz, one can obtain  $N \approx 5210$ . Moreover, because the initial frequencies under analysis are lying in the range 1520 – 1720 MHz, one can conclude that the relative accuracy of data processing can be estimated at least by the ratio  $\delta f / f_0 \approx 2.37 \cdot 10^{-5}$ . Then, the data from section 4 show that, if the total efficiency of Bragg light scattering by the difference-frequency acoustic wave is chosen to be  $I_0 = 0.03$ , i.e. 3%, one should provide  $P_{P0} \leq 0.83 \cdot 10^7$  g/s<sup>3</sup> = 0.83 W/cm<sup>2</sup> and  $P_S \leq 0.83 \cdot 10^6$  g/s<sup>3</sup> = 0.083 W/cm<sup>2</sup> due to  $\alpha = 0.1$  with  $L = 1.0$  cm, see section 4.5.

At this step, it seems quite reasonable to compare operation characteristic of the proposed KRS-5 acousto-optical cell with the corresponding characteristics of the traditional high-frequency cell. Perhaps, the best option for this purpose is connected with a crystalline cell exploiting longitudinal acoustic waves along the [100]-axis of uniquely low-loss lithium niobate (LiNbO<sub>3</sub>) single crystal with  $M_2 = 7.0 \cdot 10^{-18}$  s<sup>3</sup>/g,  $\Gamma = 0.15$  dB/(cm GHz<sup>2</sup>), and  $V_L = 6.57 \cdot 10^5$  cm/s. Each cell can be characterized in both frequency and amplitude domains. The best set of frequency characteristics for the chosen cell at the central frequency  $f_0 = 1.6$  GHz (which is neighboring to the central frequency  $f_0 = 1620$  MHz obtained for KRS – 5 crystalline cell) includes the frequency bandwidth  $\Delta f \approx f_0 / 2 = 800$  MHz, the upper signal frequency  $f_U = 2.0$  GHz, the optical aperture  $D_0 = 3 \text{ [dB]} / (\Gamma f_U^2) \approx 5.0$  cm associated with a 3 – dB level of acoustic losses at the frequency  $f_U$ , the frequency resolution  $\delta f = V/D_0 = 131.4$  KHz, the number of resolvable spots  $N = \Delta f / \delta f \approx 6010$ , and the relative accuracy of analysis  $\delta f / f_0 \approx 8.2 \cdot 10^{-5}$ . The efficiency of this cell with  $L = 1.0$  cm and a given exciting acoustic wave power density  $P_0$  can be estimated by  $I_0 = \sin^2(q_0 L)$ , where  $q_0$  can be taken from Eq.(4.5b) at  $\lambda = 671$  nm. To make the comparison with the data in the end of section 4.2, let us take as before  $I_0 = 0.03$ , i.e. 3%. In this case, one can estimate  $q_0 = I^{1/2} / L \approx 0.173$  cm<sup>-1</sup> and  $P_0 = (2I\lambda^2) / (\pi^2 L^2 M_2) \approx 0.4 \cdot 10^7$  g/s<sup>3</sup> = 0.4 W/cm<sup>2</sup>.

The above-mentioned data make it possible to conclude that the proposed KRS – 5 based cell, exploiting the collinear acoustic wave heterodyning, provides increasing both the frequency resolution and the relative accuracy of analysis by about 3.4 times in comparison with the traditional lithium niobate cell. Together with this the new KRS – 5 cell ranks below the traditional lithium niobate cell in the number of resolvable spots by 13%. Then, to make the correct decision one has to take into account a few following circumstances. First, a large optical aperture requires growing large enough boule of lithium niobate. It should be the mono-domained svilen-less single crystal exhibiting a high optical homogeneity and providing top-level conditions for propagation of both optical as well as UHF acoustic waves through a large-aperture cell. Practically, it is rather difficult to satisfy these requirements, but in the otherwise case, similar cell will have lost a significant part of its potential frequency resolution. Second, designing truly effective piezoelectric transducer with a 50% frequency bandwidth at a carrier frequency of about 1.6 GHz is not an ordinary task. The existing difficulties in technology of production as well as in subsequent acoustic and electronic matching of similar wide-band piezoelectric transducer can be resolved currently only within decreasing its efficiency or/and narrowing its bandwidth. This is why the above-noted potential frequency characteristics have to be considered as just the limiting theoretical values. Third, the estimated efficiency for a lithium niobate cell cannot be applied directly to the comparison under consideration, because the proposed new cell involves two cascades of

processing and provides an additional function, namely, the heterodyning, which needs naturally additional power consumption.

#### 4.8. CONCLUSION

The presented data demonstrate both the possibility and the potential advantages of applying a co-directional collinear wave heterodyning to essential, about an order of magnitude or more, improvement of the frequency resolution within a multi-channel parallel acousto-optical spectrum analysis of gigahertz-frequency range analogue radio-wave signals. In so doing, we have theoretically investigated the phenomenon of a co-directional collinear wave heterodyning, taken in the particular case of mixing the longitudinal acoustic waves of finite amplitudes. Then, an opportunity of implementing acousto-optical data processing with the wave heterodyning has been experimentally modeled utilizing the specially designed acousto-optical cell based on the distilled water. Together with this, the methods for estimating the total efficiency of operation and optimizing aperture parameters for the cell of a new type have been developed. The proposed technique exploits a two-cascade algorithm of processing and is intended for direct parallel and precise optical spectrum analysis and provides more than **5000**-frequency-channels for processing analogue radio-wave signals in a gigahertz-frequency range with the accuracy or, what is the same, with the relative frequency resolution about  $10^{-5}$ , which is usually unattainable for conventional direct acousto-optical methods. The obtained results reflect fruitful character of modern approaches based on applying various non-linear phenomena to improving the performance data of optical processing and give an appropriate example of this kind. At the moment, a few practical advantages of the presented approach can be noted. First, the proposed device need not additional electronic equipment for mixing the signals and selecting the resulting carrier frequency, because heterodyning can be performed directly in a cell and provides potentially the dynamic range of about **90** dB peculiar to wave processes in solids. Then, the approach under consideration decreases the required relative bandwidth of piezoelectric transducer from **50 – 100%** at the resulting frequency within a conventional cell to **15%** at the initial carrier frequency. Third, in the case of a spatially multi-channel arrangement of the acousto-optical cell, the identity of neighboring spatial channels to each other can be provided by adjusting the corresponding heterodynes. Finally, one should note that the number of isotropic or crystalline materials, which are appropriate for acousto-optical cells processing signals in a gigahertz-frequency range, is definitely restricted due to fast-growing influence of square-law frequency dependence for the acoustic attenuation in solids. For instance, one can easily show that the above-discussed **KRS – 5** cubic crystal cannot be used for creating a conventional acousto-optical cell operating with signals whose carrier frequency exceeds about **400 – 500** MHz. Nevertheless, just this crystalline material can be in principle exploited for the control over  $f_0 = 1.6$  GHz signals. Consequently, one can conclude that a two-cascade arrangement of a cell presented here allows extending the spectrum of acousto-optical materials being appropriate for direct processing of ultra-high-frequency analogue radio-wave signals.

#### 4.9. REFERENCES

- 4.1. P.A.M.Dirac. *The Principles of Quantum Mechanics*. 4-th Ed. (Oxford University Press, Oxford, 1999).
- 4.2. A.S.Shcherbakov, A.M.Bliznetsov, A.L.Castellanos, and D.Sánchez Lucero. “Acousto-optical spectrum analysis of ultra-high frequency radio-wave analogue signals with an improved resolution exploiting the collinear acoustic wave heterodyning.” *OPTIK – International Journal for Light & Electron. Optics* (Elsevier, Germany) 2009; (published electronically at [www.sciencedirect.com](http://www.sciencedirect.com); doi:1016/j.ijleo.2009.02.015).
- 4.3. A.S.Shcherbakov, D.Sánchez Lucero, A.Luna Castellanos, and O.I.Belokurova. “Direct multi-channel optical spectrum analysis of radio-wave signals using collinear wave heterodyning in single acousto-optical cell.” *Journal of Optics (UK)*, vol.12, no.4, 2010; # 045203 (published electronically by April 01, 2010 at [www.sciencedirect.com](http://www.sciencedirect.com); doi:10.1088/20408978/12/4/045203).
- 4.4. Yu.E.Sirotnin and M.P.Shaskol'skaya. *Fundamentals of Crystal Physics*. (Mir Publ., Moscow, 1982)
- 4.5. A.A.Blistanov. *Crystals for Quantum and Nonlinear Optics*. 2-nd Ed. (MISIS, Moscow, 2007).
- 4.6. V.G.Dmitriev, G.G.Gurzadyan and D.N.Nikogosyan, *Handbook of Nonlinear Optical Crystals* 3-rd Ed. (Springer, Berlin, 1999).
- 4.7. R.W.Klein and B.D.Cook. “A unified approach to ultrasonic light diffraction.” *IEEE Transactions*, V.**SU-14**, no. 3, 123-134 (1967).

- 4.8. L.D.Landau, L.P.Pitaevskij, E.M.Lifshitz, and A.M.Kosevich. *Theory of Elasticity*. 3-rd Ed. (Pergamon Press, Oxford. 1999).
- 4.9. V.V.Kludzin and V.V.Molotok. "Experimental characteristics of the elastic nonlinearity in **KRS-5** and  $\text{NaBi}(\text{MoO}_4)_2$  crystals." The 1994 IEEE Ultrasonic Symposium Proceedings, (Cannes, France), Vol.2, 851-854 (1994).
- 4.10. M.Abramovitz and I.A.Stegun. *Handbook of Mathematical Functions: with Formulas, Graphs, and Mathematical Tables*. (Dover Publications, 1965); G.A.Korn and T.M.Korn. *Mathematical Handbook for Scientists and Engineers*. 2-nd. Ed. (McGraw-Hill, 1967).
- 4.11. A.Korpel. *Acousto-Optics*. (Marcel Dekker, New-York, 1997).

## 5. ACKNOWLEDGMENTS

The work was financially supported by the CONACyT, Mexico, project # 61237. Also, the authors thank Dr. Luis Carrasco Bazua (INAOE, Mexico) for his stimulating discussion related to developing and implementing the specialized acousto-optical equipment providing a high-resolution spectrum analysis of the UHF radio-wave signals from the Mexican Large Millimeter Telescope.